The Philosophical Magazine

FIRST PUBLISHED IN 1798

A Journal of Theoretical Experimental and Applied Physics

Vol. 3 June 1958 No. 30
Eighth Series

£1 5s. 0d., plus postage
Annual Subscription £13 10s. 0d., payable in advance

Printed and Published by
TAYLOR & FRANCIS LTD
RED LION COURT, FLEET STREET, LONDON, E.C.4

THE PHILOSOPHICAL MAGAZINE

Authors wishing to submit papers for publication in the Journal should send manuscripts directly to the Publishers.

Manuscripts should be typed in *double* spacing on one side of quarto (8×10 in.) paper, and authors are urged to aim at absolute clarity of meaning and an attractive presentation of their texts.

References should be listed at the end in alphabetical order of authors and should be cited in the text in terms of author's name and date. Diagrams should normally be in Indian ink on white card, with lettering in soft pencil, the captions being typed on a separate sheet.

A leaflet giving detailed instructions to authors on the preparation of papers is available on request from the Publishers.

Authors are entitled to receive 25 offprints of a paper in the Journal free of charge, and additional offprints can be obtained from the Publishers.

The *Philosophical Magazine* and its companion journal, *Advances in Physics*, will accept papers for publication in experimental and theoretical physics. The *Philosophical Magazine* publishes contributions describing new results, letters to the editor and book reviews. *Advances in Physics* publishes articles surveying the present state of knowledge in any branch of the science in which recent progress has been made. The editors welcome contributions from overseas as well as from the United Kingdom, and papers may be published in English, French and German.

Nuclear Magnetic Resonance in Indium Antimonide
I. The Effect of Impurities†

By E. H. Rhoderick
Services Electronics Research Laboratory, Baldock, Herts.

[Received January 23, 1958; and in revised form March 5, 1958]

Abstract

A study has been made of the effect of impurities on the ^{115}In nuclear magnetic resonance in indium antimonide. In n-type (Te-doped) and p-type (Zn-doped) samples, the amplitude and width of the resonance are very sensitive to the presence of donors or acceptors, a concentration of 10^{19} cm^{-3} reducing the maximum of the derivative of the absorption curve by a factor of 10. This is ascribed to broadening arising from the interaction of the nuclear quadrupole moment with the Coulomb field of the ionized impurity atoms. The effect is slightly less pronounced in p-type than in n-type samples, which can be explained by the fact that holes are more effective than electrons in screening the ionic charges, because of their greater effective mass. Assuming the field gradient at a distance r from an ion to be given by $\partial^2 V/\partial r^2 = 2\beta e/r^3$, β must be $\simeq 350$ to fit the experiments, which implies an ' anti-shielding factor ' of $\simeq 1000$. It is suggested that this large value is associated with the smallness of the forbidden gap in InSb. The replacement of a small fraction of In atoms by Ga in an InSb–GaSb mixed crystal has a qualitatively similar effect on the ^{115}In resonance, but the concentration of Ga atoms must be about 30 times that of Te or Zn for the same reduction in resonance amplitude. Since the Ga atoms are electrically neutral, their effect is attributed to strain set up in the InSb lattice by the disparity between the sizes of the Ga and In atoms.

A search for a possible Knight shift in n- and p-type InSb containing 10^{19} carriers cm^{-3} revealed no deviation in either case from the ^{115}In resonance frequency in intrinsic material, within an experimental accuracy of 1 in 10^4. The negative result in n-type material is attributed to the small effective mass of the electrons, which reduces the Pauli susceptibility, while the p-type result provides possible evidence for the p-character of hole wave functions.

§ 1. Introduction

In recent years nuclear magnetic resonance has become widely used as a tool for solid state investigations. In particular, an extensive review article by Bloembergen (1955) has drawn attention to its potentialities for studying defects in crystals. The possibility of using nuclear resonance for this purpose arises because the precise frequency at which a particular nucleus resonates depends upon the magnetic (and in some cases electric) field which exists at the site of that nucleus; although mainly determined by the external magnetic field, this local field shows small deviations which depend on the nuclear environment.

† Communicated by the Author.

Comparatively little work has been done on nuclear resonance in semiconductors. This is mainly because the most widely studied semiconductors, silicon and germanium, do not readily lend themselves to nuclear resonance investigations since the isotopes of these elements which possess nuclear magnetic moments occur in low abundance. On the other hand, the semiconducting intermetallic compounds formed from Group III and Group V elements are particularly suitable for nuclear resonance investigations since the nuclei of all these elements are magnetically active. The present paper describes a study of indium antimonide using nuclear resonance techniques.

After the work was begun, a paper was published by Shulman *et al.* (1955) on nuclear magnetic resonance in pure indium antimonide and gallium antimonide. The research described here does not overlap their work since they confined their studies to crystals as near to perfection as they could obtain, whereas the present paper is mainly concerned with the effect of deliberately introduced imperfections. Preliminary accounts of these experiments have already appeared (Rhoderick 1956, 1957).

§ 2. Experimental Method

The nuclear magnetic resonance was observed with a radio-frequency spectrometer of the type developed by Pound, Knight and Watkins (see, for example, Pound 1952), used in conjunction with a permanent magnet having a field of 3850 gauss. The normal technique of using a lock-in amplifier was adopted, so that the derivative of the absorption ($\partial\chi''/\partial\nu$) was recorded, the line shape being plotted by varying the frequency at constant magnetic field. Measurements at liquid oxygen temperature were made using a cryostat of the heat-leak variety similar to that described by Gutowsky *et al.* (1953).

One experimental difficulty may be mentioned here. The resistivity of highly extrinsic indium antimonide at room temperature may be as low as 10^{-4} ohm cm, for which the skin depth at a frequency of 5 Mc/s is about 0·2 mm. Not only does the intensity of the absorption fall if the radio-frequency field does not completely penetrate the specimen, but distortions of the line shape may occur (Bloembergen 1952, Chapman *et al.* 1957). The difficulty may be overcome by using powdered specimens such that the particle size is much smaller than the skin depth. Initially these were embedded in an insulating matrix of paraffin wax, but this was subsequently found to be unnecessary, probably because of the high contact resistance. The resistivity of intrinsic indium antimonide at room temperature is sufficiently high for single crystals in the form of plates about 1 mm thick to be used.

The indium antimonide used in these experiments was zone-refined material which was intrinsic at room temperature. Hall effect measurements at liquid air temperature gave the excess acceptor concentration as 10^{15} cm^{-3}, the estimated total impurity concentration being less than

10^{16} cm^{-3}. 'Doped' specimens were prepared by using tellurium and zinc as donor and acceptor elements respectively. In all cases the carrier concentration obtained from Hall effect measurements agreed within 10% with the donor or acceptor concentration estimated from the weight of tellurium or zinc added.

§ 3. Results for Pure Indium Antimonide

A brief investigation of nuclear magnetic resonance in undoped indium antimonide was made, the results being in substantial agreement with those reported by Shulman *et al.* (1955). The shape of the ^{115}In absorption line in a single crystal is independent of the orientation of the crystal axes relative to the magnetic field, and its width is much greater than that to be expected from dipolar broadening. The width between points of maximum slope was found to be $9{\cdot}9 \pm 0{\cdot}4$ kc/s, which corresponds to $10{\cdot}6 \pm 0{\cdot}4$ gauss for an experiment at fixed frequency, compared with the value $9{\cdot}0 \pm 0{\cdot}2$ gauss given by Shulman *et al.* (1955). The line shape is almost symmetrical, the slight departure from symmetry being attributable to the presence of the ^{113}In isotope, which is 4% abundant, and which has a resonant frequency 7·5 kc/s lower than that of ^{115}In in a field of 3850 gauss. The high frequency half of the line, which is practically free from the distorting effect of the ^{113}In resonance, is very closely Gaussian in shape. Shulman *et al.* (1955) have shown that this can be explained in terms of the indirect exchange coupling between nuclei first postulated by Ruderman and Kittel (1954) to explain anomalously broad lines in metals. This coupling mechanism, which was subsequently extended to the case of insulators by Bloembergen and Rowland (1955), leads to an interaction of the form $A_{12}\mathbf{I}_1 . \mathbf{I}_2$ between pairs of nuclei, $\mathbf{I}$ being the nuclear spin vector. The ^{121}Sb resonance is much broader (about 17 kc/s between points of maximum slope) and weaker, and no precise measurements were made on this line.

Since the ^{115}In nucleus possesses a large quadrupole moment, it is possible that the shape of the resonance may be affected by quadrupolar interactions. If a nucleus having a quadrupole moment is placed in a non-uniform electric field, the effect of the field gradient is to split the nuclear resonance line into $2I$ equally spaced components. If $2I$ is an odd integer, as in the case of ^{115}In ($I = 9/2$), the central component is unchanged in frequency, the remaining $2I - 1$ components, known as satellites, being grouped symmetrically about this central component. In crystals having the zinc-blende structure, such as indium antimonide, the lattice symmetry is such that the gradient of the crystalline field, **grad·E**, vanishes at the position of any nucleus, so that there should be no nuclear quadrupole interaction in a perfect crystal. However, as Watkins and Pound (1953) have pointed out, the symmetry of the field may be altered by the inhomogeneous strains which accompany dislocations. The result of these strains is to produce field gradients which vary in magnitude and orientation from one nucleus to another, so that the satellites become smeared into a continuous band, leaving the central component unaffected. According

to Watkins and Pound, the dislocation density in the best crystals of potassium bromide and iodide obtainable is such that the satellites of the bromine and iodine nuclear resonances are entirely obliterated, the observed intensity corresponding to that of the central component only. Since it is of importance to know whether similar effects are present in the indium antimonide crystal, a measurement was made of the total integrated intensity of the ^{115}In resonance in the single crystal and the value obtained compared with the total intensity of th ^{1}H resonance in an equal volume of a concentrated aqueous solution of ferric chloride, the latter being used to broaden the proton resonance line and to shorten the relaxation time. In this experiment an electromagnet was used, the magnetic field being adjusted so that the ^{115}In and ^{1}H resonances occurred at the same frequency, and a calibrator was used to monitor the spectrometer sensitivity. Since the resonant frequency is the same in each case, the total integrated intensities should be proportional to $\gamma^2 NI(I+1)$, where γ and I are respectively the gyromagnetic ratio and spin of the appropriate nucleus, N is the total number of nuclei in the specimen, and quadrupolar effects are neglected. In this way the intensity of the ^{115}In resonance was found to be $0{\cdot}8 \pm 0{\cdot}1$ times the intensity to be expected on the assumption that all the satellites contribute to the observed absorption. (There can be no quadrupolar effects in the case of the proton resonance, since nuclei with spin $\frac{1}{2}$ have no quadrupole moment.) Since for $I = 9/2$ the central component contributes only 25/165 of the total intensity, almost the entire contribution from the satellites was observed. It follows, therefore, that any quadrupolar broadening effects arising from dislocations are far weaker in indium antimonide than in the alkali halides studied by Watkins and Pound. Observations of etch pits in indium antimonide single crystals similar to the one used in this experiment show that the dislocation density is of the order of 10^3 cm^{-2} (Allen 1957), which is of the same order as that found in good crystals of silicon and germanium, whereas Watkins and Pound assumed densities of 10^8 cm^{-2} to explain the alkali halide results. Since one of the causes of dislocations is the stress associated with thermal gradients after solidification, the low dislocation density in the former group of materials as compared with the alkali halides may be partly due to their higher thermal conductivity; another contributing factor may be the higher energy necessary to form a dislocation, arising from the directional nature of the bonds in the predominantly covalently bound semiconductors.

The results of the present experiments differed from those reported by Shulman *et al.* (1955) in two respects. Firstly, the ^{115}In resonance was found to be weaker and broader when the material was crushed to a powder. This effect is attributed to quadrupolar broadening resulting from the introduction of dislocations during the crushing process, and will be discussed more fully in a future paper. Secondly, the resonance in the single crystal appears to be about 10% wider at liquid oxygen temperature than at room temperature, as can be seen from fig. 1, which shows the high

frequency halves of the derivative curves plotted directly from the recorder chart. The reason for this is not clear. There can be no ' motional narrowing ' of the line at room temperature, since self diffusion in indium antimonide is known to be completely negligible at 290°K (Eisen and Birchenall 1957), and in any case an $A_{12}\mathbf{I}_1 . \mathbf{I}_2$ type of interaction does not average to zero. The theory of indirect exchange coupling as applied to insulators or semiconductors (Bloembergen and Rowland 1955, Shulman *et al.* 1955) shows that the constant A_{12} depends on the energy gap, E_g, on the distance between neighbouring nuclei, R_{12}, and on the quantity

$$\langle|\Delta_{12}|^2\rangle_{\mathrm{Av}} = (16\pi\beta_N\beta/3)^2 g_1 g_2 \langle u_k(\mathbf{r}_1) u_{k'}{}^*(\mathbf{r}_1) u_k(\mathbf{r}_2) u_{k'}{}^*(\mathbf{r}_2)\rangle_{\mathrm{Av}}$$

where β and β_N are the Bohr and nuclear magnetons respectively, g_i and $\mathbf{r}_i$ the g-factor and position vector of the ith nucleus, and $u_k(\mathbf{r})$ and $u_{k'}(\mathbf{r})$

Fig. 1

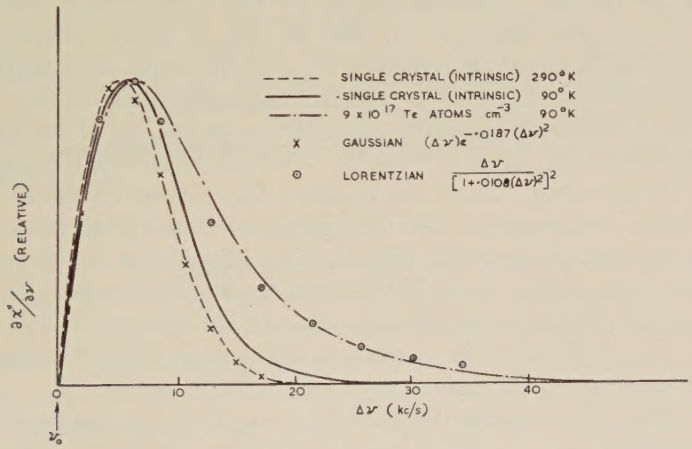

High frequency halves of ^{115}In resonance in intrinsic and Te-doped InSb. The curves show the derivative of the absorption at a frequency $\nu_0 + \Delta\nu$, where ν_0 is the centre frequency. The high and low frequency halves were identical for the doped sample.

the periodic parts of the Bloch wavefunctions for electrons with momentum vectors $\mathbf{k}$ and $\mathbf{k}'$. All three quantities depend on temperature since they are functions of the lattice parameter. E_g is known to be about 30% larger at 90°K than at room temperature for indium antimonide (Roberts and Quarrington 1955), but, as Shulman *et al.* (1955) have pointed out, A_{12} is not very sensitive to E_g; moreover, A_{12} should decrease as E_g increases, giving a narrower line at 90°K. The quantity Δ_{12} is reminiscent of the factor $\langle|\psi(0)|^2\rangle_F$ which occurs in the expression for the Knight shift (Townes *et al.* 1950), and which is known to increase as the temperature decreases. McGarvey and Gutowsky (1953) found their results on the temperature variation of the Knight shift in gallium and caesium to be

consistent with $\langle|\psi(0)|^2\rangle_F \propto v_a^{-1}$, where v_a is the atomic volume, and if we tentatively suppose that Δ_{12} shows the same behaviour, then the product $R_{12}^{-4}\langle|\Delta_{12}|^2\rangle_{Av}$, to which A_{12} is proportional, should vary as $v_a^{-10/3}$. This is in the right direction to explain the broadening of the line at 90°K, but is unlikely to lead to an increase in A_{12} of more than 1% or so. For the present, the origin of this broadening remains obscure.

§ 4. Frequency of Resonance

It is well known that nuclear resonance frequencies in metals are higher by some tenths of 1% than the resonance frequencies of the same nuclei in insulators. This effect, known as the Knight shift (Knight 1949), is due to the Pauli paramagnetism of the conduction electrons, which increases the effective magnetic field acting on a nucleus. Only those electrons near the Fermi surface contribute to the Pauli susceptibility (χ_p), and this makes χ_p proportional to $n^{1/3}$ for a degenerate electron gas, n being the electron density. In view of this, it is just possible that a small Knight shift might be detectable in a highly extrinsic semiconductor with about 10^{19} carriers cm^{-3}. Careful measurements of the ^{115}In resonance frequency were therefore made in n-type indium antimonide with an electron concentration of 10^{19} cm^{-3}. This material is highly degenerate, having a Fermi energy about $30kT$ above the bottom of the conduction band at room temperature. No deviation was found from the resonance frequency in intrinsic material, within an experimental accuracy of 1 in 10^4. The explanation of this is probably that the Pauli susceptibility is very low on account of the small effective mass of the electrons ($m^* = 0{\cdot}02m_e$), since χ_p is proportional to the density of states at the Fermi surface, which is proportional to m^* for a given electron density.

The situation is somewhat different in p-type indium antimonide. Here the larger effective mass of the holes ($m^* = 0{\cdot}2m_e$) makes χ_p considerably larger than in the n-type case for the same carrier concentration. The experiment was therefore repeated with p-type material with 10^{19} holes cm^{-3}, but again no Knight shift was detected. To interpret this result it is necessary to consider the theoretical expression for the fractional Knight shift, which is $\Delta\nu/\nu = (8\pi/3)\chi_p v_a \langle|\psi(0)|^2\rangle_F$. Here v_a is the atomic volume, and $\psi(0)$ the wave function of a hole at the nucleus, ψ being normalized to unity within an atomic volume. The expression $\langle|\psi(0)|^2\rangle_F$, which will be designated by P_F, represents an average taken over the Fermi surface. If we calculate χ_p using the Pauli formula modified for the case of intermediate degeneracy, viz. $\chi_p = n\beta^2 F'/kTF$, where n is the carrier density, β the Bohr magneton, and $F = F_{1/2}(\zeta/kT)$ is the usual Fermi–Dirac integral, we obtain the value $\chi_p = 9 \times 10^{-9}$ e.m.u. cm^{-3}. From measurements of the Knight shift in metals, it is usually found that P_F is within about 50% of the value of $|\psi(0)|^2$ relating to the valence electrons in a free atom. If we assume the hole wave function to have s-character, and substitute for P_F the value of $|\psi(0)|^2$ appropriate to the

$5s$ electron in the In^{2+} ion, which is known to be $1{\cdot}5 \times 10^{26}$ cm^{-3} from hyperfine structure determinations (Campbell and Davis 1939), we find

$$\Delta\nu/\nu = 4 \times 10^{-4},$$

which is four times the probable error of our measurements. In this calculation we have taken v_a to be one half the volume per In–Sb pair. If the value adopted for χ_p be assumed correct, the absence of an observable Knight shift implies that the value used for P_F is too large. This is not unexpected, since in the case of germanium and silicon it seems well established that the hole wave functions are predominantly p-like, and, bearing in mind that $\psi(0)$ vanishes for a p wave function, we can explain the small value of P_F by assuming that the same is true of indium antimonide. There is another factor which may depress the value of P_F, namely, the suggestion by Slater and Koster (1954) that the valence band is predominantly built up of antimony $5s$ and $5p$ orbitals, so that the hole wave functions tend to be concentrated around Sb atoms. However, assuming that the valence electron distribution is such as to give approximate charge neutrality around each atom, this effect cannot be large. The result of this experiment can be stated more specifically by saying that, assuming the value of 9×10^{-9} e.m.u. cm^{-2} for χ_p, the value of $\langle|\psi(0)|^2\rangle_F$ for holes in indium antimonide must be less than 4×10^{25} cm^{-3} at the position of an indium nucleus.

§ 5. The Effect of Ionized Impurities

In the course of the experiments mentioned in § 4, it was found that the intensity of the ^{115}In nuclear resonance in InSb, as represented by the maximum value of $\partial\chi''/\partial\nu$, was very sensitive to the presence of donor or acceptor atoms. This is shown in fig. 2, which shows the maximum value of the derivative of the room temperature absorption plotted against tellurium concentration. For concentrations of 10^{18} atoms cm^{-3}, the effect of crushing mentioned in § 2 is completely swamped by the effect of the impurity atoms. This decrease in intensity is accompanied by an increase in width, as is evident from fig. 1, which shows the line shape for the specimen with 9×10^{17} Te atoms cm^{-3} at 90°K; this has much more pronounced wings than the single crystal curves and approximates more closely to a Lorentzian than to a Gaussian line shape. No asymmetry could be detected in the absorption lines of any of the doped samples, since the additional broadening brought about by the impurities tends to reduce the asymmetry which is already very small in the case of the single crystal. In fig. 1 the ordinates are scaled to make each curve have the same maximum value, which helps to emphasize the differences in shape. With the exception of the single crystal, all samples showed the same line shape and same relative intensities at 90°K as at 290°K; provided saturation effects were avoided, the increase in the absorption intensity at the lower temperature corresponded to the increase in the Boltzmann factor which determines the difference in the populations of adjacent Zeeman levels.

The various ways in which the presence of impurities could conceivably broaden the nuclear resonance line can be divided into two categories. Firstly, it is possible that the spin-lattice relaxation time (T_1) may be shortened in some way and so give rise to ' lifetime broadening '. Such a mechanism was invoked by Reif (1955) to explain the effect of Cd^{2+} ions in broadening the Br resonance in silver bromide. Reif assumes that the relaxation mechanism arises from quadrupolar coupling of the Br nuclei to the electric fields associated with rapidly diffusing Ag^+ vacancies. Other processes by which T_1 may be shortened are the Heitler–Teller mechanism associated with the extrinsic conduction electrons, in which a

Fig. 2

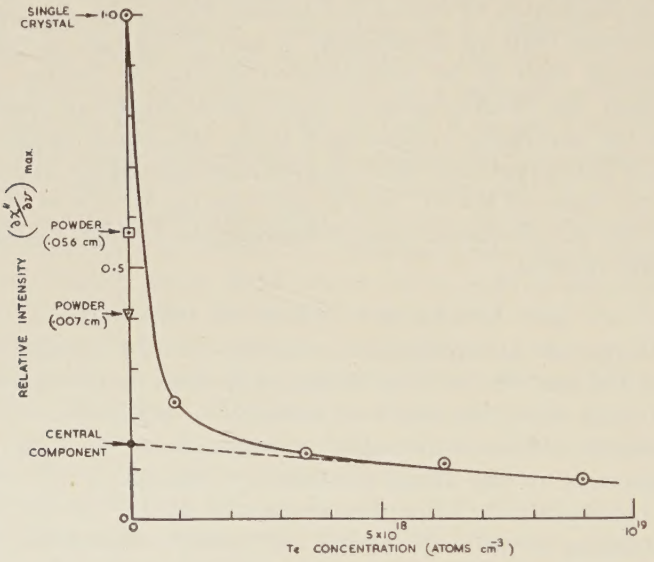

Variation with Te concentration of derivative of ^{115}In resonance in InSb (290°K). The value relating to the pure single crystal is taken as unity. Also shown are results for two particle sizes of the pure powdered material.

nucleus and a conduction electron mutually flip their spins, and its quadrupolar analogue (Mitchell 1957). All these processes should be negligible in indium antimonide at room temperature, even with 10^{19} conduction electrons cm^{-3}. To verify that this is so, a brief study of the relaxation time in pure and impure samples was made, using the saturation method. Figure 3 shows relative values of $(\partial\chi''/\partial\nu)_{max}$ plotted against the radio-frequency voltage across the coil for the ^{115}In resonance in a pure sample at both 290°K and 90°K. The spin-lattice relaxation time for this sample, deduced from the saturation curves, is of the order of 10^{-2} sec at 290°K and 0·16 sec at 90°K. This comparatively short value of T_1 at room temperature suggests that the relaxation mechanism probably involves

quadrupolar coupling of the nuclei to the lattice vibrations (Pound 1950). Also shown are experimental points for a doped sample containing 10^{19} Te atoms cm^{-3} at 90°K, the signal-to-noise ratio for this sample being too poor for saturation measurements to be made at room temperature. Although the scatter of the points relating to the doped sample is considerable, there is clearly no significant difference between the low temperature relaxation times in the pure and impure samples. Furthermore, a relaxation time of 10^{-2} sec or more is much too long to explain the observed broadening.

The second class of broadening mechanisms comprises those which modify the field at the position of the nuclei. One obvious explanation is that the tellurium may give rise to paramagnetic defects which produce strong local magnetic fields. However, the tellurium atoms enter the InSb

Fig. 3

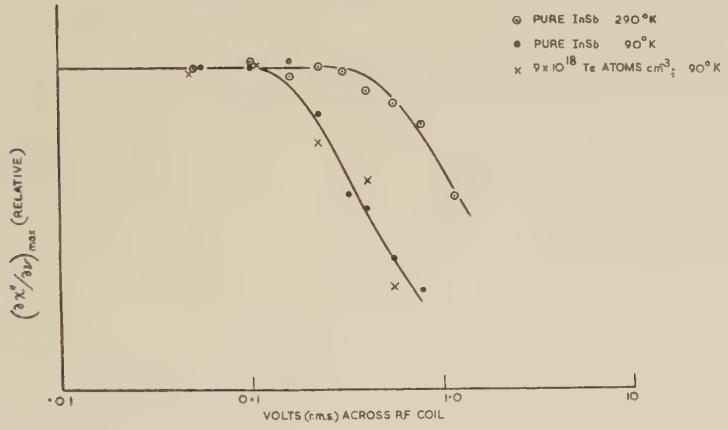

Saturation curves of ^{115}In resonance in pure and Te-doped InSb.

lattice as Te$^+$ ions, since there is one conduction electron per donor, and there is considerable evidence that they take the place of Sb atoms, the surplus Sb atoms segregating at grain boundaries. Since a Te$^+$ ion is isoelectronic with the Sb atom it replaces, one would expect no unpaired electrons and therefore no paramagnetic centres. To check this, a search for paramagnetic resonance in a sample with 10^{19} Te atoms cm^{-3} was kindly made by Dr. E. E. Schneider, of King's College, Newcastle, using a high sensitivity spectrometer. No resonance was observed, and from the known sensitivity of the spectrometer it is possible to say that, if paramagnetic defects were present, the paramagnetic resonance line width was more than 500 gauss. Another possible explanation is that the conduction electrons freed from the Te atoms may increase the constant A_{12} of § 3 and so broaden the resonance. In the case of indium antimonide with 10^{19} electrons cm^{-3} the degeneracy is so high that we may apply the theory

developed by Ruderman and Kittel (1954) for the case of metals. According to their calculation the contribution of the conduction electrons should be negligible in this case; moreover the pronounced departure from Gaussian shape suggests that this mechanism is not the one responsible for the observed broadening. A third possible broadening mechanism which belongs to this category differs from the preceding ones in that it involves an electric rather than a magnetic interaction, namely, the interaction of the nuclear quadrupole moment with the Coulomb field of the Te^{+} ion. Since both the magnitude of **grad·E** and the direction of its symmetry axis vary from nucleus to nucleus, the satellites become smeared into a continuous band, as mentioned in § 3 in connection with the possible role of dislocations. This is believed to be the mechanism responsible for the observed broadening.

According to the explanation given above, the maximum effect that quadrupole interactions can have is the complete obliteration of the satellites, the central component remaining unaltered. This is true as long as the quadrupolar perturbation is treated only to first order; if the second order perturbation is considered, it is found that the central component is also broadened. For $I = 9/2$, the central component contributes $25/165 = 0{\cdot}15$ of the total intensity in an unstrained crystal, and since fig. 2 shows that with 9×10^{18} Te atoms cm^{-3} the maximum value of $\partial\chi''/\partial\nu$ falls to 7% of the value for the pure material, it is evident that second order effects must be contributing. Figure 2 can now be interpreted as follows. The initial rapid fall in intensity with Te concentration is due to first order broadening of the satellites, while the subsequent slow decrease, which extrapolates smoothly to the value 0·15 at zero concentration, is due to second order broadening of the central component. According to theory, the second order perturbation should lead to an asymmetric line, but there was no clear evidence of asymmetry in the line shape of the most heavily doped sample, although the signal-to-noise ratio was too poor to allow any definite conclusion to be drawn. The maximum value of the derivative is apparently a more sensitive function of impurity content than is the asymmetry.

This explanation in terms of quadrupole interactions implies that ionized acceptors should have the same effect as donors, since reversing the sign of **grad·E** merely makes a particular satellite change places with its mirror image. The table gives a comparison between p-type samples obtained by doping with zinc and the n-type samples doped with tellurium. The slightly larger intensity in the p-type specimens can be explained by the partial screening of the charged ions by the carriers. The theory of this screening has been given by Mott and Jones (1936) for metals and extended to the case of semiconductors by Mansfield (1956). According to Mansfield, the potential due to the screened Coulomb field of an ion is

$$V(r) = (e/\epsilon r)\exp(-qr),$$

where $q^2 = 16\pi^2 e^2 (2m^*)^{3/2} \sqrt{(kT)} F'_{1/2}(\eta)/\epsilon h^3$. Here m^* is the effective mass

of the carriers, ϵ the dielectric constant, and $F_{1/2}(\eta) = F_{1/2}(\zeta/kT)$ is the usual Fermi–Dirac integral. The field gradient at a distance r from the ion now becomes (see Cohen and Reif 1957)

$$\frac{\partial^2 V}{\partial r^2} = \frac{2e}{\epsilon r^3} \exp(-qr)\{1 + qr + \tfrac{1}{3}q^2r^2\}. \quad . \quad . \quad . \quad . \quad (1)$$

With 10^{19} carriers cm $^{-3}$ in InSb, q has the value $1{\cdot}5 \times 10^6$ cm $^{-1}$ for electrons ($m^* = 0{\cdot}02m_e$) and $4{\cdot}2 \times 10^6$ cm $^{-1}$ for holes ($m^* = 0{\cdot}2m_e$). With 10^{19} impurity atoms cm^{-3}, the maximum distance which any nucleus can be from an ionized atom is about 50 Å. Using this value of r, the term in eqn. (1) arising from the screening amounts to 0·92 for electrons and 0·56 for holes. The effect of screening is therefore almost negligible for n-type material with 10^{19} electrons cm $^{-3}$, but in the case of the p-type specimen the screening reduces the field gradient by an amount which is of the right order to explain the difference between the resonance intensities in the two cases. For 10^{18} carriers cm $^{-3}$, q is $1{\cdot}95 \times 10^6$ cm^{-1} for holes

Sample	Relative intensity
Intrinsic (single crystal)	1·00
n-type ($n_d = 10^{18}$ cm^{-3})	$0{\cdot}23 \pm 0{\cdot}01$
p-type ($n_a = 10^{18}$ cm^{-3})	$0{\cdot}25 \pm 0{\cdot}01$
n-type ($n_d = 10^{19}$ cm^{-3})	$0{\cdot}07_3 \pm 0{\cdot}005$
p-type ($n_a = 10^{19}$ cm^{-3})	$0{\cdot}13_0 \pm 0{\cdot}008$
compensated $\begin{cases} n_d + n_a = 10^{19} \text{ cm}^{-3} \\ n_d - n_a = 2 \times 10^{18} \text{ cm}^{-3} \end{cases}$	$0{\cdot}07_5 \pm 0{\cdot}005$

and 7×10^5 cm^{-1} for electrons, so the effect of screening is very small in both cases. For a partially compensated specimen with

$$n_d + n_a = 10^{19} \text{ cm}^{-3} \text{ and } n_d - n_a = 2 \times 10^{18} \text{ cm}^{-3}$$

the amplitude of the resonance is indistinguishable from that with $n_d = 10^{19}$ cm^{-3}, since the screening is negligible and the number of ions is the same in both cases.

While this explanation in terms of the interaction of the quadrupole moment of the nucleus with the screened Coulomb field of the ions gives a good qualitative interpretation of the data, the quantitative agreement is more speculative. First order perturbation theory shows that the change in frequency of the $m \longleftrightarrow m-1$ satellite due to a charge e at a point (r, θ) relative to the nucleus is given by

$$\Delta\nu = \frac{3eQ(2m-1)}{4I(2I-1)h} \cdot \frac{\partial^2 V}{\partial z^2}$$

$$= \frac{3eQ(2m-1)}{4I(2I-1)h} \cdot \frac{\beta e(3\cos^2\theta - 1)}{r^3} \quad . \quad . \quad . \quad . \quad . \quad . \quad (2)$$

where I is the nuclear spin, Q its quadrupole moment, and the direction of the magnetic field is taken as z axis (Pound 1950). Within a solid, the field gradient will be modified due to polarization effects, and we allow for this by incorporating in the right-hand side of eqn. (2) an empirical multiplicative constant β (strictly speaking a tensor). To calculate the shape of the broadened line it would be necessary to find the distribution of values of $\Delta\nu$ for different nuclei resulting from a random distribution of impurity atoms. This is an exceedingly complex problem, and it is simpler to calculate the second moment of the resonance line†. From eqn. (2) it is possible to show that, neglecting lattice structure and assuming a perfectly random distribution of impurities, the broadening of the resonance absorption due to first order quadrupole interactions with charged impurities gives rise to a second moment

$$\overline{(\Delta\nu)^2} = \frac{3\pi}{5} \cdot \frac{\beta^2 e^4 Q^2 (2m-1)^2}{I^2(2I-1)^2 h^2} \cdot \frac{N}{r_c^3} \quad . \quad . \quad . \quad . \quad . \quad (3)$$

where N is the impurity concentration, and the effect on a given nucleus of impurities lying within a distance r_c of that nucleus is neglected‡. The use of this cut-off radius is necessary to prevent the second moment diverging; its introduction is also physically plausible since the lattice structure and ionic size set a lower limit to the distance between an impurity atom and a nucleus. In practice, however, r_c is determined by other considerations. As the line shape in the doped sample approaches a Lorentzian form, the second moment converges more and more slowly since the contribution from the wings becomes increasingly important. As the wings eventually become lost in noise, it is impossible to measure the second moment of the entire curve, and one is driven to the expedient of a cut-off frequency $(\Delta\nu)_c$. The simplest procedure is therefore to determine $(\Delta\nu)_c$ experimentally as that frequency beyond which the signal-to-noise ratio is too poor for accurate measurement, and then to find r_c by substituting this value of $(\Delta\nu)_c$ in eqn. (2) with the angular factor set equal to unity. (This slightly overestimates r_c since, on account of the angular term, some impurities less than r_c from a given nucleus will still give $\Delta\nu < (\Delta\nu)_c$.)

---

† An exhaustive treatment of the effect on the line shape of quadrupolar broadening by point defects is given by Cohen and Reif (1957), who show that for small concentrations of defects the contribution to the line shape from a given pair of satellites becomes Lorentzian. Since the central component is unaltered, the line shape in this particular case should be a superposition of one Gaussian and four different Lorentzian curves. The author is indebted to Professor Cohen for letting him see the manuscript of this paper in advance of publication.

‡ This expression can be obtained using an approximate method due to Bloembergen (1955) if one writes β for Bloembergen's $(1 + |\gamma_\infty|)$ and corrects a numerical error in his expression for $\overline{(\Delta\nu)^2}$. It can be obtained more rigorously by a method similar to that used by Reif (1955) to treat second order broadening.

In this way we find

$$\left[\overline{(\Delta\nu)^2}\right]_0^{(\Delta\nu)_c} = \frac{4\pi N}{5}\cdot\frac{e^2Q\beta(2m-1)}{I(2I-1)h}\cdot(\Delta\nu)_c \quad . \quad . \quad . \quad . \quad (4)$$

This equation applies only to the contribution from the $m \leftrightarrow m-1$ satellite, which has an asymmetric line shape. If we consider the contributions from the $m \leftrightarrow m-1$ and $-m \leftrightarrow -(m-1)$ satellites together, the resulting line shape is symmetric and has a second moment given by eqn. (4). We may use this expression for $\overline{(\Delta\nu)^2}$ to include all satellites by taking $+5/2$ as a mean value for m. Figure 1 shows that the line shape for the sample with 9×10^{17} Te atoms cm^{-3} approximates quite closely to the derivative of the Lorentzian curve $g(\Delta\nu)\propto[(9{\cdot}6\text{ kc/s})^2+(\Delta\nu)^2]^{-1}$ up to $\Delta\nu=30$ kc/s. Assuming this analytical form for the curve, we find $\left[\overline{(\Delta\nu)^2}\right]_0^{30\text{ kc/s}}=137\,(\text{kc/s})^2$. The Gaussian line shape in the pure material has $\overline{(\Delta\nu)^2}=29(\text{kc/s})^2$, so the quadrupolar contribution to $\left[\overline{(\Delta\nu)^2}\right]_0^{30\text{ kc/s}}$ is $108\,(\text{kc/s})^2$. Substituting this in eqn. (4) with $(\Delta\nu)_c=30$ kc/s and $Q=1{\cdot}16\times10^{-24}$ cm^2, we find $\beta=350$.

To interpret this large value of β we write it in the form $\beta=\beta_\epsilon\beta_0$, following Reif (1955), where β_ϵ and β_0 have the following significance. Let us imagine a spherical hole in the InSb crystal formed by removing one indium atom. We consider the field gradient at the centre of this sphere and suppose it to be given by $2\beta_\epsilon e/r^3$, so that β_ϵ describes the effect of the polarization of the surrounding medium. We then replace the indium atom and consider the effect of the distortion of its own electron cloud on the field gradient at the nucleus, supposing this to be equivalent to multiplication by the factor β_0. This is admittedly a rather artificial procedure, since indium antimonide is a predominantly covalently bound compound, and the concept of a sphere with a complete atom inside and the others outside lacks realism, but it should at least serve as a rough model sufficiently exact to assess orders of magnitude. If the polarization of the surrounding medium produces an internal field of the Lorentz type, so that $E_{\text{eff}}=E+4\pi P/3$, then $\beta_\epsilon=(\epsilon+2)/3\epsilon\simeq\frac{1}{3}$, since $\epsilon=16$. On the other hand, if the internal field is of the Drude type, as in the case of ionic crystals where there is considerable overlap of the ions (Mott and Gurney 1948), then $E_{\text{eff}}=E$ and $\beta_\epsilon=1/\epsilon$. The correct value of β_ϵ will lie somewhere between these two extremes, but we will take $\beta_\epsilon=\frac{1}{3}$ since this demands a lower value of β_0, namely, $\beta_0\simeq1000$†.

It is well known that in diatomic polar molecules the interaction of the quadrupole moment of either nucleus with the electric field is much greater than that arising from a field gradient $2e/r_0^3$, where r_0 is the internuclear distance. This has been attributed to the distortion of the closed electron shells, which under certain conditions may have an ' anti-shielding ' effect.

---

† By using a more refined argument, Cohen and Reif (1957) arrive at the result $\beta_\epsilon=(2\epsilon+3)/5\epsilon$, which is slightly higher than the value adopted here. In view of the roughness of the approximation, it makes little difference which of the two expressions is used.

The anti-shielding factor, which we may indentify with β_0, has been calculated for ions having the inert gas configuration by Foley *et al.* (1954). Interpolating between their results for Rb^+ and Cs^+, we may estimate $\beta_0 \simeq 70$ for Ag^+, which is isoelectronic with In^{3+}. The value of β_0 for In^{3+} will probably be lower because, having a larger nuclear charge, In^{3+} is more tightly bound. It seems, therefore, that the distortion of the indium core electrons is much too small to explain the large value of β_0 required to fit the experiments. This suggests that the effect may be due to distortion of the valence electron distribution, and that this should be so is not surprising if one considers how the distortion arises. The electron distribution around the In nucleus can be distorted only by mixing with the unperturbed wave function new wave functions corresponding to excited states. The extent to which these perturbing wave functions are admixed depends, among other things, on the energy difference between the initial state and the excited states involved. In the case of the In^{3+} core, the lowest excited state above the full N-shell is the $5s$ state, which is more than 10 ev higher. However, in the case of the In atom in InSb, the energy difference between the top of the valence band and the lowest unoccupied state is only of the order of the forbidden gap, i.e. about 0·18 ev. We might therefore expect the valence electrons to be much more easily distorted than the core, and it is significant that the quadrupolar part of the hyperfine interaction in the $(5s)^2 5p\ ^2P_{3\,2}$ state of the free indium atom corresponds to a value of $(3eQ\partial^2 V/\partial z^2)/4I(2I-1)h$ of 37 mc/s (Mann and Kusch 1950), so that we need a distortion equivalent to the addition of only 0·1% of a $5p$ orbital to give a first-order broadening of about 30 kc/s in solid indium antimonide.

If these ideas are correct, we should attribute the very large value of β_0 in indium antimonide, as compared with polar molecules and ionic crystals, to the smallness of the forbidden gap. This implies that there should be some correlation between the value of β_0 and the inverse of the gap width, rather like the relation between ϵ and E_g suggested by Briggs *et al.* (1954). Some preliminary experiments carried out in this laboratory on indium arsenide, which has an energy gap of 0·34 ev, show that the ^{115}In resonance is affected by impurities in much the same way as in indium antimonide, but that the value of β_0 is smaller, which is consistent with the above hypothesis.

§ 6. The Effect of Neutral Impurities

The decrease in intensity of the ^{115}In nuclear resonance on doping with tellurium or zinc has been attributed to the effect of the Coulomb field of the charged ions. An obvious method of verifying this hypothesis would be to neutralize the ions by lowering the temperature. Unfortunately this is not practicable in indium antimonide, which has zero activation energy for ionization of donors, and an activation energy for acceptors which is zero except at liquid helium temperatures. An alternative approach is to dope the material with impurities belonging to the same

group as one of the constituents, which would be electrically neutral. Through the kind cooperation of Dr. J. C. Woolley, of Nottingham University, the ^{115}In resonance has been observed in a series of mixed crystals of indium antimonide diluted with gallium antimonide. These compounds are isomorphous, and combine to form a single phase over the entire range of compositions, providing the annealing time is long enough (Woolley *et al.* 1956). Figure 4 shows that the effect of a small concentration of GaSb on the ^{115}In resonance at room temperature is similar to that of Te atoms,

Fig. 4

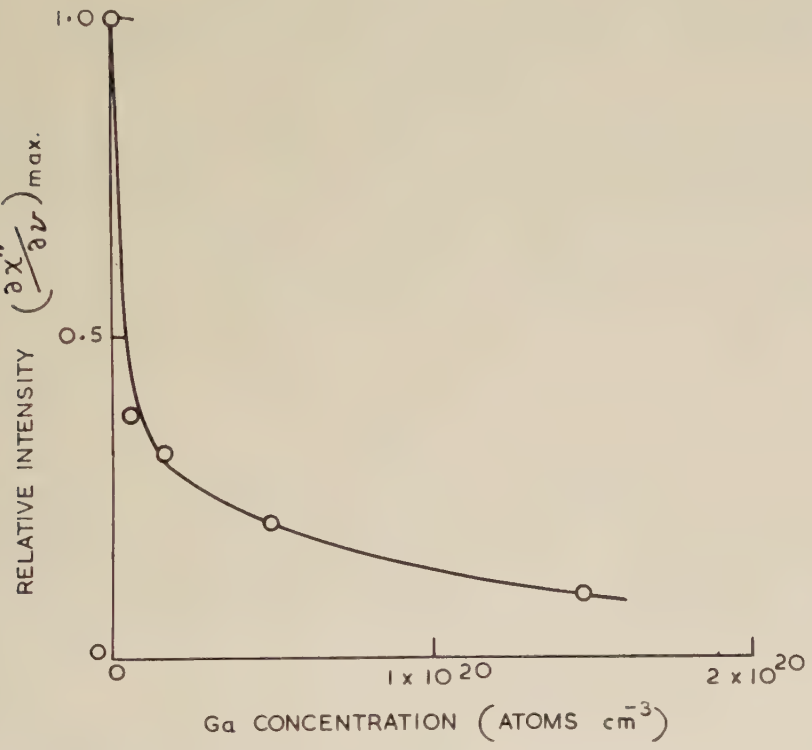

Variation with Ga concentration of derivative of ^{115}In resonance in InSb–GaSb mixed crystal (290°K).

except that for a given reduction in intensity the Ga concentration has to be about thirty times greater than that of the Te. This large difference confirms the view that the effect of the Te atoms arises almost entirely from the charge of the Te^+ ion. The much smaller effect of the gallium can be attributed to strain in the InSb lattice in the neighbourhood of a Ga atom. The distance between nearest neighbours is 2·80 Å in InSb and 2·65 Å in GaSb, so if we assume that the length of the Ga–Sb bonds associated with an isolated Ga atom which is substituted for In in the InSb

lattice tends to be the same as the Ga–Sb distance in pure GaSb, then the InSb lattice around the Ga atom must be in a state of tension. This strain destroys the tetrahedral symmetry of the perfect lattice and gives rise to quadrupolar broadening. Although detailed studies of the line shapes in the GaSb–InSb mixed crystals have not been made, a rough order of magnitude interpretation of the results may be made as follows. If the material within a sphere of radius a_1 in an isotropic elastic medium is contracted to radius a_2, then the strain at a distance r from this defect is a pure radial one whose magnitude is given by ordinary elasticity theory as

$$-\Delta r/r = [(a_1 - a_2)/a_1] \times (a_1/r)^3.$$

At some distance from a Ga atom, we may apply this continuum model and assume the radial strain to be given by this formula with

$$a_1 - a_2 = (2{\cdot}80 - 2{\cdot}65)\ \text{Å},$$

and a_1 equal to the ' tetrahedral covalent radius ' of a Ga atom, which according to Pauling (1940) has the value 1·26 Å. The relation between the field gradient and the strain at a given point in the lattice is a tensor one which has been studied experimentally for the case of InSb by Shulman *et al.* (1957). These authors find a relation between the diagonal components of the field gradient and stress tensors of the form

$$\partial^2 V/\partial x^2 = C_{11}[X_{xx} - \tfrac{1}{2}(X_{yy} + X_{zz})]$$

(and cyclic permutations), where x, y, and z lie along the cubic axes, X is the usual stress tensor, and C_{11} is a ' gradient-elastic ' constant having the value $\pm 2{\cdot}4 \times 10^4$ e.s.u./dyne. We may write this in a form involving the strain rather than the stress as follows :

$$\partial^2 V/\partial x^2 = C_{11}(c_{11} - c_{12})[e_{xx} - \tfrac{1}{2}(e_{yy} + e_{zz})] \quad . \quad . \quad . \quad . \quad (5)$$

Here c_{11} and c_{12} are the usual elastic constants which have been measured for InSb by Potter (1956), and e is the strain tensor. For a pure radial strain of the form $\Delta r/r = k/r^3$, one can show $e_{xx} = k(r^2 - 3x^2)/r^5$, etc. If we suppose the magnetic field to coincide with one of the cube axes and call this the z-axis, then we finally obtain

$$\partial^2 V/\partial z^2 = 3kC_{11}(c_{11} - c_{12})(1 - 3\cos^2\theta)/2r^3 \quad . \quad . \quad . \quad . \quad (6)$$

This has the same dependence on r and θ as the field gradient due to a point charge, $\beta e(3\cos^2\theta - 1)/r^3$, which was used in eqn. (2). We may therefore use eqn. (4) for the case of strain by substituting $3kC_{11}(c_{11} - c_{12})/2$ for βe. Using Potter's values for c_{11} and c_{12} and the above mentioned values of k and C_{11}, we find $3kC_{11}(c_{11} - c_{12})/2 = \pm 2{\cdot}75 \times 10^{-9}$ e.s.u., which is equivalent to a value of β of 6. In the absence of a detailed knowledge of the line shape, the second moment cannot be estimated, but we may note that eqn. (4) involves β and the concentration of defects N only through the product βN. We have seen from the results with the Te-doped samples that the charge effect demands a value of β of 350. Since the strain effect is equivalent to a value of β of 6, we might expect that, if the line shapes are roughly the same in two the cases, we should require a concentration

of Ga atoms about 60 times that of the Te atoms for the same effect on the nuclear resonance intensity. This compares reasonably well with the factor of about 30 which is obtained by comparing figs. 2 and 4. The assumption that the magnetic field is parallel to one of the cubic axes implies the use of a single crystal ; in fact, the material was polycrystalline, but it is unlikely that this will materially affect the broad conclusions of this analysis.

The conclusion that the broadening produced by Ga atoms is attributable to strain has relevance to the interpretation of the tellurium experiments, since the Te atoms must also produce some strain in the lattice, and it is important to know the relative magnitude of the strain and charge effects. In In_2Te_3, which is a ' deficit ' semiconductor with the zinc-blende structure having one third of the In sites vacant (Welker 1954), the In–Te distance is 2·66 Å, which is almost indistinguishable from the Ga–Sb distance of 2·65 Å in GaSb. If we assume that the In–Te bond length in Te-doped InSb is approximately the same as the distance between nearest neighbours in In_2Te_3, then the strain caused by the substitution of a Te^+ ion for an Sb atom in InSb should have a broadening effect comparable with that of a Ga atom, which we have seen to be about two orders of magnitude less than the observed effect of the Te atoms. We can therefore say fairly confidently that the effect of the Te^+ (and Zn^-) ions must be due to their charge.

§ 7. Conclusion

The aims of this research were twofold. The object of the search for a possible Knight shift was to investigate the *s*- or *p*-character of the electron and hole wave functions. The results are consistent with the hole wave functions being predominantly *p*-like, but in the case of n-type samples, the results are ambiguous because of the small effective mass of the electrons.

The motive for studying the dependence of nuclear resonance intensity on impurity concentration was the hope that the results might be interpretable in the simple way which Bloembergen and Rowland (1953) used to explain their results on the Cu resonance in α-brass. In the case of a metal, the Coulomb field of an impurity is rapidly damped out by the screening of the conduction electrons, and the crystalline field is only modified in the immediate vicinity of the impurity atom. Bloembergen and Rowland found that their results could be explained by assuming the existence of a critical radius around a Cu nucleus such that, if there is a Zn atom inside this radius, the quadrupolar interaction is so large as to obliterate the contribution of that nucleus, whereas, if there is no Zn atom inside this radius, the resonance of the Cu nucleus is unmodified. In this way they showed that the extra electron on a Zn atom is shared with a Cu atom in the 18 nearest and next-nearest neighbour positions. A similar result is possible in insulators if the interaction is so weak that it is appreciable only in the immediate vicinity of an impurity,

in which case the r^{-3} variation (or r^{-6} in the case of the second order interaction) may allow discrimination between nearest and next-nearest neighbour positions (Kawamura *et al.* 1956). The initial hope was that a similar situation might arise in InSb, i.e. that the quadrupolar interaction would be appreciable only for nuclei in the immediate vicinity of a defect, and that in this way it might be possible to prove, for instance, whether the impurities enter the lattice substitutionally or not. Unfortunately, the large value of β in InSb makes the interaction appreciable even at points more than 50 Å from the impurity, and at these large distances the lattice structure ceases to play a significant part. Paradoxically, nuclear resonance in InSb is too sensitive to the presence of imperfections to be helpful in studying the immediate vicinity of a defect, and the usefulness of nuclear resonance in this respect tends to be restricted to those materials which have much smaller values of β and Q. With this in mind, it is proposed to make a brief investigation of the applicability of the technique to other intermetallic semiconductors, especially those having higher energy gaps.

Acknowledgments

The author wishes to express his indebtedness to Dr. J. C. Woolley for providing the InSb–GaSb mixed crystals, and to Dr. E. E. Schneider for carrying out the paramagnetic resonance experiment. Acknowledgment is made to the Admiralty for permission to publish this paper.

References

Allen, J. W., 1957, *Phil. Mag.* **2,** 1475.

Bloembergen, N., 1952, *J. appl. Phys.*, **23,** 1383 ; 1955, *Report of the Bristol Conference on Defects in Crystalline Solids* (London : Physical Society), p. 1.

Bloembergen, N., and Rowland, T. J., 1953, *Acta Metallurgica*, **1,** 731 ; 1955, *Phys. Rev.*, **97,** 1679.

Briggs, H. B., Cummings, R. F., Hrostowski, H. J., and Tannenbaum, M., 1954, *Phys. Rev.*, **93,** 912.

Campbell, J. S., and Davis, J. R., 1939, *Phys. Rev.*, **55,** 1125.

Chapman, A. C., Rhodes, P., and Seymour, E. F. W., 1957, *Proc. phys. Soc. Lond.* B, **70,** 345.

Cohen, M. H., and Reif, F., 1957, *Solid State Physics*, Vol. 5 (New York : Academic Press), p. 321.

Eisen, F. H., and Birchenall, C. E., 1957, *Acta Metallurgica*, **5,** 265.

Foley, H. M., Sternheimer, R. M., and Tycko, D., 1954, *Phys. Rev.*, **93,** 734.

Gutowsky, H. S., Meyer, L. H., and McClure, R. E., 1953, *Rev. sci. Instrum.*, **24,** 644.

Kawamura, H., Otsuka, E., and Ishiwatari, K., 1956, *J. phys. Soc., Japan*, **11,** 1064.

Knight, W. D., 1949, *Phys. Rev.*, **76,** 1259.

Mann, A. K., and Kusch, P., 1950, *Phys. Rev.*, **77,** 427.

Mansfield, R., 1956, *Proc. phys. Soc. Lond.* B, **69,** 76.

McGarvey, B. R., and Gutowsky, H. S., 1953, *J. chem. Phys.*, **21,** 2114.

Mitchell, A. H., 1957, *J. chem. Phys.*, **26,** 1714.

Mott, N. F., and Gurney, R. W., 1948, *Electronic Processes in Ionic Crystals* (Oxford : University Press), p. 15.

Mott, N. F., and Jones, H., 1936, *Properties of Metals and Alloys* (Oxford: University Press), p. 86.
Pauling, L., 1940, *The Nature of the Chemical Bond* (Oxford: University Press), p. 179.
Potter, R. F., 1956, *Phys. Rev.*, **103**, 47.
Pound, R. V., 1950, *Phys. Rev.*, **79**, 685; 1952, *Prog. nucl. Phys.*, **2**, 21.
Reif, F., 1955, *Phys. Rev.*, **100**, 1597.
Rhoderick, E. H., 1956, *Report of the meeting on semiconductors* (London: Physical Society), p. 147; 1957, paper read at Physical Society conference on solid state physics, Nottingham University (unpublished).
Roberts, V., and Quarrington, J. E., 1955, *J. Electronics*, **1**, 152.
Ruderman, M., and Kittel, C., 1954, *Phys. Rev.*, **96**, 99.
Shulman, R. G., Mays, J. M., and McCall, D. W., 1955, *Phys. Rev.*, **100**, 692.
Shulman, R. G., Wyluda, B. J., and Anderson, P. W., 1957, *Phys. Rev.*, **107**, 953.
Slater, J. C., and Koster, G. F., 1954, *Phys. Rev.*, **94**, 1498.
Townes, C. H., Herring, C., and Knight, W. D., 1950, *Phys. Rev.*, **77**, 852.
Watkins, G. D., and Pound, R. V., 1953, *Phys. Rev.*, **89**, 658.
Welker, H., 1954, *Physica*, **20**, 893.
Woolley, J. C., Smith, B. A., and Lees, D. G., 1956, *Proc. phys. Soc. Lond.* B, **69**, 1339.

Nuclear Magnetic Resonance in Impure Indium Antimonide†

By M. H. Cohen
Cavendish Laboratory, University of Cambridge

[Received March 11, 1958]

Abstract

An analysis of Rhoderick's experiments on the nuclear quadrupole broadening of the nuclear magnetic resonance of ^{115}In in impure indium antimonide is carried out which is based on a detailed theory of the line shape. It results in values of 580 for the multiplication factor and 1300 for the Sternheimer antishielding factor of In in InSb.

Rhoderick (1958) has shown that addition of impurities to indium antimonide causes quadrupolar broadening of the ^{115}In nuclear magnetic resonance. In n-type (Te-doped) and p-type (Zn-doped) samples, the broadening arises through interaction of the nuclear quadrupole moment with the gradient of the electrostatic field of the ionized impurity atoms. The broadening is first-order at low concentrations of impurity. In particular, the line is approximately Lorentzian with a half-width of 9·6 kc/s in a sample containing 9×10^{17} atoms per cm^3, a concentration at which screening effects are unimportant. From this result, Rhoderick has estimated that the multiplication factor β is approximately 350 for In in InSb. The estimate is based on an approximate calculation of the second-moment of the resonance line. We give here an independent estimate of β based on a detailed theory of the line shape (Cohen and Reif 1957).

If the resonance line were sharp in the pure crystal, the shape of the component arising from transitions $m\longleftrightarrow m-1$, $m\neq\frac{1}{2}$, in the impure crystal would be Lorentzian with half-width Γ_m,

$$\Gamma_m=|2m-1|\frac{2\pi^2}{3\sqrt{3}}\frac{N\beta e^2Q}{I(2I-1)h} \quad . \quad . \quad . \quad . \quad . \quad . \quad (1)$$

where N is the number of impurity atoms per unit volume. The resonance line is actually broadened by indirect exchange in the pure crystal (Shulman *et al.* 1955) so that the (normalized) intensity per unit frequency interval is

$$g_m(\nu)=\frac{1}{\pi}\int_{-\infty}^{\infty}\frac{\Gamma_m}{\Gamma_m{}^2+\nu'^2}f_m(\nu-\nu')\,d\nu' \quad . \quad . \quad . \quad . \quad . \quad (2)$$

in the impure crystal if it is $f_m(\nu)$ in the pure crystal. The frequency ν is measured from the centre of the line. If Γ_m is larger than the line width in the pure crystal, eqn. (2) becomes

$$g_m(\nu)=\frac{1}{\pi}\frac{\Gamma_m}{\Gamma_m{}^2+\nu^2}+\tfrac{1}{2}\sigma_m{}^2\frac{d^2}{d\nu^2}\frac{1}{\pi}\frac{\Gamma_m}{\Gamma_m{}^2+\nu^2}+\ldots \quad . \quad . \quad . \quad (3)$$

† Communicated by the Author. Guggenheim Fellow, 1957–1958, on leave from Institute for the Study of Metals, University of Chicago.

where $\sigma_m{}^2$ is the second moment of $f_m(\nu)$. At frequencies such that ν^2 is greater than $\Gamma_m{}^2$, $g_m(\nu)$ becomes

$$g_m(\nu)=\frac{\Gamma_m}{\pi\nu^2}\left(1-\frac{\Gamma_m{}^2-3\sigma_m{}^2}{\nu^2}+\ldots\right). \quad . \quad . \quad . \quad . \quad (4)$$

In the wings of the resonance line, where the central component does not contribute, the line is a superposition of these components, each weighted according to its relative intensity $I(I+1)-m(m-1)$. The total (normalized) intensity per unit frequency interval is

$$g(\nu)=\sum_{m\neq\frac{1}{2}} p_m g_m(\nu), \quad . \quad . \quad . \quad . \quad . \quad . \quad . \quad . \quad (5)$$

where p_m is the weight of the mth component and $g_m(\nu)$ is given by eqn. (4). Combining eqns. (4) and (5) we obtain

$$g(\nu)=\frac{\overline{\Gamma}}{\pi\nu^2}-\frac{1}{\pi\nu^4}\sum_{m\neq\frac{1}{2}} p_m\Gamma_m(\Gamma_m{}^2-3\sigma_m{}^2), \quad . \quad . \quad . \quad . \quad (6)$$

where $\overline{\Gamma}$ is obtained by replacing the $|2m-1|$ in Γ_m by $\overline{|2m-1|}$,

$$\overline{|2m-1|}=\sum_{m\neq\frac{1}{2}} p_m|2m-1|. \quad . \quad . \quad . \quad . \quad . \quad . \quad (7)$$

The spin of ^{115}In is 9/2, for which $\overline{|2m-1|}$ is 4·28. This corresponds to an 'average' value of m of 2·64, which is close to the value of 5/2 assumed by Rhoderick.

The wings of the line are indistinguishable from those of a single Lorentzian of half-width $\overline{\Gamma}$ if we neglect the second term in (6). The value of the half-width of a Lorentzian giving a good *overall* fit to the line shapes for the Te-doped ($N=9\times10^{17}$) sample is 9·6 kc/s. Inspection of Rhoderick's fig. 1 suggests that $\overline{\Gamma}$ is actually somewhat less than 9·6 kc/s. We therefore obtain a value of 580, or perhaps somewhat less, for β. The correction term in (6) may be estimated by using the approximation

$$g(\nu)=\frac{\overline{\Gamma}}{\pi\nu^2}\left(1-\frac{\overline{\Gamma}^2-3\sigma^2}{\nu^2}\right) \quad . \quad . \quad . \quad . \quad . \quad . \quad . \quad (8)$$

where σ^2 is the second moment in the pure crystal. The correction is small when eqn. (6) is valid.

The multiplication factor can be decomposed by means of the approximation

$$\beta=(1+\gamma)[(2\epsilon+3)/5\epsilon] \quad . \quad . \quad . \quad . \quad . \quad . \quad . \quad (9)$$

where $1+\gamma$ is the Sternheimer antishielding factor (Foley *et al.* 1954, Cohen and Reif 1957), the remaining factor is the polarization correction (Cohen and Reif 1957), and ϵ is the dielectric constant. The polarization correction is 0·437 for InSb for which $\epsilon=16$. Rhoderick's estimate of β yields $1+\gamma\simeq800$; the present estimates yields $1+\gamma\gtrsim1300$. This difference in $1+\gamma$ is probably within the error of eqn. (9), which is based on a highly idealized model more suitable to ionic crystals than to semiconductors.

Acknowledgment

I am grateful to Dr. Rhoderick for permission to use his results before their publication.

References

Cohen, M. H., and Reif, F., 1957, *Solid State Physics*, **5**, 321.
Foley, H. M., Sternheimer, R. M., and Tycko, D., 1954, *Phys. Rev.*, **93**, 734.
Rhoderick, E. H., 1958, *Phil. Mag.*, **3**, 545.
Shulman, R. G., Mays, J. M., and McCall, D. W., 1955, *Phys. Rev.*, **100**, 692.

The Giant Photonuclear Resonance in the Rare Earth Region†

By D. H. Wilkinson
Clarendon Laboratory, Oxford

[Received March 24, 1958]

Abstract

The giant resonances of nuclear photodisintegration show a strong correlation between their width and the distance from doubly closed shells. In particular the width becomes very great in the rare earth region of large permanent nuclear deformations. It is shown, with the aid of the Nilsson level schemes for a deformed harmonic oscillator potential, that the independent particle model of the giant resonance is capable of providing a quantitative explanation of this broadening.

§ 1. Introduction

Two apparently conflicting models seek to explain the phenomena associated with the giant resonance of nuclear photodisintegration. The first is the collective model (Goldhaber and Teller 1948, Jensen and Jensen 1950, Danos 1952) in which the resonance is pictured due to a bulk oscillation of all the protons of the nucleus against all the neutrons. The second model ascribes the resonance to excitations of individual nucleons within the general framework of the shell and optical models (Wilkinson 1954, 1956, Rand 1957).

Many of the predictions of these opposed models are surprisingly similar: this is true of the energy of the resonance and its trend with atomic weight and of the strength of absorption in the resonance. The independent particle model has enjoyed certain specific successes, notably its satisfactory treatment of the anomalous emission of fast protons by heavy nuclei. This success stems from the fact that it is a much more detailed model from the point of view of nuclear structure and so may be immediately applied to any phenomenon in which the behaviour of single nucleons is of importance. It is not clear that the collective model could not be broken down so as to enable one to form a picture of the behaviour of the individual nucleons. Equally it is not clear how this could or should be done and it certainly seems at first sight that the conceptual basis of that model, totally different from that of the independent particle model, precludes our concentration of the energy of excitation on a single nucleon such as is necessary to explain the anomalous emission (see however, Brown and Levinger 1958). We might therefore maintain that the phenomenon of proton emission argues in favour of the shell model and

† Communicated by the Author.

against the collective model. Such a judgment would not necessarily be wrong but would be hasty. In fact Brink (1957) has shown that in one extreme case—the pure harmonic oscillator without damping forces—the models are formally identical. He argues that this surprising identity will persist in some form for real nuclei and so, by implication, that it is futile to attempt to distinguish between the models. Be this as it may the confrontation of the models continues and will do so until a full analysis of the relationship has been effected.

An advantage enjoyed by the collective model is that it is always easy to make predictions with it because the motion envisaged is so simple and general. It is doubtful whether any of its important results were unknown to the third Lord Rayleigh. The shell model is relatively slow off the mark because a large amount of computation must precede the getting of any quantitative result. This is of course the price paid for our ability to make detailed predictions.

This note describes a preliminary application of the shell model to an aspect of the experimental situation—the width of the giant resonances —which has recently acquired some topical interest following the first careful giant resonance studies among the rare earths (Petree *et al.* 1957).

§ 2. The Resonance Width

For spherical nuclei the collective model makes no simple prediction about the width of the giant resonance because the width is due to 'frictional' forces which are not included in the model. The shell model can make some prediction because the two chief components of the width for doubly magic nuclei, the spread in energy between the several independent particle transition energies and the smearing in position of each due to the imaginary part of the optical model potential, are both fairly well understood. If the latter effect is set at 3 Mev full width at half maximum the total predicted width for a doubly-magic nucleus is 4–5 Mev (see later for an example) which accords well with experiment.

It has recently been found (*loc. cit.*) that in the region of the rare earths the resonance width becomes very much greater and may even exceed 10 Mev. This is the familiar region where nuclei are permanently deformed into prolate ellipsoids of appreciable eccentricity as is revealed by the rotational structure of their low-lying level schemes and by their greatly enhanced probabilities for E2 transitions (see e.g. Bohr and Mottelson 1953).

The collective model is able to make an immediate and dramatic prediction about the giant resonance in this region: it should split into two. Classically speaking if the neutrons and protons vibrate against each other along a minor axis they would be expected to do so at a higher frequency than along the major axis. This splitting, whose magnitude depends on the particular version of the collective model which is employed, will be seen at least as an increased width to the resonance and possibly even as a separation into two peaks. This has been treated by Okamoto (1958) and

Danos (1956, 1958) and provides a semi-quantitative account of the experimental data although the full width of the resonance is probably not accounted for.

It is clear that qualitatively the same effect is expected from the independent particle model since in the deformed ellipsoidal potential the independent particle levels are split up in the manner first discussed in detail by Nilsson (1955) and so what in the spherical potential is a single transition now becomes several. A glance at the Nilsson diagram shows that the levels in the ellipsoidal potential become completely interlaced at quite modest values of the deformation and so it may be thought that no resonance structure will persist. This however is wrong because in the strongly deformed potential new selection rules arise (Strominger and Rasmussen 1957) which limit the possible transitions.

§ 3. The Deformed Potential

The only way to see what is happening to the independent particle model of the giant resonance is to recompute it for the distorted potential. This is a most laborious and uncertain operation and it is not pretended that the present results have much more than an illustrative significance. However a completely consistent calculation would imply a complete solution of the problem of the distorted nucleus and to this we cannot presently aspire.

For the present purpose we have used Nilsson's results. This is unsatisfactory in that they are based on a harmonic oscillator potential which is unrealistic in such heavy nuclei and it is well known that these level schemes do not give as good an account of the ground state spins in the rare earths as do more realistic potentials. However the Nilsson Hamiltonian contains a spin-orbit term and also a further arbitrary term proportional to l^2 which is made to caricature, for spherical nuclei, the level ordering prescribed by nature. The great advantage of the Nilsson scheme is that it can be made to apply to nuclei of any mass by a suitable adjustment of the fundamental isotropic oscillator spacing. We have therefore used it for this preliminary examination of the distorted nuclei.

An immediate difficulty lies in the choice of the parameters of the model. We may adopt the simple plan of using the same parameters as are suggested in Nilsson's paper and then finally taking that value of the fundamental oscillator spacing that locates the giant resonance at the right absolute energy. In this way the predictions would be unambiguous. This procedure of course involves us in the use of considerably greater values of the oscillator spacing than were envisaged by Nilsson in recommending suitable values for the other parameters. This large oscillator spacing is not in itself objectionable, being associated with the use of the reduced mass (velocity dependent potential) in the calculation of the level positions (Wilkinson 1956). It has in fact been shown by Frahn and Lemmer (1957) that a velocity dependence of the interaction for nucleons moving in a spheroidal harmonic oscillator potential gives a level scheme

that is approximately that of Nilsson. Their numerical estimates of the effective Nilsson parameters for a reduced nucleon mass of 0·5 times the free mass (Brueckner 1955) are close to those originally recommended by Nilsson. Their effective oscillator spacing for these parameters is $82A^{-1/3}$ Mev which is itself close to the value needed to give agreement in absolute position between the experimental and calculated giant resonance energies. This work thus constitutes the justification for our simple procedure of using the Nilsson scheme with a final adjustment of energy scale on account of the velocity dependence of the potential to fit the absolute resonance energy.

It is to be hoped that calculations such as those of Gottfried (1956) for a deformed finite square well will become available over a range of atomic weight and will use both a velocity dependent potential and a radius adjusted to reproduce the experimental density of nuclear matter. The final refinement of a diffuse edge to the nucleus would also be welcome.

§ 4. The Nuclear Deformation

The deformation δ used by Nilsson is related to the intrinsic quadrupole moment Q_0 by:

$$Q_0 \simeq 0{\cdot}8ZR^2\delta(1+\tfrac{2}{3}\delta).$$

Fig. 1

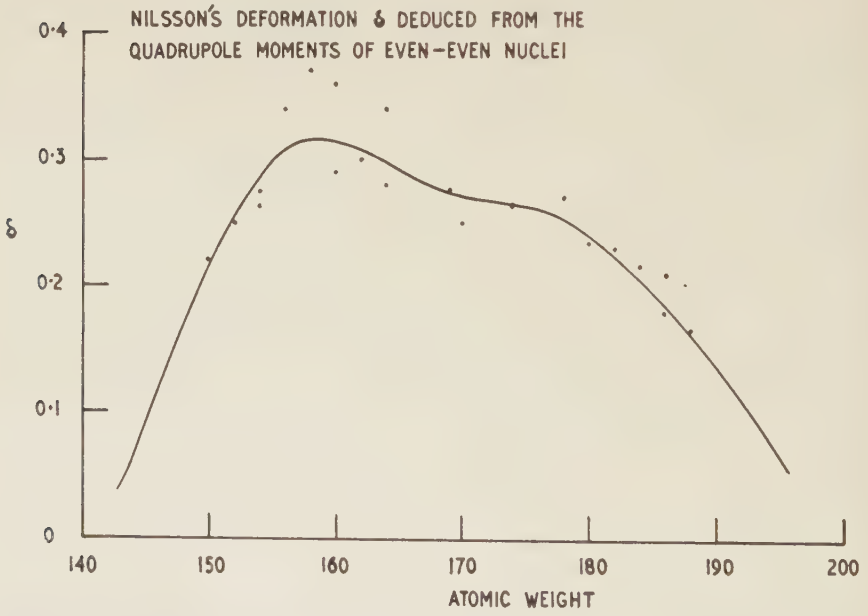

The nuclear deformation δ as defined by Nilsson deduced from the quadrupole moments of even–even nuclei in the rare earth region. The full line represents the trend of δ used for the present computation of the resonance widths.

The values of δ deduced from this expression, and using $R = 1{\cdot}2A^{1/3}$ fermis, are shown in fig. 1. The Q_0 we have taken from a variety of sources for even–even nuclei only (see e.g. Alder *et al.* 1956). Values of δ derived from nuclei of odd mass are in accord with those shown on the figure. The full line of the figure shows the trend of δ with A that we have assumed in the subsequent computations.

§ 5. The Computations

A number of values of A, Z throughout the range shown in fig. 1 were chosen, with their appropriate values of δ, for detailed computation. For each A, Z, δ value the Nilsson diagram was filled with the appropriate number of neutrons and protons and the energies and strengths of the E1 transitions were calculated. In order to limit the complexity of the work only transitions of the parent type $1l \rightarrow 1l+1$ and $2l' \rightarrow 2l'+1$ were considered since they provide the overwhelming bulk of the total E1 absorption strength (Wilkinson 1956).

The energies and strengths of all possible transitions, several dozens for each nucleus, were tabulated and then each transition was smeared into a Gaussian with a full width at half maximum of 3 Mev † to represent the effect of the imaginary part of the optical model potential. The resulting transition strengths were then grouped at equal energy intervals and plotted as shown on figs. 2 to 5. These figures represent deformations $\delta = 0$, 0·1, 0·2, and 0·3 for elements working backwards in mass from Pb to about Ho. The computed points are represented by the bold dots and the line has been put smoothly through them by eye. In order to fit the absolute energies of the experimental resonances we must set one of the arbitrary energy units of these figures equal to about 2 Mev.

The widths are seen to increase with δ in the way qualitatively expected. For $\delta = 0$ the assembly of transitions is remarkably symmetrical and has a width of 4·4 Mev for Pb in complete accord with experiment. As δ increases the resonance broadens and develops an asymmetry on the high energy side which, for $\delta = 0{\cdot}3$, becomes an actual splitting of the resonance into two. This behaviour runs closely parallel to that predicted by the collective model and gives the impression that perhaps here again we have a phenomenon that cannot be used to distinguish between the models. There is a tendency for the transitions in the higher energy peak of fig. 5 to come from the larger values of Ω, the projection on to the nuclear symmetry axis of the individual j of the nucleon in question, while the smaller Ω values are found in the lower peak. This result is qualitatively to be expected and is confirmed by a glance at the Nilsson diagram. High values of Ω correspond classically to orbits lying in the plane of the minor

† Doubtless this should depend on δ and on the levels concerned but we have no data on which to assess such a dependence. It is not necessarily to be expected that the smearing will increase with increasing transition energy since a high *transition* energy does not necessarily imply that the excited nucleon is placed high in the continuum.

axes of the ellipsoid and low values of Ω to nucleon motion in planes at right angles to this. This makes complete the qualitative correspondence with the collective model and suggests that, for example, experiments

Fig. 2

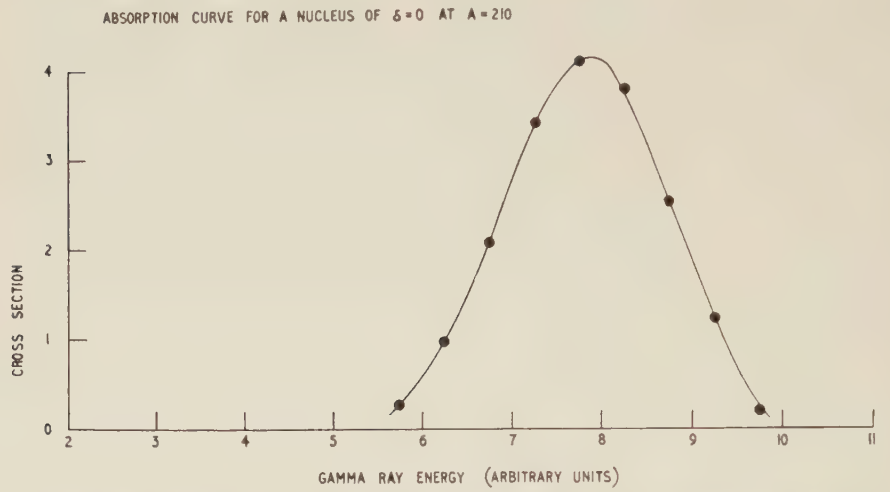

The calculated absorption curve of a nucleus with $\delta = 0$ in the region of $A = 210$. The computed transitions each smeared into a Gaussian of full width 3 MeV, are grouped in equal energy intervals and are represented by the bold dots. The energy scale is in arbitrary units and we must set one of these units equal to about 2 MeV to fit the absolute experimental energy of the resonance correctly.

Fig. 3

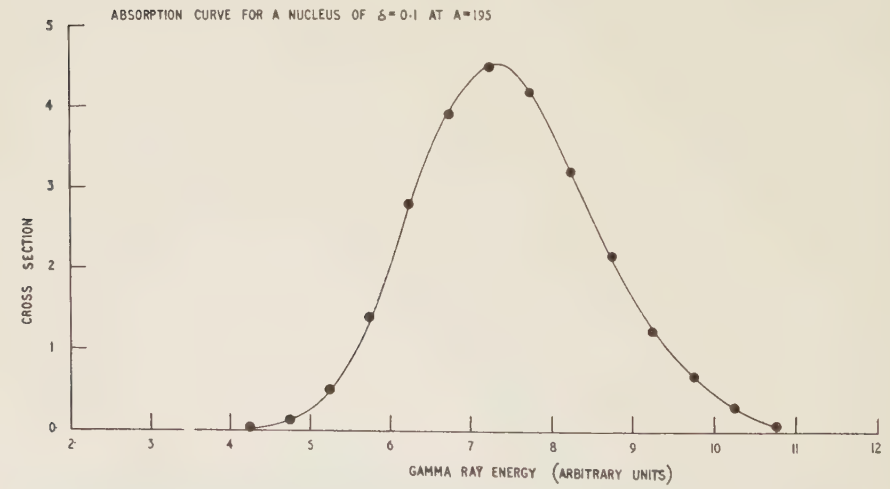

The calculated absorption curve of a nucleus with $\delta = 0{\cdot}1$ in the region of $A = 195$. See also caption to fig. 2.

using oriented nuclei and, or, polarized gamma-rays would not distinguish between the models any more than simple measurements of the widths seems to do.

Fig. 4

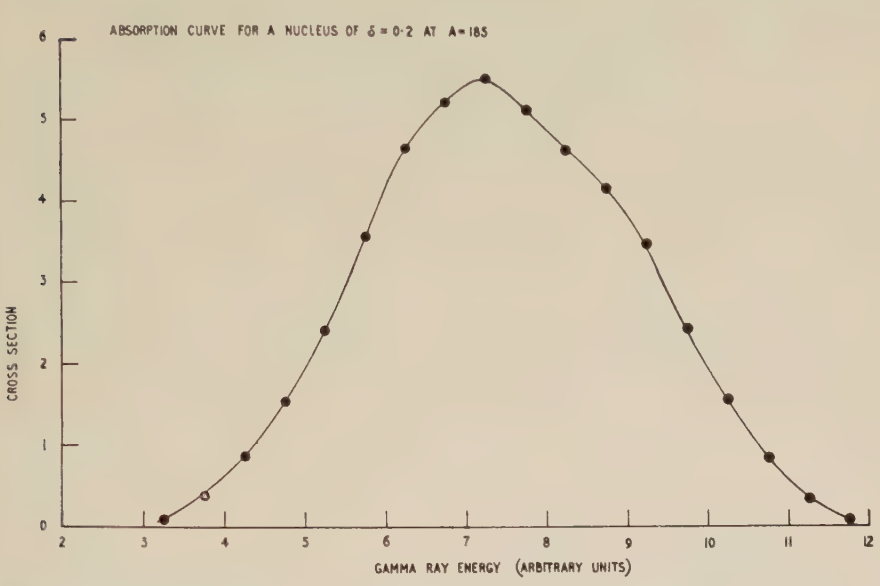

The calculated absorption curve of a nucleus with $\delta = 0{\cdot}2$ in the region of $A = 185$. See also caption to fig. 2.

Fig. 5

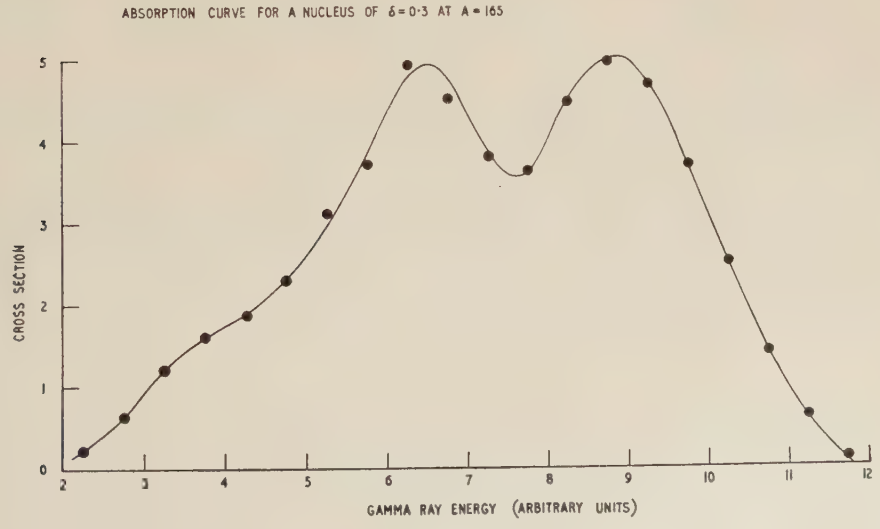

The calculated absorption curve of a nucleus with $\delta = 0{\cdot}3$ in the region of $A = 165$. See also caption to fig. 2.

Figure 6 shows the dependence of the resonance width on δ for a hypothetical nucleus of $A \sim 160$ and variable deformation. The resonance maximum is taken as 15·5 MeV for this figure.

Fig. 6

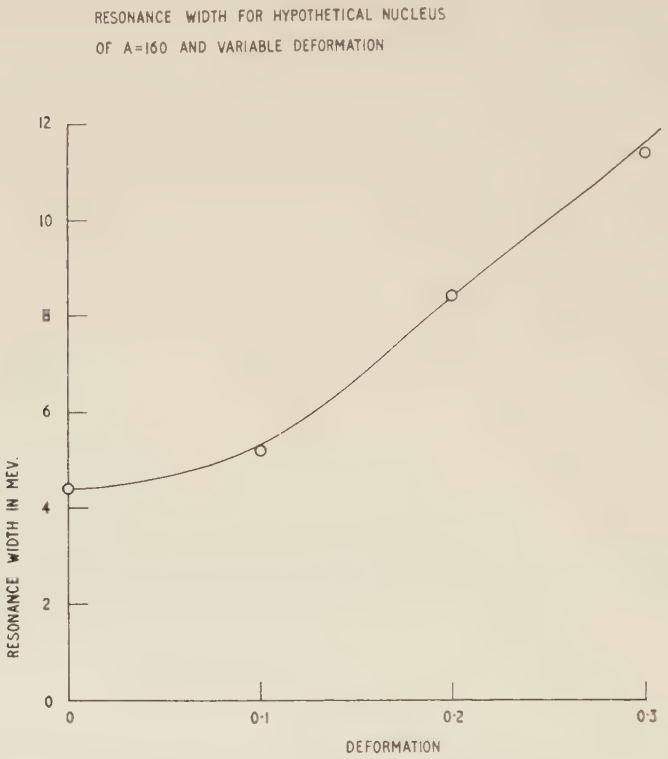

The calculated width of the giant resonance for a hypothetical nucleus of $A \sim 160$ and variable deformation whose resonance maximum occurs at 15·5 MeV. The computed points are shown by the circles.

Finally fig. 7 shows the comparison between the calculated resonance widths evaluated over the whole range of interest and the experimental results. In order to avoid systematic errors the experimental work from a single laboratory (the National Bureau of Standards, Washington) has been used in this comparison†.

§ 6. Discussion

Figure 7 shows that the independent particle model gives an excellent account of the great increase in giant resonance width in the region of strongly deformed nuclei. We must however stress that the computations,

† The experimental data are quoted from the work of Okamoto and are private communications to him from the NBS group (Petree, Weiss and Fuller).

lengthy as they are, are not wholly satisfactory and that they probably somewhat over-estimate the resonance widths for the more deformed nuclei. We must also recognize that the Nilsson diagram is least reliable for the cases of large deformation and large energy difference with which we are chiefly concerned here. A full computational programme which

Fig. 7

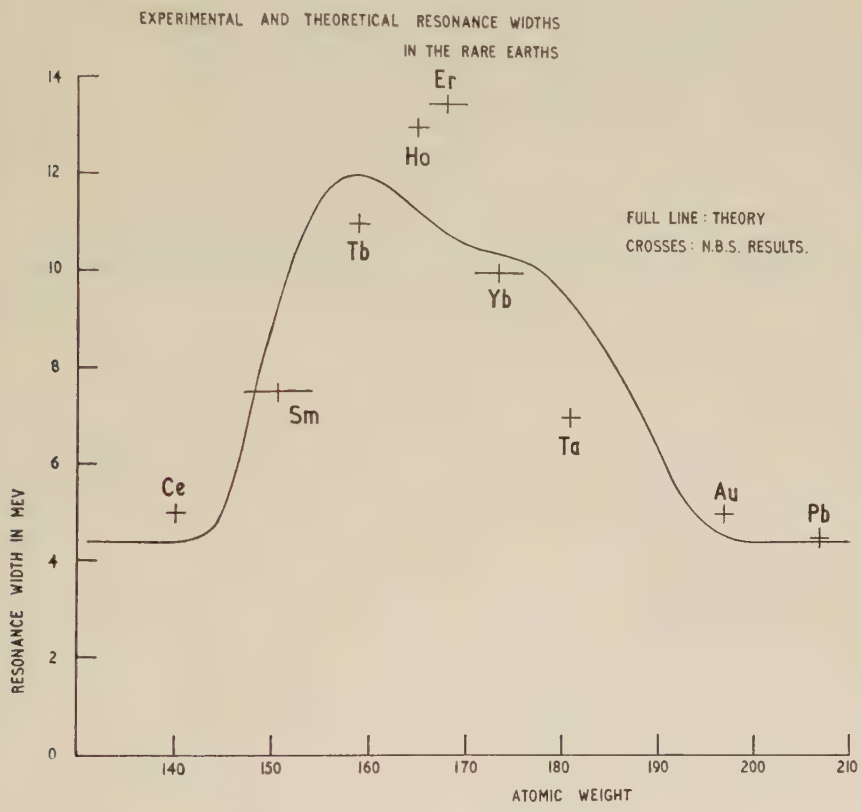

The comparison between the computed and experimental widths of the giant resonance through the region of the rare earths. Mono-isotopic elements or those with a strongly predominating isotope are shown by a small cross. For the others the horizontal bar spans the mass values of the abundant isotopes. All these experimental data come from the National Bureau of Standards, Washington. The vertical bars are not intended to indicate the accuracy of the experimental results.

aims at a simultaneous account of the single-particle level spacings and the ground state properties in this region of the periodic table would be extremely complex and lengthy. Until it is carried through we may adopt the present results as a semi-quantitative indication that the independent particle model of the giant resonance has it well within its power to give an account of the experimental situation.

References

Alder, K., Bohr, A., Huus, T., Mottelson, B. R., and Winther, A., 1956, *Rev. mod. Phys.*, **28,** 432.

Bohr, A., and Mottelson, B. R., 1953, *Dan. Mat. Fys. Medd.*, **27,** No. 16.

Brink, D., 1957, *Nuclear Phys.*, **4,** 215.

Brown, G. E., and Levinger, J. S., 1958, *Proc. phys. Soc. Lond.*, **71,** 733.

Brueckner, K. A., 1955, *Phys. Rev.*, **97,** 1353.

Danos, M., 1952, *Ann. d. Phys.*, **10,** 265 ; 1956, *Bull. Amer. phys. Soc.*, **1,** 135 ; 1958, *Nuclear Phys.*, **5,** 23.

Frahn, W. E., and Lemmer, R. H., 1957, *Nuovo cim.*, **6,** 664.

Goldhaber, M., and Teller, E., 1948, *Phys. Rev.*, **74,** 1046.

Gottfried, K., 1956, *Phys. Rev.*, **103,** 1017.

Jensen, J. H. D., and Jensen, P., 1950, *Z. Naturf.*, **5a,** 343.

Nilsson, S. G., 1955, *Dan. Mat. Fys. Medd.*, **29,** No. 16.

Okamoto, K., 1958, *Phys. Rev.* (in course of publication).

Petree, B., Weiss, M., and Fuller, E. G., 1957, *Bull. Amer. phys. Soc.*, **2,** 16.

Rand, S., 1957, *Phys. Rev.*, **107,** 208.

Strominger, D., and Rasmussen, J. O., 1957, *Nuclear Phys.*, **3,** 197.

Wilkinson, D. H., 1954, *Proceedings of* 1954 *Glasgow Conference on Nuclear and Meson Physics* (London : Pergamon Press), p. 161, 1957, *Physica*, **22,** 1039.

The Energy and Angular Distributions of the Protons from the Reaction ^{60}Ni(n, p)^{60}Co Induced by 13·5 MeV Neutrons†

By P. V. March and W. T. Morton
Department of Natural Philosophy, University of Glasgow

[Received March 25, 1958]

Abstract

The energy spectrum and angular distribution of the protons emitted from ^{60}Ni on bombardment with 13·5 MeV neutrons have been studied using photographic emulsions. About 30% of the protons emitted can be attributed to direct interaction processes.

§ 1. Introduction

In a previous communication (March and Morton 1958) henceforth referred to as I, the authors reported their results on the protons emitted from ^{54}Fe and ^{56}Fe; for each of these isotopes the angular distributions of the protons emitted with energies greater than 7 MeV showed a marked peak at forward angles.

It was considered desirable to make a similar study of a different medium weight element. The isotope ^{60}Ni was chosen for study because its Q value for the n, p) reaction lies between those of ^{54}Fe and ^{56}Fe so the cross section should also be intermediate between those of the ^{54}Fe and ^{56}Fe. The effects of the Coulomb barrier in ^{60}Ni should be similar to those in the isotopes of iron.

§ 2. Experimental Procedure

The nickel isotope (99·2% ^{60}Ni) consisted of a layer 7 mg/cm^2 in thickness and 1 cm^2 in area electroplated on to a gold foil. The exposure arrangements and the procedure for the examination of the photographic emulsions were those described in I. Only protons making angles between 0° and 140° with the direction of the incident neutrons were measured. The total number of protons observed in the area of emulsion examined was 2498 of which 792 were background protons. The neutron flux at the isotope layer was determined by scanning a known volume of emulsion for recoil protons as described in I. The neutron energy was $13{\cdot}5 \pm 0{\cdot}1$ MeV.

† Communicated by the Authors.

§ 3. Results

The angular distributions of the protons emitted from ^{60}Ni for three different ranges of proton energy are given in fig. 1. The total cross section for the emission of protons was obtained by extrapolating the angular distribution to 180°. The value obtained was 233 ± 25 mb.

Fig. 1

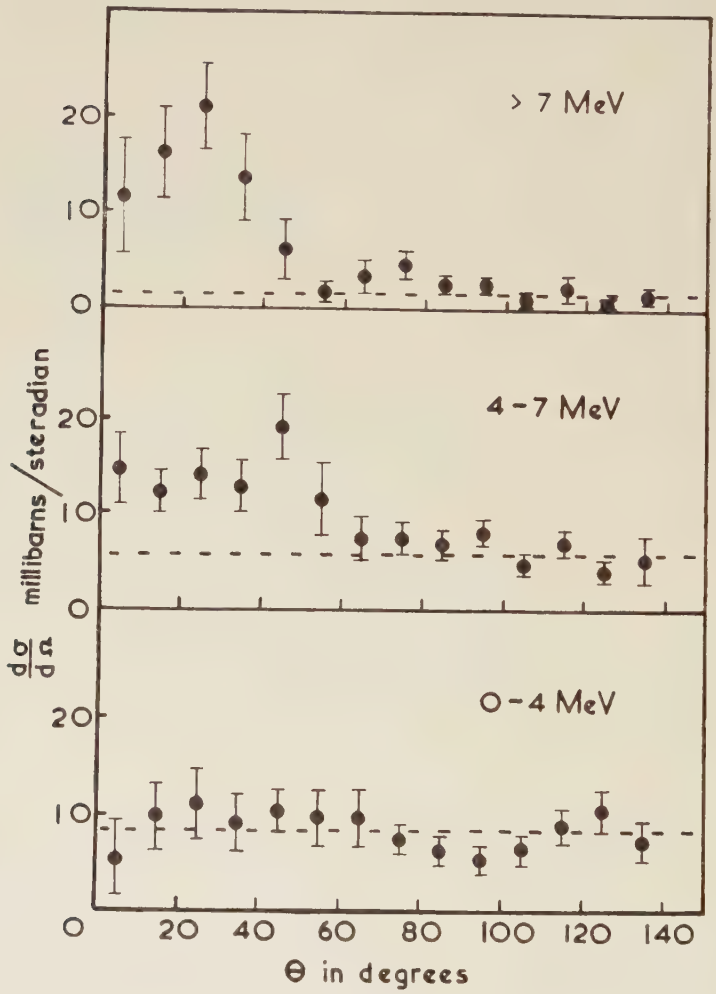

Angular distributions of the protons emitted from ^{60}Ni.

The energy spectra of the protons emitted in three different angular intervals are given in fig. 2.

The solid line curves in fig. 2 are the proton energy distributions expected for the (n, p) reaction on the basis of the statistical theory of Weisskopf

and Ewing (1940). The calculated energy distribution was normalized to the observed distribution for proton energies greater than 4 MeV in the angular range 90°–140°. The majority of the protons emitted with energies below 4 MeV are due to the (n, np) reaction and the broken line was drawn through the observed distribution of these protons for the

Fig. 2

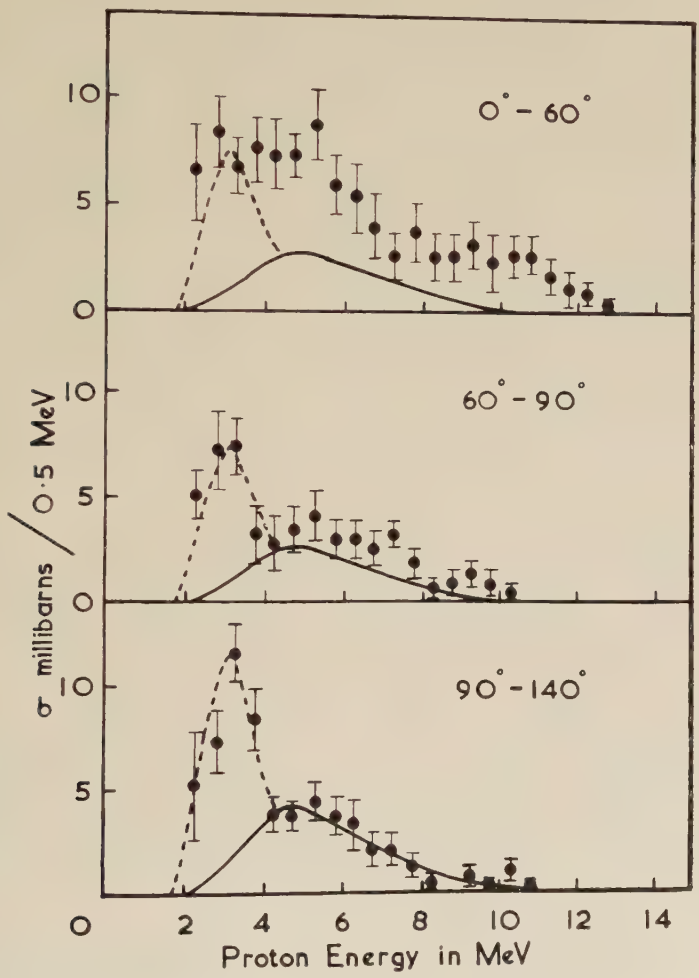

Energy spectra of the protons emitted from ^{60}Ni.

angular range 90°–140°. The curves drawn on the other two angular intervals were obtained by assuming that the protons from these two compounds nucleus processes were emitted isotropically.

§ 4. Discussion

The isotropic angular distribution of the protons emitted at backward angles and the good fit of the calculated energy spectrum to the distribution of protons with energy greater than 4 Mev emitted in the angular interval 90°–140° suggest that these protons result from the decay of a compound nucleus.

The Q values for the reactions (n, p), (n, np) and (n, 2n) are $-2{\cdot}0$, $-9{\cdot}6$ and $-11{\cdot}5$ Mev respectively, hence at a bombarding energy of 13·5 Mev the maximum energy of a proton from the (n, np) reaction is 3·9 Mev and at proton energies of about 2 Mev the (n, np) reaction is favoured relative to the (n, 2n) reaction. Thus the large number of low energy protons observed is probably due to the (n, np) reaction. Figures 1 and 2 show that these protons are emitted isotropically in agreement with a compound nucleus process.

The broken line on the angular distributions was drawn through the mean of the experimental points at backward angles and illustrates any departure from isotropy at forward angles. It is seen that the high energy protons are emitted preferentially in the forward direction. These protons are probably due to the direct interaction of the incident neutron with a proton of the target nucleus (e.g. Austern *et al.* 1953, Brown and Muirhead 1957). The energy spectra show that the energy spectrum of the protons from direct interaction is approximately flat above 4 Mev and there is no evidence of marked structure in their spectrum similar to that observed by Gugelot (1954) and Cohen (1957) in the inelastic scattering of protons by nuclei.

If the isotropic part of the proton distributions is attributed to the decay of a compound nucleus and the excess at forward angles to a direct interaction, the cross sections obtained are, compound nucleus: 155 mb (87 mb (n, p) and 68 mb (n, np)) and direct interaction: 68 mb.

The results for ^{60}Ni bear a strong resemblance to those obtained for ^{54}Fe and ^{56}Fe described in I. Similar results for medium weight elements have been reported by Allen (1957) and by Brown *et al.* (1957) using photographic emulsions and by Colli and Facchini (1957) using a counter technique. Colli *et al.* (private communication) have measured the angular distribution of the protons emitted from natural nickel (67·4% ^{58}Ni, 26·7% ^{60}Ni) and find that the proton spectrum is much more intense at forward than backward angles.

An estimate of the nuclear temperature for the compound nucleus part of the (n, p) reaction may be obtained by plotting $\log_e N(E_p)/\sigma_{c,p}E_p$ against E_p, where $N(E_p)$ is the number of protons observed with an energy E_p in the angular interval 90°–140° and $\sigma_{c,p}$ is the cross section for the formation of the compound nucleus by a proton of energy E_p. This plot is shown in fig. 3. The slope of the line gives the nuclear temperature at the average excitation energy. The change of slope at 4 Mev illustrates the onset of the (n, np) reaction. The value obtained for the nuclear temperature for the (n, p) reaction is 1·0 Mev.

Fig. 3

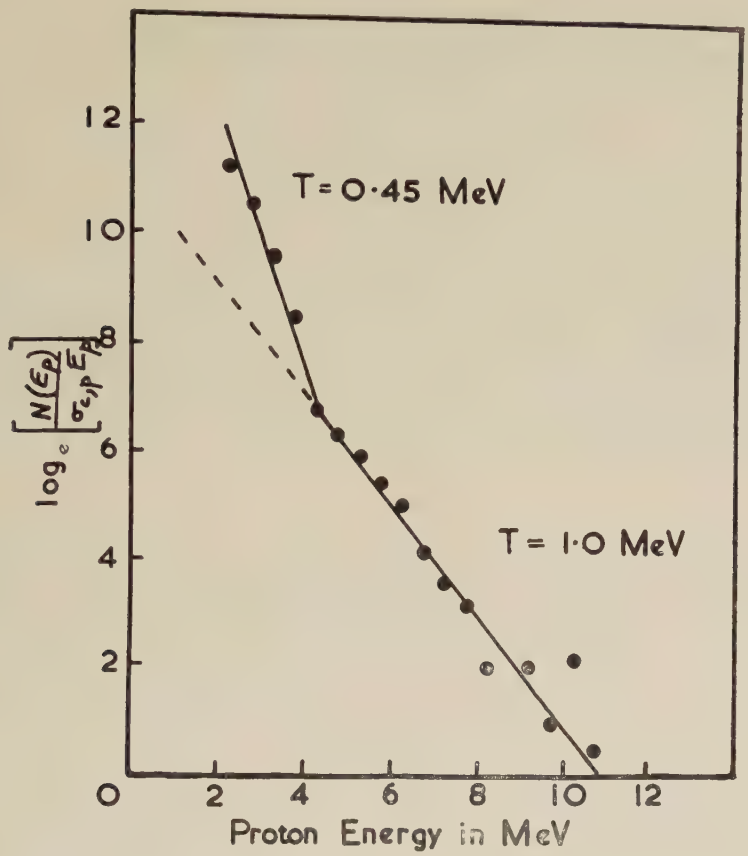

Proton spectra of ^{60}Ni corrected for Coulomb barrier penetrabilities.

Acknowledgments

The authors wish to thank Dr. G. Brown and Dr. H. Muirhead for valuable advice, Dr. A. Ward for running the H.T. set, Miss E. Rose and Miss J. Stewart for help with the microscope work, and A.E.R.E., Harwell for providing the separated isotope. One of us (W. T. M.) wishes to thank the Department of Scientific and Industrial Research for a maintenance grant.

References

Allan, D. L., 1957, *Proc. phys. Soc. Lond.* A, **70,** 195.
Austern, N., Butler, S. T., and McManus, H., 1953, *Phys. Rev.*, **92,** 351.
Brown, G., Morrison, G. C., Muirhead, H., and Morton, W. T., 1957, *Phil. Mag.*, **2,** 785.
Brown, G., and Muirhead, H., 1957, *Phil. Mag.*, **2,** 473.
Cohen, B. L., 1957, *Phys. Rev.*, **105,** 1549.
Colli, L., and Facchini, U., 1957, *Nuovo Cim.*, 1957, **5,** 309.
Gugelot, P. C., 1954, *Phys. Rev.*, **93,** 425.
March, P. V., and Morton, W. T., 1958, *Phil. Mag.*, **3,** 143.
Weisskopf, V. F., and Ewing, D. H., 1940, *Phys. Rev.*, **57,** 472.

Do the 'Constants of Nature' change with Time?†

By D. H. Wilkinson
Clarendon Laboratory, Oxford

[Received March 24, 1958]

Abstract

The age of minerals determined by radioactive methods agrees roughly with the age of the galaxy. This suggests that radioactive alpha-decay constants have probably changed by less than a factor of 3 or 4 during the last 3 or 4×10^9 years. It is shown that this implies that many 'Constants of Nature', particularly e, h and c probably change more slowly than 10^{-12} parts per year. The meson coupling constant also appears to change more slowly than this and the beta-coupling constants by less than 10^{-9} parts per year.

The question of a possible time-dependence of the 'Constants of Nature' is occasionally raised (e.g. Dirac 1938). The evidence for their constancy over great periods of time is not very good although Teller (1948) has given reasons for believing that the gravitational constant G probably changes by less than 10^{-9} parts per year. The usual interpretation of the red-shift of the spectral lines from distant galaxies probably implies a comparable constancy of the relevant atomic constants.

It seems that we can sharpen these estimates by considering the phenomenon of alpha-particle decay. This is because the rate of this decay is governed chiefly by the penetration of the charged particles through the Coulomb barrier which surrounds the nucleus and so tends to depend exponentially on the constants. Small changes in the constants would bring large changes in the decay rates.

The 'age of the earth' is estimated through the relative concentrations of the various radiogenic leads and their parent bodies in unaltered minerals (Nier *et al.* 1941, Holmes 1946, 1947). The age so deduced, about $3–4 \times 10^9$ years, is just about the same as is estimated for the galaxy (see e.g. Bondi 1952), the best current estimates running at about $7–8 \times 10^9$ years. We may take it that this coincidence is not due to chance. The implication is then that the decay constants λ of the various radioactive bodies concerned in these estimates (^{235}U, ^{238}U, ^{232}Th) have not changed by more than a factor of 3 or 4 over the last 3 or 4×10^9 years. Supplementary evidence of an essentially similar nature comes from a study of pleochroic haloes (Henderson 1934).

The decay constant λ is dominated by the penetrability factor so that we may write, to a first approximation;

$$\lambda = \text{constant} \times \exp(-\Lambda)$$

† Communicated by the Author.

where $\Lambda = 8\pi^2 Ze^2/hv$. Here Z is the atomic number of the radioactive body and v is the speed with which the alpha-particle of energy E is emitted. This approximation, which neglects the effect of the nuclear radius on the decay rate, would be very poor for calculating the actual barrier penetrability but is quite adequate for our present crude estimate of the way in which λ depends on e.

If now e were to change slightly there would be no first order effect on the nuclear wave functions since these are determined chiefly by the much stronger nuclear forces which we leave unchanged for the present argument. We may for example estimate that a 1% increase in e would dilate the nucleus by less than 0·1%. The intrinsic probability of the alpha-particle emission therefore changes very little and any effect on λ is due chiefly to changes in Λ through e and v. The change in v comes about because the Coulomb energy changes with e. Writing the Coulomb energy classically and ignoring the effect of the change in R, which is unimportant, we have:

$$\frac{dv}{v}\Big/\frac{de}{e} = \frac{12}{5}\frac{e^2 Z}{RE}.$$

With the earlier equation this gives:

$$\frac{d\lambda}{\lambda}\Big/\frac{de}{e} = -\Lambda\left(2 - \frac{12}{5}\frac{e^2 Z}{RE}\right) = 1{\cdot}5 \times 10^3$$

for the bodies of interest. We have used $R = 1{\cdot}2A^{1/3}$ fermis.

This estimate is in error because we have neglected the effect of the radius in diminishing Λ and have neglected the effect of the change in radius in reducing the change in v. When these omissions are corrected the above simple estimate of the sensitivity of λ to e is lowered by about 20%.

We see that the increase in decay rate due to the increase in v on increasing e more than offsets the extra difficulty in escape due to the increased height of the Coulomb barrier. This we can understand qualitatively. As we increase e to the first approximation the height of the Coulomb barrier at the nuclear surface increases but the depth of the nuclear potential below the top of the barrier remains the same so the whole nuclear level system is simply lifted with the barrier, the alpha-particle escaping with greater energy but at the same energy below the top of the barrier. The barrier however has become thinner at a given energy below its top because it has been raised so the penetrability increases. When we take into account also the increased Coulomb effects within the nucleus itself and not just up to the nuclear surface we see that in fact the energy at which the alpha-particle escapes below the top of the barrier decreases as the barrier is raised so on this account also the penetrability increases.

We noted earlier that a change of λ by a factor of 3 or 4 in 3 or 4×10^9 years is unlikely so the present result implies that a rate of change of e by 10^{-12} parts per year is unlikely.

A similar analysis of the sensitivity of λ to changes in h (through Λ) suggests that h changes by less than 10^{-11} parts per year but here the situation is complicated because of the involvement of h in the nuclear wave functions. However it is unlikely that the effect of a change in h, through the nuclear wave function, if of the opposite sign, would nearly cancel that due to the change in penetrability. We may therefore let this estimate stand as probably conservative.

We may likewise discuss the stability of the nuclear forces. It is difficult to do this from a fundamental viewpoint because we are not yet able to relate the real part of the effective nuclear potential to the internucleonic forces in any simple way. We may however discuss possible changes in the effective nuclear potential itself. If we consider the alpha-particle to be formed from nucleons which are near the top of a Fermi-sea in a potential of depth V and of fixed radius then:

$$\frac{d\lambda}{\lambda}\Big/\frac{dV}{V} = \frac{16\pi^2 Ze^2}{hv} \times \frac{V}{E} = 5 \times 10^3.$$

We have set $V = 55$ Mev. The sensitivity of λ to changes in R for a potential of fixed depth is roughly twice as great as this. It therefore seems likely that the parameters of the effective nuclear potential change by less than 10^{-12} parts per year. Since the nuclear forces certainly depend on h/mc where m is a mesonic mass it seems likely that h, c and the masses of elementary particles themselves change by less than this order per year. We may similarly include the (π) meson–nucleon coupling constants in this list.

We can also make some remarks about the constancy of the coupling constants for beta-decay. From the pleochroic haloes in mica we get a picture of the natural radioactive series integrated over geological time (Henderson 1934, Henderson and Turnbull 1934). These series contain certain bodies which at the present epoch emit alpha-particles and beta-rays in competition with each other. One such point in the ^{235}U series is at Ac which branches 1·2% by alpha emission to AcK, the rest by beta emission to RdAc. Another point is at AcC′ which branches 99·7% by alpha emission to AcC″ and the rest by beta emission to AcC″. A particularly well-measured specimen is the Renfrew biotite of Henderson and Turnbull (1934) which is about 1×10^9 years old. It shows good haloes called F and H of radii 15·4 μ and 19·4 μ due respectively to Ra + UII + Io and to Rn + RaF. The halo due to alpha-particles from Ac is expected at 17·5 μ radius which is almost exactly in the middle of a rather clean and halo-free gap between haloes F and H. This is consistent with the present day branching of a factor of 80 in favour of beta-decay of Ac. If however 10^9 years ago the beta-coupling constant had been 10 times less the rate of decay of Ac by alpha-emission would have been equal to the rate of decay by beta-emission and a visible halo would have formed in the present gap. Similarly had the constant been greater by this same order a halo due to the alpha-particles of AcC′ should be found at a radius of 32·6 μ in another

rather clean gap between halo C at $27{\cdot}4\,\mu$ (due to AcC + An) and halo A at $34{\cdot}6\,\mu$ (due to RaC'). This suggests that the beta-coupling constants do not change in either direction by 10^{-8} parts per year.

We must stress that all these estimates are crude but probably good to orders of magnitude and, where open to considerable error, as in the discussion of nuclear forces, are probably conservative. We must also admit that we cannot detect a conspiracy among the Constants of Nature by which some or all might change in such a way as to preserve the constancy of λ. This, however, would surely be the ultimate *lusus naturae*. Nor could we detect rapid fluctuations of the constants (say with a period of 10^7 years) about their mean values. We have effectively assumed that their change is monotonic in time.

Note added in proof.—I am grateful to Dr. K. I. Mayne for pointing out to me that the ages of minerals determined by the A–K and Sr–Rb methods, which depend on the beta-couplings, are in agreement with the ages determined by alpha-decay methods to a degree which implies constancy of the beta-coupling constants to the order of 10^{-9} parts per year. See, e.g. J. T. Wilson, R. D. Russell and R. M. Farquhar, 1956, *Handbuch der Physik*, **47,** 288, for modern references.

References

Bondi, H., 1952, *Cosmology* (Cambridge: University Press).
Dirac, P. A. M., 1938, *Proc. roy. Soc.* A, **165,** 199.
Henderson, G. H., 1934, *Proc. roy. Soc.* A, **145,** 591.
Henderson, G. H., and Turnbull, L. G., 1934, *Proc. roy. Soc.* A, **145,** 582.
Holmes, A., 1946, *Nature, Lond.*, **157,** 680; 1947, *Ibid.*, **159,** 127.
Nier, A. O., Thompson, R. W., and Murphey, B. F., 1941, *Phys. Rev.*, **60,** 112.
Teller, E., 1948, *Phys. Rev.*, **73,** 801.

Viscosity of Liquid Helium II near the Lambda Point†

By J. G. Dash
Royal Society Mond Laboratory, Cambridge

[Received February 28, 1958]

Abstract

The theory of Landau and Khalatnikov for the viscosity of liquid He II is examined in the neighbourhood of the lambda point. Arguments are advanced against the validity of the ideal gas approximation for rotons, and a qualitative roton liquid model is proposed. The temperature dependence of viscosity of the liquid model is found to correspond to the observed viscosity above 1·8°K, and with the discontinuity in the temperature derivative of viscosity at the lambda point.

The viscosity of liquid He II, as measured by the technique of oscillating discs or by rotation viscometer, rises monotonically as the temperature is decreased from 1·8° to 1°K. This trend is successfully described by Landau and Khalatnikov (1949, hereafter referred to as LK) in terms of the phonon and roton excitations of liquid ^{4}He below its lambda point temperature T_λ. At about 1·8°K, however, the observed temperature derivative of viscosity changes sign, the viscosity increasing by about a factor of two between 1·8°K and T_λ, and a theoretical explanation of this behaviour has not yet been proposed. The success of the LK model at lower temperatures can be taken as evidence for the validity of their theory; we here suggest a means for extending it to temperatures near T_λ.

The detailed calculations of LK show that the important processes giving rise to viscosity above 1°K are the scattering of phonons by rotons and of rotons by rotons. The two types of processes are each characterized by separate coefficients, respectively called 'phonon viscosity' η_p and 'roton viscosity' η_r, and the total viscosity η of the liquid is given by the sum of these two contributions.

The temperature dependence of η_p is given by LK as

$$\eta_p = \text{const.}/N_r$$

where N_r is the number of rotons per unit volume of liquid. Since the density ρ_n of normal fluid at temperatures $T > 1$°K is almost wholly due to the rotons, and N_r is proportional to $\rho_n T$, the phonon viscosity can be written in terms of the measured fraction $x = \rho_n/\rho$ of normal fluid,

$$\eta_p = a/xT, \quad a = \text{constant}, \quad . \quad . \quad . \quad . \quad . \quad . \quad (1)$$

---

† Communicated by the Author. Guggenheim Fellow 1957–8, on leave from Los Alamos Scientific Laboratory.

for the region $T > 1°$K. A re-examination by Khalatnikov (1956) of the characteristic times for achieving equilibrium among the scattered phonons indicates that the coefficient a of eqn. (1) varies with the temperature, but much more weakly than x. The coefficient is known in terms of certain empirical parameters of the liquid, and in that sense, the value of a is not completely arbitrary. There are, however, large discrepancies among the several experimental determinations of the fundamental parameters, leading to a considerable uncertainty in the magnitude of the phonon viscosity. We shall therefore treat the coefficient a itself as an empirical parameter. In addition, we neglect its variation with temperature. Errors that may result from this simplification may lead to a poorer description of the data near 1°K, where the phonon viscosity is dominant. Such errors will not affect the principal object of this paper, which is concerned with the behaviour of roton viscosity at higher temperatures.

The roton viscosity is found by LK to be temperature independent. This result stems from the high self-energy Δ compared to the kinetic energy $\sim kT$, the assumption of a hard-sphere roton–roton interaction potential, and the assumption of relatively low density N_r. Under these conditions, the rotons behave as quasi-particles, having a viscosity independent of N_r, as characteristic of an ideal gas of real massive molecules. This prediction appears to be confirmed by experiment, for the value of η (exp.) $-\eta_p$ (theor.) is about 10 micropoise between 1·2° and 1·8°K although x changes by a factor of 15 in this interval. We should, however, accept the result with some reservation, since η_p becomes increasingly dominant at low temperatures and the many measurements of viscosity do not agree well below 1·6°K.

The high temperature region of He II, from 1·8°K to T_λ, is the region in which the behaviour of η_r is dominant, and it is in this range that the LK theory does not correspond to the experiments. The failure, as Landau and Khalatnikov indicate, arises from the use of the ideal gas model. Such an approximation is justified in the case of low density, when each ' particle ' spends only a small fraction of its time under the influence of others. In the low density limit, the roton–roton interactions can be described as elastic two-body collisions, and the empirical collision cross section contains in integral form whatever moderate range interaction potential may exist. As in the case of real molecules, details of the roton–roton potential become increasingly important as the density increases. The existence of such a potential is indicated by the theoretical examination of phonon exchange processes given by Cohen and Feynman (1957), and by Khalatnikov's (1956) semi-empirical description of the ' non-ideality ' of the roton gas. Furthermore, the LK ideal gas approximation suggests a high probability for many-body collisions, even at 1·8°K; on the basis of their calculations, the roton–roton collision-radius r (related to the collision cross section σ by $\sigma = \pi r^2$) at this temperature is of the order of the mean free path, and the time between collisions is $\sim 10^{-12}$ sec, comparable with the period of atomic vibrations. A gas model seems

completely unsuitable in these circumstances, and it should be more profitable to compare the assembly of rotons to the molecules of a liquid. Such a comparison is not too badly handicapped by our ignorance of the detailed interaction as long as we are primarily interested in the qualitative dependence of viscosity on temperature and density, and can forgo the much more difficult problem of calculation of magnitudes. For our purposes, the qualitative theory of viscosity of liquids (Frenkel 1946) is adequate. We therefore accept, for the description of the motion of rotons in the high density region, the microscopic model of liquids, called at times the ' hole theory ', which has achieved moderate success in describing the dependence of viscosity of ordinary simple liquids upon temperature and pressure. According to this model, the motion of a molecule in the liquid is considered to be quite constrained by the close presence of its immediate neighbours; in contrast to the trajectories in a gas of low density, it is here taken to correspond to a sporadic migration through an equilibrium configuration of other molecules. Details of the interaction need not be known if we assume a density-dependent activation energy W opposing the dislocation of an individual molecule from its ' equilibrium ' position. The viscosity then behaves according to the exponential law

$$\eta_{\mathrm{liq}} = A \exp{}^{(W/kT)},$$

where A is approximately constant. The variation of η with density is given by expanding W about its value W_0 corresponding to a standard state of numerical density n_0;

$$W = W_0 + \alpha(n - n_0) + \beta(n - n_0)^2 + \ldots .$$

Using the proportionality of N_r and normal fluid fraction x above 1 °K, and neglecting terms higher than the first, we obtain for the viscosity of the ' roton liquid '

$$\eta_r = b \exp(cx) \quad . \quad . \quad . \quad . \quad . \quad . \quad . \quad . \quad . \quad (2)$$

where b and c are approximately constant: that is, neglecting the variation of T in comparison with the much more strongly varying function $x(T)$. Equation (2) corresponds approximately to ' Andrade's Law ' (Andrade 1934) relating the viscosity and density of ordinary liquids. The equation for η_r is also of the correct form in the region of low roton density, for it approaches the constant value b at low temperatures as for a gas; this is a fortuitous result of the rapid variation of x with temperature. We therefore obtain, for the viscosity of normal fluid in He II in the range 1 °K–T_λ, the sum of roton and phonon contributions

$$\eta = \frac{a}{xT} + b \exp(cx). \quad . \quad . \quad . \quad . \quad . \quad . \quad . \quad (3)$$

Comparison of eqn. (3) with the observed viscosity (Dash and Taylor 1957) in the range 1·2 °K–T_λ yields the empirical constants

$$a = 0{\cdot}675\ \mu\mathrm{P\ deg}; \quad b = 10\ \mu\mathrm{P}; \quad c = 0{\cdot}95,$$

which may be compared to the values

$$a \simeq 0{\cdot}8\ \mu\text{P deg}; \quad b = 11{\cdot}5\ \mu\text{P}; \quad c = 0,$$

given by Khalatnikov (1956). Equation (3) appears to correspond closely to the observed viscosity above 1·2°K, as shown in the figure; mean deviation between our equation and the measured values is of the order of 5%.

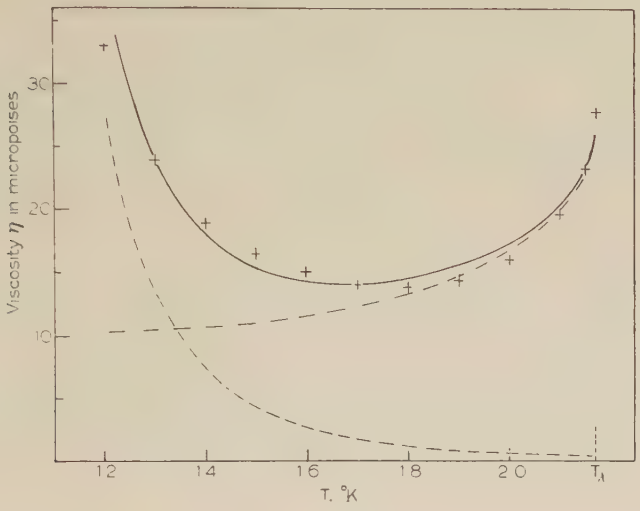

Viscosity of He II above 1·2°K.
– – – – – η_p, Landau and Khalatnikov.
— · — · η_r, liquid model.
————, $\eta_p + \eta_r$.
\+ , smoothed experimental values, Dash and Taylor (1957).

This liquid model of roton viscosity appears to present a simple explanation for the observed singularity in $d\eta/dT$ at the lambda point. Experiments (Dash and Taylor 1957, Taylor and Dash, 1957, Welber, private communication) have shown that both $d\eta/dT$ and $d\rho_n/dT$ have strong discontinuities at T_λ, but that the kinematic viscosity η/ρ_n changes quite smoothly through the transition temperature. From the latter observation we have

$$\left[\frac{d}{dT}\left(\frac{\eta}{\rho_n}\right)\right]_{T_\lambda - dT} = \left[\frac{d}{dT}\left(\frac{\eta}{\rho_n}\right)\right]_{T_\lambda + dT},$$

and since

$$\left(\frac{d\rho_n}{dT}\right)_{T_\lambda + dT} = \left(\frac{d\rho}{dT}\right)_{T_\lambda + dT} \simeq 0,$$

$$\left(\frac{d\eta}{dT}\right)_{T_\lambda - dT} - \left(\frac{d\eta}{dT}\right)_{T_\lambda + dT} = \left(\frac{\eta}{\rho}\right)_{T_\lambda} \left(\frac{d\rho_n}{dT}\right)_{T_\lambda - dT}. \quad . \quad . \quad (4)$$

From eqn. (2) we obtain the temperature derivatives of the roton liquid viscosity on each side of the lambda point:

$$\left(\frac{d\eta_r}{dT}\right)_{T_\lambda+dT}=0, \quad \left(\frac{d\eta_r}{dT}\right)_{T_\lambda-dT}=c\left(\frac{\eta_r}{\rho}\right)_{T_\lambda}\left(\frac{d\rho_n}{dT}\right)_{T_\lambda-dT}.$$

Since the empirical value $c=0{\cdot}95$, this is seen very nearly to satisfy the observed condition, eqn. (4). Thus, although we do not consider the mechanisms of viscosity in He I, the discontinuity in $d\eta/dT$ at the lambda point appears to arise as a direct consequence of the abrupt halt in the increase of roton density with temperature.

Acknowledgment

I should like to thank Drs. D. Shoenberg and W. F. Vinen for helpful comments and suggestions.

References

Andrade, E. N. da C., 1934, *Phil. Mag.*, **17,** 497, 698.
Cohen, M., and Feynman, 1957, *Phys. Rev.*, **107,** 13.
Dash, J. G., and Taylor, R. D., 1957, *Phys. Rev.*, **105,** 7.
Frenkel, J., 1946, *Kinetic Theory of Liquids*, Ch. IV (Oxford : University Press).
Khalatnikov, I. M., 1956, *Adv. phys. Sci., Moscow*, **59,** 673.
Landau, L. D., and Khalatnikov, I. M., 1949, *J. exp. theor. Phys.*, **19,** 637, 709.
Taylor, R. D., and Dash, J. G., 1957, *Phys. Rev.*, **106,** 398.

Superconductivity of Thorium below 1°K†

By Norman M. Wolcott and Robert A. Hein
United States Naval Research Laboratory, Washington, D.C.

[Received March 11, 1958]

Abstract

The critical magnetic field of thorium has been determined between 0·1°K and 1·37°K, the transition temperature, where the initial slope of the critical field curve is 190 gauss/deg. The data indicate a value of 162 gauss for the critical field at absolute zero. The critical field curve departs from a parabola near the transition temperature. The electronic specific heat, $11{\cdot}1 \times 10^{-4}T$ cal/mole-deg, deduced from the magnetic measurements is in substantial agreement with the previously determined calorimetric value.

§ 1. Introduction

As the result of electrical resistivity measurements, Meissner (1929) reported the superconductivity of thorium at about 1·4°K. Later Shoenberg (1939) investigated the critical field of thorium down to 1°K using a moment measuring technique. His measurements indicated that thorium had superconducting properties similar to those found in ' soft ' superconductors; in particular, the superconducting-normal transitions in a magnetic field were very sharp. Since extremely pure thorium is now available, we thought it would be of interest to extend the critical field measurements below 1°K to determine the shape of the critical field curve in this region and also to obtain a magnetic value for the electronic specific heat coefficient, γ.

§ 2. Experimental Details

A polycrystalline rod of thorium prepared by the van Arkel process was obtained from Metal Hydrides, Inc., Beverly, Massachusetts. The chemical analysis provided with the material indicated the following impurities in parts per million:

N	30	Cu	12·5	Al	2·5	H	8
Fe	23	Ni	4·0	Ca	2·5	Sn, Co, Zn, Zr, Ge, P, As, Cd, Sb,	
Si	33	Pb	2·5	Mg	2·5	Ba, Be, V, Mo, Bi, Ta, Hg not detected	
Cr	22	Mn	2·5	O	30·0		

The specimen was in the form of a rod 6 mm in diameter and 25 mm long. It was cemented (GE 7031 adhesive) into two split copper cylinders; one of these was in thermal contact with a pill of potassium chrome alum, while a carbon resistor used as a resistance thermometer was cemented to the other. In order to reduce heat leak from the surrounding liquid

† Communicated by the Authors.

helium bath to the sample assembly, the suspension threads and leads to the carbon resistor were passed through a ballast pill of manganous ammonium sulphate.

Temperatures below 1°K were obtained by adiabatic demagnetization of the chrome alum from fields up to 30 000 gauss at an initial temperature of 1·3°K. After demagnetization, the procedure was to observe the temperature (differential susceptibility) of the chrome alum pill by a ballistic mutual inductance technique and to follow the resistance of the carbon thermometer. Comparison of the two temperatures indicated that the time for thermal equilibrium between the salt and the thorium was about two minutes. A steady external field was then applied and the differential susceptibility of the thorium was observed as the system slowly warmed up. As the chrome alum and the thorium were centred in different measuring coils, the differential susceptibility of each could be measured independently. When the transition temperature was reached for the particular applied field, a sudden change in the differential susceptibility of the thorium was observed. The applied field was then reduced until the metal again became superconducting. In this way, two to three points on the critical field curve could be obtained from a single demagnetization.

§ 3. Results

A typical warm up curve is shown in fig. 1. The solid curve is the galvanometer deflection (proportional to the differential susceptibility of the thorium) obtained with the ballistic measuring field parallel to the applied external field, while the dotted curve represents the galvanometer deflection obtained with measuring field opposite to the applied field. The deflections obtained with the metal in the normal and superconducting states respectively are shown on the margin and denoted by N and SC. The magnitude of the change observed between the completely superconducting and completely normal deflections indicates that 95 to 100% of the thorium became superconducting.

The qualitative interpretation of the curve is as follows: Following demagnetization a galvanometer deflection corresponding to complete superconductivity is observed. An external field is then applied until the galvanometer deflection indicates a differential paramagnetism ($t = 1$ hour in fig. 1). The excess differential paramagnetism above the normal is due to the inverse Meissner effect, for near the transition temperature in a magnetic field the small applied measuring field (about one gauss) causes a large amount of expelled flux to re-enter the superconductor, thus giving rise to an apparent paramagnetic differential moment which can be quite large. For about one hour after the measurements began, the applied external field dropped as the solenoid coils warmed up. This caused the galvanometer deflection to decrease during this period. The deflection then remained very near the normal value for about two hours. In fact during the first experiment, it was suspected

that the metal might actually be normal; and only the fact that identical deflections were not obtained with the measuring field reversed indicated that superconducting material was still present. As the transition temperature is approached, the inverse Meissner effect becomes more pronounced and large paramagnetic deflections are obtained. This 'differential' paramagnetic effect has been discussed by Steele (1952). In this case the maximum paramagnetic deflection was more than ten times the diamagnetic deflection corresponding to complete superconductivity. As the transition temperature is passed, the deflection suddenly returns to its normal value. When the measuring field is reversed (dotted curve in fig. 1), the paramagnetic deflections are shifted

Fig. 1

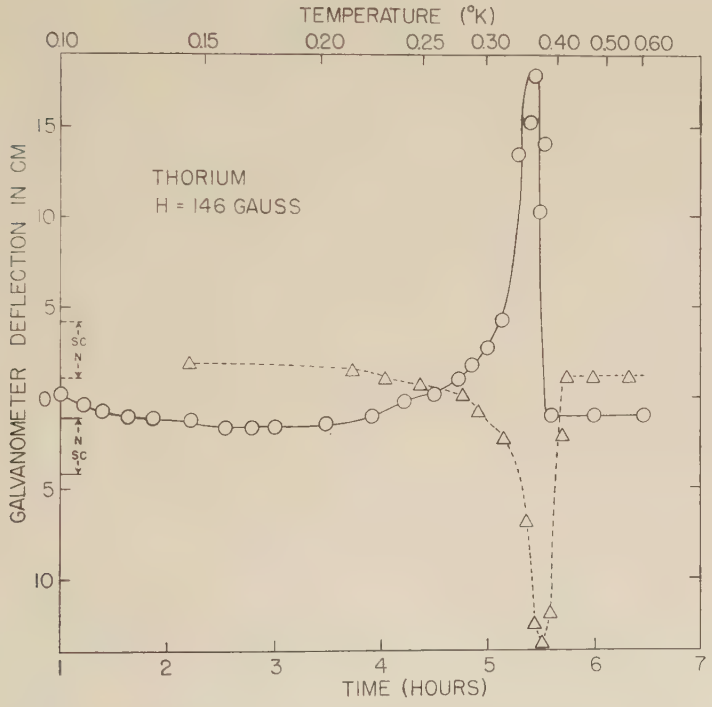

Galvanometer deflection as a function of temperature and time after demagnetization.

——o—— Measuring field parallel to applied field.
- - - △ - - - Measuring field anti-parallel to applied field.
N Galvanometer deflection in normal state.
SC Galvanometer deflection in superconducting state.

to higher temperatures since the external field is reduced by the measuring field; and the metal becomes normal at a slightly higher temperature. The transition temperature in the present experiments was defined as the

temperature at which the differential susceptibility returned to its normal value. The sharpness of the differential paramagnetic effect allowed this temperature to be obtained very accurately; this is in contrast to the results obtained with uranium, another actinide element, for which Hein *et al.* (1957) found spread-out transitions with no sharp Meissner effect.

Fig. 2

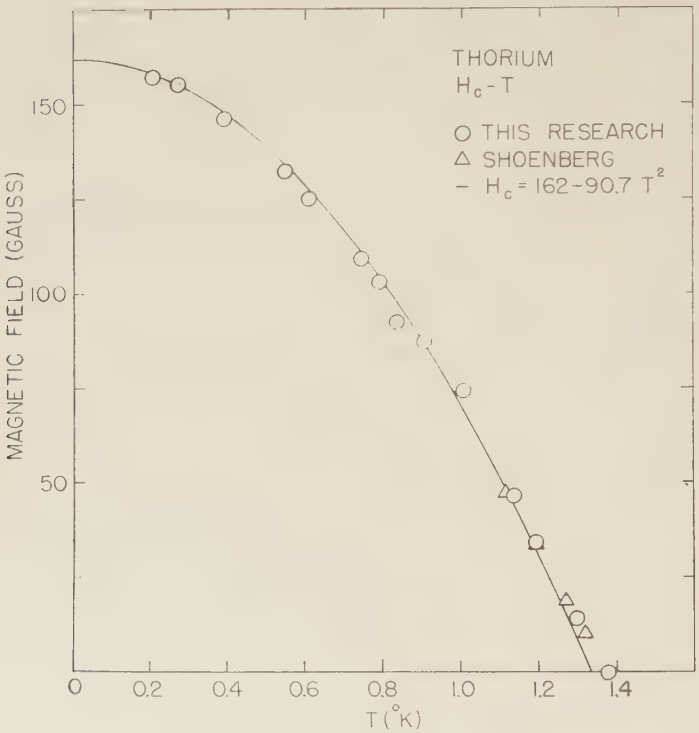

Critical magnetic field curve of thorium versus temperature.

With no applied field, the transition temperature was 1·37°K(T_c) in agreement with the earlier value of Shoenberg. The transition temperatures in various applied fields are shown in fig. 2 along with the earlier results of Shoenberg. It appears that the critical field departs from a parabola (shown as a solid line) near T_c. The measured points indicate that the slope of the critical field curve at the transition temperature, $(dH_c/dT)_{T=T_c}$, is 190 gauss/deg, also in agreement with Shoenberg.

§ 4. Discussion

In order to obtain an estimate of H_0, the critical field at absolute zero H_c was plotted *vs.* T^2 as shown in fig. 3. An extrapolation of this curve (which is linear over most of its range) to $T=0$ yields a value of H_0 of

162 gauss. Over the region where H_c is linear in T^2, the critical field is given by $H_c = H_0 - \lambda T^2$ with $H_0 = 162$ and $\lambda = 90{\cdot}7$; this is the parabola which is indicated by the solid line in fig. 2.

From the critical field curve a value of the electronic specific heat coefficient γ can be obtained, provided that the critical field curve represents the boundary for reversible superconducting–normal transitions. Application of thermodynamics to the transition indicates that (Daunt 1955) in general $\gamma = -(V/8\pi)(d^2H_c/dT^2)_{T=0}$ where V is the molar

Fig. 3

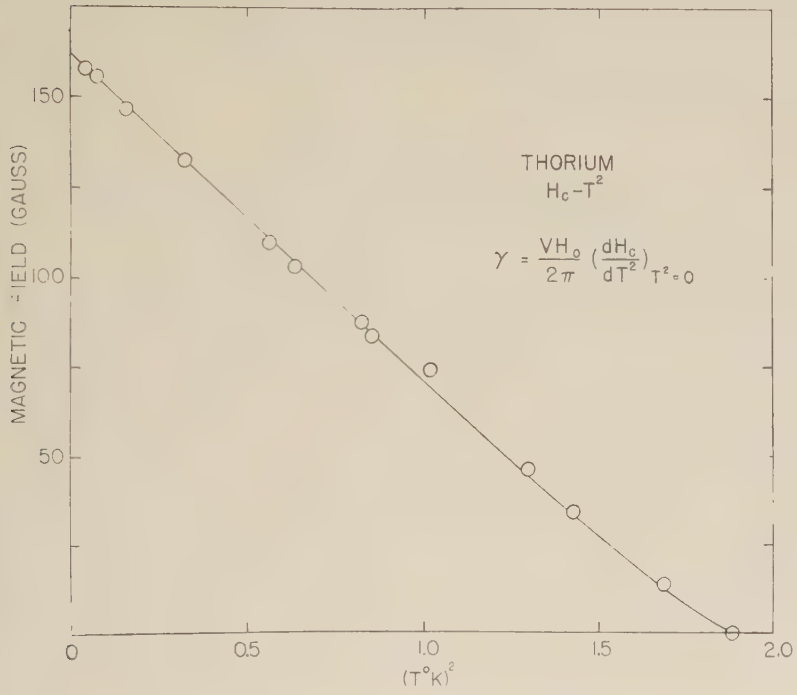

Critical magnetic field versus T^2 for thorium.

volume. If the critical field curve is parabolic in T, then this formula can be rewritten $\gamma = (V/8\pi)(dH_c/dT)^2_{T=T_c}$. When information about the critical field curve is only known near T_c, then this formula must be used. Using Shoenberg's value for $(dH_c/dT)_{T=T_c}$, Daunt obtained a value of $\gamma = 7{\cdot}1 \times 10^{-4}$ cal/mole-deg^2. Since the present measurements show that the critical field curve is not parabolic, it is not surprising that this value of γ disagrees with the calorimetric one.

In order to determine γ from a measured critical field curve near $T = 0$, it is necessary to evaluate the general relationship for γ. For this purpose,

it is convenient to change the variable of differentiation from T to T^2; when this is done, it becomes

$$\gamma = -\left(\frac{VH_0}{2\pi}\right)\left(\frac{dH_c}{dT^2}\right)_{T^2=0}.$$

Both H_0 and $(dH_c/dT^2)_{T^2=0}$ can be obtained from fig. 3, the former being the intercept and the latter the slope of the line at $T^2=0$. Using the values $H_0=162$ and $(dH_c/dT^2)_{T^2=0}=-90{\cdot}7$, the value $\gamma=11{\cdot}1\times10^{-4}$ cal/mole-deg^2 is obtained. This is in good agreement with the calorimetric value of $\gamma=11{\cdot}2\times10^{-4}$ cal/mole-deg^2 reported by Smith and Wolcott (1955).

In summary, we may say that thorium behaves in many ways like an ideal superconductor, that the critical field curve though not a parabola is parabolic over much of its range, and that values for the electronic specific heat coefficient, γ, obtained from magnetic and calorimetric data are in substantial agreement.

References

Daunt, J. G., 1955, *Progress in Low Temperature Physics* (Amersterdam : North Holland Pub. Co.).

Hein, R. A., Henry, W. E., and Wolcott, N. M., 1957, *Phys. Rev.*, **107**, 1517.

Meissner, W., 1929, *Naturwissenschaften*, **17**, 390.

Shoenberg, D., 1940, *Proc. Camb. phil. Soc.*, **36**, 84.

Smith, P. L., and Wolcott, N. M., 1955, *Bulletin de l'Institut International du Froid* Supplement 1955–3 (January 1956), p. 283.

Steele, M. C., 1952, *Phys. Rev.*, **87**, 1137.

The Cleavage of Metal Single Crystals†

By A. N. Stroh
Department of Physics, University of Sheffield

[Received March 13, 1958]

Abstract

A model of cleavage applicable to metals cleaving on the slip plane is developed in which a crack is initiated at the end of a low angle tilt boundary terminating inside the crystal. The strength of the metal is determined by the difficulty of growth of the crack. Satisfactory agreement is obtained with the experimental results for zinc.

§ 1. Introduction

Recently attempts have been made to account for the brittle fracture of metals in terms of the stress concentrations due to piled-up groups of dislocations at the ends of slip lines. Though this treatment has had some success with polycrystals (cf., for example, Stroh 1957) two difficulties are met when we try to apply it to single crystals. First, it is not easy to think of suitable obstacles in the slip plane able to withstand the large piled-up groups needed for fracture, since the grain boundaries which fulfill this role in polycrystals are no longer available. Secondly, a number of metals, of which zinc and bismuth are examples, have a single predominant slip plane which is also the cleavage plane; and since piled-up groups produce no tensile stress normal to their own slip plane they would not produce in these crystals the kind of stress magnification needed for fracture even if they could be formed. It seems therefore worthwhile to consider other possible mechanisms for fracture; in this paper a mechanism which is particularly adapted for the case in which slip and cleavage planes coincide is investigated.

§ 2. Initiation of Cracks

Orowan (1954) has pointed out that if a sub-grain boundary, i.e. a wall of dislocations, terminates within a crystal there will be a high stress concentration at its end which may be great enough to produce a crack. Such a terminating wall may be formed from a complete wall extending right across the crystal if part of this is held up against an obstacle and the other part is pulled on by the applied stress (fig. 1). Friedel (1956) has estimated the stresses which will occur at the end of such a wall and concludes that a crack should form if the wall corresponds to a misorientation of 5° or more; this estimate is necessarily somewhat rough as it reflects

† Communicated by the Author.

our ignorance of the exact value of the theoretical strength of the ideal lattice. This uncertainty, however, is of no great importance for the application to be made here, for our treatment will be based on the idea that the strength of the crystal which is observed is determined by the growth of the crack and not by its initiation; then we need only know that, for some sufficiently great misorientation, a crack can be initiated at the end of a wall of dislocations.

Cracks formed in this way have been directly observed by Gilman (1954); fig. 2, Pl. 25 shows two such cracks formed in zinc under a compressive load. A second example of crack formation, also due to Gilman (1957), is shown in fig. 3, Pl. 25 and we suggest that the same mechanism is operating here; we consider this case in some detail. The figure shows a symmetric

Fig. 1

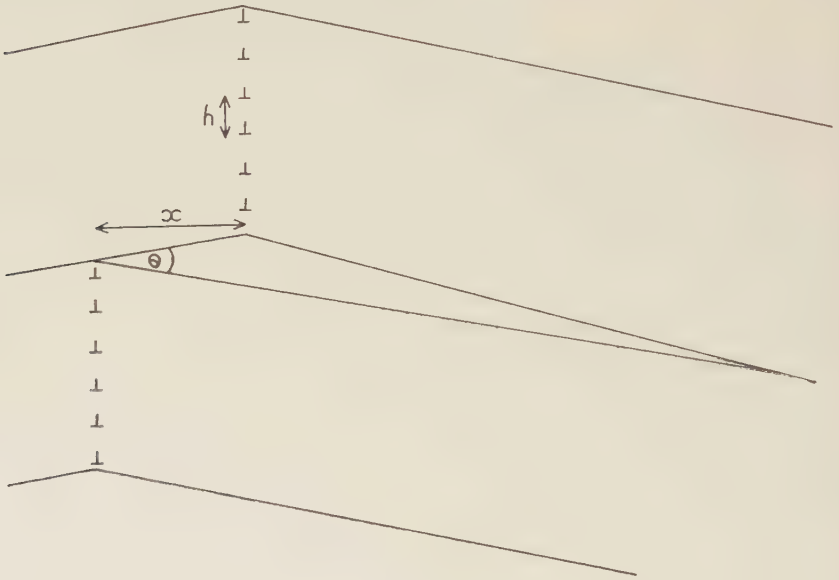

Cleavage at a divided dislocation wall.

bicrystal of zinc which has been tested under tension, the tensile axis being parallel to the grain boundary; since such bicrystals were found to have the same yield stress, rate of strain hardening and ductility as single crystals it is reasonable to assume that the same processes occur in these bicrystals and in single crystals. If we compare slip lines such as A and B lying on either side of the crack we see that while the slip lines on the side A are very nearly straight, those on side B are curved; thus the slip lines B must contain an excess of dislocations of one sign, but not the slip lines A. Since the slip lines are curved and not polygonized, the dislocations cannot all lie in a single boundary plane as in fig. 1 and fig. 2, Pl. 25; nevertheless the curvature occurs only in a fairly narrow region and so it will

be a reasonable approximation to suppose that here also the dislocations form a plane sub-boundary. The direction of bending of the slip planes shows that the extra half atomic planes terminating on the dislocations are on the side further from the crack; under the applied stress (a tension parallel to the grain boundary) such dislocations would move from left to right in the figure.

We therefore suggest that the following sequence of events has occurred. A dislocation wall formed on the left of the grain boundary and under the applied stress moved towards the grain boundary. Though the orientations of the two crystals are such that the boundary is transparent to dislocations and slip can continue through it from one crystal to the other, the grain boundary will nevertheless offer some resistance to the passage of dislocations. In the present case part of the wall has been held up at the grain boundary while the remaining part has been pulled through it into the second grain. Thus the wall has been split into two, and we have the situation shown in fig. 1 where a crack has been formed by the stress concentration at the end of the wall.

The misorientations in figs. 2 and 3, Pl. 25 are 14° and 8° respectively; Friedel's estimate of 5° as minimum misorientation to produce a crack is consistent with these results.

Some sort of barrier, for example the grain boundary in the case shown in fig. 3, Pl. 25, is still needed to hold back part of the wall while the other part is pulled on by the applied stress. But now the barrier may be relatively weak since a large number of dislocations can become blocked simultaneously, whereas in a piled-up group only the leading dislocation is blocked and the other dislocations all push against it. A possible barrier is now a low angle boundary formed from dislocations intersecting the slip plane; such a boundary corresponding to a misorientation of 1° or even less should be quite adequate as a barrier.

It is interesting to note that the present mechanism for initiating a crack accounts for the tendency for fracture (in single crystals of zinc, for example) to occur near the grips in a tensile test if the greatest possible care is not taken in mounting the specimen. For then inhomogeneous strains will develop near the grips and low angle boundaries will form most readily here.

§ 3. Spread of the Crack: Approximate Treatment

We shall now accept that cracks can be initiated in the manner discussed above and consider the conditions under which they will grow; the stress at which this occurs will determine the strength of the crystal.

When a wall of dislocations divides into two, the dislocations on either side of the division will attract each other and so oppose the separation of the two parts of the wall. If the distance between these parts is x the number of dislocations in each which interact is of order x/h, where h is the spacing of the dislocations in the wall. There are thus $(x/h)^2$ pairs of dislocations each interacting with a force of about $Gb^2/2\pi x$, and so the

resulting force tending to reunite the wall is $Gb^2x/2\pi h^2 = G\theta^2 x/2\pi$, with $\theta = b/h$ the misorientation across the wall. If the applied load produces a resolved shear stress σ_s and so a force $\sigma_s b$ on each dislocation, the total force on a wall of length L is $\sigma_s b(L/h) = \sigma_s L\theta$. Hence the two parts of the wall will attain an equilibrium separation x given by

$$G\theta x/2\pi = \sigma_s L. \quad . \quad . \quad . \quad . \quad . \quad . \quad . \quad . \quad (1)$$

Now consideration of the geometry of fig. 1 shows that, as far as its effect in causing the crack to spread is concerned, the divided wall is equivalent to a wedge of thickness θx driven into the cleavage plane; such a wedge may be shown (Stroh 1954) to produce a crack of length

$$c = (\theta x)^2 G/8\pi\gamma, \quad . \quad . \quad . \quad . \quad . \quad . \quad . \quad . \quad (2)$$

where γ is the energy per unit area of the new surfaces formed. On substituting for θx from (1), this becomes

$$c = \pi\sigma_s{}^2 L^2/2\gamma G. \quad . \quad . \quad . \quad . \quad . \quad . \quad . \quad . \quad (3)$$

Once it has formed the crack will be subjected to the normal component σ_n of the applied stress which will extend it in the manner considered by Griffith (1920); the condition that a crack of length c should spread catastrophically is then

$$\sigma_n{}^2 c = 8\gamma G/\pi. \quad . \quad . \quad . \quad . \quad . \quad . \quad . \quad . \quad (4)$$

From (3) and (4) we obtain the condition for fracture of the material as

$$\sigma_s \sigma_n L = 4\gamma G/\pi. \quad . \quad . \quad . \quad . \quad . \quad . \quad . \quad . \quad (5)$$

This equation which constitutes our main result will be discussed in § 5. The derivation which has just been given, however, involves a number of simplifying approximations which have been made so that the physical ideas involved will not be obscured by purely mathematical complexities. We therefore reconsider the argument in the following section under less restrictive assumptions.

§ 4. Spread of Crack: More Exact Treatment

Our previous treatment was deficient in two respects which will be remedied here. First, various approximations were introduced which result in the constant on the right-hand side of eqn. (5) being incorrect by a numerical factor. Secondly, the material was assumed to be elastically isotropic which will certainly not be the case for single crystals. As we shall be particularly interested in the variation of the strength with crystal orientation, we wish to be sure that no errors are introduced by neglecting the anisotropy of the crystal. Though in this paper we shall confine our discussion of experimental results to those for zinc, we shall not assume hexagonal symmetry, but consider the general triclinic case. In this way our equations will be directly applicable to other crystals when experimental results for these become available. This will not complicate

the treatment in any way. The main approximation which remains is that we assume that, after the dislocation wall has divided, its two parts are plane; in fact they are likely to curve slightly under their mutual attraction.

A general discussion of some problems in anisotropic elasticity has been given by Stroh (1958) and we follow here the treatment and notation of that paper, referring to it for fuller details. We take x_3 axis parallel to the dislocation lines so that the stresses depend only on x_1 and x_2, and introduce three complex variables $z_\alpha = x_1 + p_\alpha x_2$, $(\alpha = 1, 2, 3)$ and their complex conjugates $\bar{z}_\alpha = x_1 + \bar{p}_\alpha x_2$; p_α and $\bar{p}_\alpha$ are defined as the roots of a certain sextic equation whose coefficients are the elastic constants. We shall also need a set of complex constants $L_{i\alpha}$ $(i, \alpha = 1, 2, 3)$ which depend on the elastic constants, and we denote the reciprocal of the matrix $[L_{i\alpha}]$ by $[M_{\alpha i}]$. d_i are the components of a real vector which is essentially the product of an elastic modulus and the Burgers vector. All these constants will be eliminated from our final equations and we do not need here to know their precise values. It may be shown that three of the components of the stress field due to a dislocation lying along the x_3 axis are

$$\sigma_{i2} = (1/4\pi) \sum_\alpha (L_{i\alpha} z_\alpha^{-1} M_{\alpha j} + \bar{L}_{i\alpha} \bar{z}_\alpha^{-1} \bar{M}_{\alpha j}) d_j, \quad . \quad . \quad . \quad . \quad (6)$$

where we have used the convention that a repeated Latin suffix is to be summed. (Summation over Greek suffices will always be indicated explicitly as in eqn. (6).) The stress components not included in (6) will not be needed here.

We have now to sum the stresses (6) over all the dislocations in the divided wall, the position of which we suppose is given by $x_1 = 0$, $x_2 < 0$ and $x_1 = x$, $x_2 > 0$. In finding the stress at a point $P(x_1, x_2)$ at a distance from the wall large compared with the spacing h between the dislocations we may replace the summation by an integration. Then considering the part of the wall $x_1 = 0$, $x_2 < 0$, we see that the factor z_α^{-1} in (6) must be replaced by

$$\frac{1}{h} \int_{-L'}^{0} \frac{d\eta}{x_1 + p_\alpha (x_2 - \eta)} = -\frac{1}{p_\alpha h} \log (x_1 + p_\alpha x_2) + \frac{1}{p_\alpha h} \log p_\alpha L' + \frac{\pi i}{p_\alpha h},$$

if the length L' of this section of the wall is large. In the same way we obtain from the section of the wall of length L in the plane $x_1 = x$, a contribution of

$$\frac{1}{p_\alpha h} \log (x_1 - x + p_\alpha x_2) - \frac{1}{p_\alpha h} \log p_\alpha L;$$

and taking both sections of the wall together we see that z_α^{-1} in (6) must be replaced by

$$(p_\alpha h)^{-1} \log (z_\alpha - x)/z_\alpha - (p_\alpha h)^{-1} \log (L'/L) + \pi i / p_\alpha h \quad . \quad . \quad . \quad (7)$$

to give the stress of the whole wall. Now we specify that the wall is to be a simple tilt boundary. Such a wall, when undivided, produces no remote stress field; hence the stresses we obtain must vanish when $x = 0$, and so

the terms independent of x in (7) can give no contribution to the stress. Dropping these terms we obtain from (6) and (7) the stresses due to the divided wall

$$\sigma_{i2} = (1/4\pi h) \sum_{\alpha} \{ L_{i\alpha} M_{\alpha j} p_\alpha^{-1} \log (z_\alpha - x)/z_\alpha + \bar{L}_{i\alpha} \bar{M}_{\alpha j} \bar{p}_\alpha^{-1} \log (\bar{z}_\alpha - x)/\bar{z}_\alpha \} d_j. \quad . \quad . \quad . \quad (8)$$

The force on each dislocation of the wall due to the remainder is $b\sigma_{12}$, and the total force on one section of the wall is obtained by summing the forces on all the dislocations composing it. Replacing as before the summation by an integration, we find the attractive force between the two parts of the wall is

$$F = (b^2 x/2\pi h^2)\{\mu_1(1 + \log (L/x)) + \mu_2\}, \quad . \quad . \quad . \quad . \quad . \quad . \quad . \quad . \quad (9)$$

where

$$\mu_1 = \tfrac{1}{2} \sum_{\alpha} (L_{2\alpha} p_\alpha^{-1} M_{\alpha j} + \bar{L}_{2\alpha} \bar{p}_\alpha^{-1} \bar{M}_{\alpha j}) d_j/b, \quad . \quad . \quad . \quad . \quad . \quad (10)$$

and

$$\mu_2 = \tfrac{1}{2} \sum_{\alpha} (L_{2\alpha} p_\alpha^{-1} \log p_\alpha M_{\alpha j} + \bar{L}_{2\alpha} \bar{p}_\alpha^{-1} \log \bar{p}_\alpha \bar{M}_{\alpha j}) d_j/b\,; \quad . \quad (11)$$

in obtaining this, we have used the result that the constants are related by $L_{1\alpha} + p_\alpha L_{2\alpha} = 0$. Since d_j is proportional to b, μ_1 and μ_2 depend only on the elastic constants of the crystal. The force due to the applied stress separating the two parts of the wall is $\sigma_s bL/h$ and on equating this to F, eqn. (9) shows that the equilibrium separation x is given by

$$x\{\mu_1(1 + \log L/x) + \mu_2\} = 2\pi h L \sigma_s/b. \quad . \quad . \quad . \quad . \quad (12)$$

Now suppose that a crack has been formed in the plane $x_2 = 0$ by the stresses of the dislocations as in fig. 1. The normal stress σ_{22} across this plane is from eqn. (8) and (10)

$$\sigma_{22} = (b\mu_1/2\pi h) \log |(x_1 - x)/x_1|. \quad . \quad . \quad . \quad . \quad . \quad (13)$$

We choose as unit of length half the length of the crack, so that the crack extends from $x_1 = 0$ to $x_1 = 2$. Stroh (1958) has shown that the stresses near the tip of the crack $x_1 = 2$ under a variable stress σ_{22} are the same as if a uniform tension

$$T_2 = \pi^{-1} \int_0^2 \sigma_{22} x_1^{1/2} (2 - x_1)^{-1/2} dx_1 \quad . \quad . \quad . \quad . \quad . \quad (14)$$

acted on the crack. Substituting (13) in (14) we find that in the present case the mean tension is

$$T_2 = b\mu_1 x/2\pi h,$$

or if the crack has length $2c$ the effective tension on it is

$$T = \sigma_{\prime\prime} + b\mu_1 x/2\pi hc. \quad . \quad . \quad . \quad . \quad . \quad . \quad . \quad . \quad (15)$$

where the normal component $\sigma_{\prime\prime}$ of the applied stress has now been added.

We assume that the spread of the crack depends only on the tensile component of the stress at its tip, and this is completely determined by T. To ascertain the value of T for which the crack will spread we follow Griffith (1920), and consider the energy of a crack of length $2c$ under a

uniform tension T. The elastic energy is $\frac{1}{2}\pi B_{22}T^2c^2$, where B_{22} depends on the elastic constants of the material, and so, on adding the surface energy, the total energy of the crack is

$$W = -\tfrac{1}{2}\pi B_{22}T^2c^2 + 4\gamma c.$$

The condition $dW/dc = 0$ for the critical size of the crack, gives

$$Tc^{1/2} = (4\gamma/\pi B_{22})^{1/2}. \quad . \quad . \quad . \quad . \quad . \quad . \quad . \quad (16)$$

On substituting (15), we see that our cracks will just be able to extend if

$$\sigma_n c^{1/2} + b\mu_1 x/2\pi h c^{1/2} = (4\gamma/\pi B_{22})^{1/2}; \quad . \quad . \quad . \quad . \quad (17)$$

but if the left-hand side of this equation is less than the right-hand side growth of the crack will increase the energy of the system and so cannot occur. The left-hand side is a minimum when $c = b\mu_1 x/2\pi h\sigma_n$, and on substituting this value in (17) the condition that the crack can grow at every stage becomes

$$b\mu_1 x\sigma_n/h = 2\gamma/B_{22}. \quad . \quad . \quad . \quad . \quad . \quad . \quad . \quad (18)$$

Finally eliminating x between eqns. (12) and (18), we obtain

$$\sigma_s\sigma_n L = (\gamma/\pi B_{22})\{\log(\mu_1\theta/\sigma_s) + \delta\}, \quad . \quad . \quad . \quad . \quad . \quad (19)$$

where $\delta = 1 + \mu_2/\mu_1$: this equation may be regarded as the more precise form of eqn. (5).

The constant δ may be shown to be zero for an isotropic material; generally it will be small compared with the logarithmic term and so may be neglected. Then μ_1 appears only in the argument of a logarithm and it is sufficient to know it in order of magnitude, which will be that of an elastic modulus. Thus the elastic constant of the material enter eqn. (19) essential only through B_{22}. The general relation between B_{22} and the elastic constants is fairly complicated, though B_{22} may always be calculated numerically by a straightforward procedure (Stroh 1958). For hexagonal metals

$$B_{22} = -(s_{11}s_{33} - s_{13}^2)s_{11}^{-1}\mathscr{I}(p_1^{-1} + p_2^{-1}), \quad . \quad . \quad . \quad (20)$$

where p_1 and p_2 are the two roots with positive imaginary part of

$$p^4(s_{11}^2 - s_{12}^2) + p^2(s_{11}s_{44} + 2s_{11}s_{13} - 2s_{13}^2) + s_{11}s_{33} - s_{13}^2 = 0. \quad (21)$$

In these expressions s_{MN} are the elastic coefficients referred to the conventional axes, i.e. with the x_3 axis along the hexagonal axis, and not to the axes used elsewhere in this paper.

§ 5. Comparison with Experiment

In order to put eqn. (19) in a form more suitable for comparison with the experimental results we make a few minor modifications. If the crystal has diameter D the greatest value of L which we can obtain is $D/\cos\chi$ where χ is the angle the specimen axis makes with the slip plane; since large values of L give the weakest crystals it is this value of L which will determine the strength. Also, in the previous section it was assumed that the dislocations were free to move under any stress no matter how small; in fact there will be a resistance to the motion, due to intersecting dislocations, impurities, the Peierls–Nabarro force etc. We may allow

for this by taking the effective shear stress on a dislocation to be not σ_s but $\sigma_s - \sigma_0$ where σ_0 is a constant stress which measures the resistance to the motion.

Then eqn. (19) may be written

$$\sigma_s - \sigma_0 = k \cos \chi / \sigma_n, \quad . \quad . \quad . \quad . \quad . \quad . \quad . \quad . \quad (22)$$

where

$$k = (\gamma / \pi B_{22} D) \log (\mu_1 \theta / \sigma_s). \quad . \quad . \quad . \quad . \quad . \quad . \quad . \quad (23)$$

If we neglect a small variation due to the logarithm we may regard k as a constant and independent of the crystal orientation. For a given crystal orientation σ_s and σ_n are readily calculated from the applied tensile stress and so (22) expresses the variation of the crystal strength with orientation. The comparison with experiment can most conveniently be made

Fig. 4

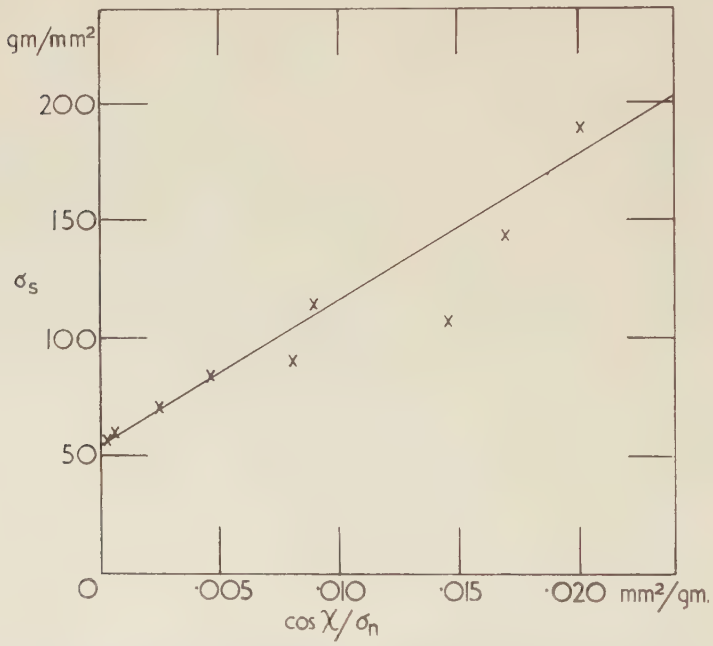

Variation of strength with orientation. Experimental values for zinc due to Deruyttere and Greenough (1956).

by plotting σ_s against $\cos \chi / \sigma_n$. Deruyttere and Greenough's results (1956) for zinc shown in fig. 4 agree with the linear relation predicted by eqn. (22). Similar results for bismuth have been obtained by Vickers (1958) and will be published elsewhere. From the slope of the line in fig. 4 we obtain a value of k equal to $6{\cdot}2 \times 10^3 \, (\mathrm{g/mm^2})^2$ which is in reasonable agreement with the value $8{\cdot}1 \times 10^3 \, (\mathrm{g/mm^2})^2$ calculated from eqn. (23).

The intercept in fig. 4 gives a value of σ_0 of $55 \, \mathrm{g/mm^2}$. The axis corresponds to crystals with their basal planes normal to the stress axis and for

such crystals the ductility tends to zero. Crystals in other orientations have an observable ductility and for these the flow stress was found to be independent of the orientation; the initial flow stress of Deruyttere and Greenough's crystals was 55 g/mm², agreeing with the value of σ_0.

When the basal plane is nearly perpendicular to the stress axis ($\chi \simeq 90°$) the resolved shear stress σ_s is small compared with the tensile stress; or, since σ_s must be at least equal to σ_0 before the dislocations can move and fracture can occur, the strength of the crystal will be large in these orientations. This is in accord with the observation of Gilman (1957) who obtained a fracture stress as high as 4500 g/mm² for a zinc crystal with $\chi = 89°$. In this orientation σ_n will be large and eqn. (22) reduces to the simple condition that $\sigma_s = \sigma_0$, or fracture occurs as soon as the dislocations can move. Using the value of $\sigma_0 = 55$ g/mm obtained above we estimate the strength when $\chi = 89°$ to be 3000 g/mm². Since this value depends very sensitively on the orientation this is as good agreement with Gilman's result as we can expect ($\chi = 89° 15'$ would give exact agreement); it shows, however, that our model is able to account for the high stresses he observes.

We are also able to understand from our model the variation of ductility with orientation observed by Deruyttere and Greenough (1956). We have seen that when $\chi \simeq 90°$, cleavage occurs as soon as the dislocations can move, so the ductility tends to zero in this orientation. For other values of χ, plastic flow will occur as soon as the applied stress is such that $\sigma_s = \sigma_0$, but according to eqn. (22), cleavage will not occur until σ_s and the applied tensile load have increased; hence plastic flow must take place to work-harden the metal before fracture can occur, and a finite ductility is observed.

§ 6. Polycrystals

If the model which has just been developed is accepted for single crystals, it is natural to ask whether the same mechanism can occur in polycrystals. However, this mechanism becomes more difficult in a polycrystal since the constraint of the surrounding grains will oppose the movement of a subgrain boundary across a grain; while, on the other hand, it is the very presence of the grain boundaries that provides the obstacles which make a piled-up group mechanism possible. Thus it may well be that different mechanisms operate in single and polycrystals. It might be possible to decide between these two mechanisms for polycrystals by considering the variation of fracture strength σ with grain diameter d. On the model of this paper we obtain (taking the length L of eqn. (19) proportional to d)

$$(\sigma - \sigma_0)\sigma = k' d; \quad . \quad . \quad . \quad . \quad . \quad . \quad . \quad . \quad . \quad (24)$$

this law has also been proposed recently by Cottrell (1958) from a different model. The model based on piled-up groups of dislocations gives

$$(\sigma - \sigma_0)^2 = k' d. \quad . \quad . \quad . \quad . \quad . \quad . \quad . \quad . \quad . \quad (25)$$

Equations (24) and (25) agree provided the constant stress σ_0 is small; this is the case for zinc (Greenwood and Quarrel 1954). However in the case of magnesium the experimental values (Hauser *et al.* 1956) seem to fit eqn. (25) better than eqn. (24) suggesting that piled-up groups are responsible for fracture here.

Acknowledgment

I wish to thank Dr. A. R. Entwisle for a number of helpful discussions.

References

Cottrell, A. H., 1958, *Amer. Inst. min. (metall.) Engrs* (Inst. Met. Div., Annual Lecture).

Deruyttere, A., and Greenough, G. B., 1956, *J. Inst. Metals*, **84**, 337.

Friedel, J., 1956, *Les Dislocations* (Paris: Gauthier-Villars).

Gilman, J. J., 1954, *Trans. Amer. Inst. min. (metall.) Engrs*, **200**, 621; 1957, *Amer. Inst. min. (metall.) Engrs* (Inst. Met. Div., Fall Meeting).

Greenwood, G. W., and Quarrel, A. G., 1954, *J. Inst. Metals*, **82**, 551.

Griffith, A. A., 1920, *Phil. Trans.* A, **221**, 163.

Hauser, F. E., Landon, P. R., and Dorn, J. E., 1956, *Trans. Amer. Inst. min. (metall.) Engrs*, **206**, 589.

Orowan, E., 1954, *Dislocations in Metals*, Ed. M. Cohen (New York: Amer. Inst. min. (metall.) Engrs), p. 69,

Stroh, A. N., 1954, *Proc. roy. Soc.* A., **223**, 404; 1957, *Advanc. Phys.*, **6**, 418; 1958, *Phil. Mag.*, **3** (in the press).

Vickers, W., 1958 (to be published).

Intensity Calculation of Some Optical Absorption Lines in Hydrated Manganous Salts†

By S. Koide‡ and M. H. L. Pryce
H. H. Wills Physics Laboratory, University of Bristol

[Received March 14, 1958]

Abstract

The ligand field theory is applied to the hydrated manganous salts. The splitting of the degenerate levels of $^4A_{1g}$ and ^4E_g is first investigated, and then the intensities of the transitions from the ground sextet $^6A_{1g}$ to these levels are calculated. The properties of the odd vibrations responsible for these transitions are also discussed. It is found that the calculated oscillator strengths are in good agreement with experiment if an appropriate model is used for the vibrations.

§ 1. Introduction

It is now generally admitted that the optical absorption spectra of inorganic complex ions are interpreted as transitions between the various d^n or f^n electronic configurations of the metallic ions involved, and, so far as the so-called ionic complexes are concerned, general features of these spectra are explained fairly well by the ligand field theory (Moffit and Ballhausen 1956, Jørgensen 1957). The probabilities of these transitions are very small because initial and final states have the same parity in the case of free ions. Though it is well established qualitatively that these transitions are electric dipole ones caused by the odd vibrations of the complexes Van (Vleck 1937, Broer *et al.* 1945, Satten 1957), as to the quantitative calculation of the intensities there is only the recent work of Liehr and Ballhausen (1957) for Ti (III) and Cu (II) complexes which can be treated as one-electron systems.

In various complexes of the first transition group elements, $Mn^{2+}(3d^5)$ complexes are rather special because all absorption lines correspond to spin forbidden intersystem transitions and the intensities are quite small. This is due to the fact that the ground state $^6A_{1g}$ is the only sextet obtained from the $3d^5$ configuration. To explain the spectra, therefore, it is necessary to take the spin–orbit interaction into account. There are two approaches in the calculation based on the ligand field theory. In the *weak field* scheme, energy levels of the free ions are first determined by taking account of the Coulomb interactions between electrons, and the ligand field is regarded as giving rise to the mixing of these free ion states and to

† Communicated by the Authors.

‡ Permanent address: Institute of Physics, College of General Education, University of Tokyo.

cause the change of level structure. Orgel's calculation (Orgel 1952) is based on this point of view. In most part of the present paper, however, we shall adopt the so-called *strong field* scheme extensively developed by Tanabe and Sugano (1954). According to this model, the field acting on each electron is considered to be of cubic symmetry. The fivefold orbital degeneracy of d-electrons is lifted in such a field, and we get the lower triplet $d\epsilon$ orbits of T_{2g} symmetry and the upper doublet $d\gamma$ orbits of E_g symmetry. After accommodating the electrons in these orbits, we introduce the Coulomb interactions. The energy differences between $d\epsilon$ and $d\gamma$ orbits, usually denoted by Δ or $10Dq$, is considered to express the measure of the strength of the ligand field. Both approaches eventually lead to the same result. Figure 1 shows the positions of the lowest quartet levels as functions of the parameter Δ in the case of cubic ligand field.

Fig. 1

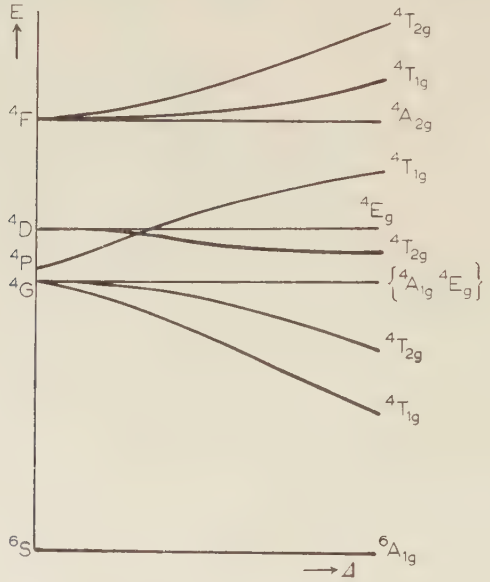

It is easily seen that the transitions in which electrons jump from $d\epsilon$ to $d\gamma$ or vice versa correspond to the transitions between curves with different slopes in this Orgel diagram. Such transitions are usually observed as broad bands or complex patterns consisting of numerous lines. This may be interpreted as the result of excitation of even vibrations due to the change of ionic radius, because the charge cloud makes appreciable change in such electronic transitions.

To avoid inessential complexity, therefore, we shall restrict our attention to the transitions from ground state $^6A_{1g}$ to the levels of $^4A_{1g}$ and ^4E_g which are degenerate in the cubic field and henceforth denoted by $\{^4A_{1g}; {}^4E_g\}$. These are transitions between the $d\epsilon^3 d\gamma^2$ configuration, and

are observed as a narrow band in the spectra obtained at not very low temperatures (Jorgensen 1954, Holmes and McClure 1957). Recent experiment carried out by Pappalardo (1957) at very low temperatures has revealed the existence of fine structure of this band, which gives us some information about the detailed mechanism of the transitions. The aim of the present calculation is to clarify the mechanism by analysing this fine structure quantitatively.

§ 2. Wave Functions in the Case of Cubic Field

We shall start from the Mn^{2+} ion placed in a cubic field. Explicit forms of the wave functions can be easily written out by following Tanabe and Sugano's (1954) scheme. Let the three $d\epsilon$ and the two $d\gamma$ functions be denoted by ξ, η, ζ and u, v. Angular variations of these functions are of the forms yz/r^2, zx/r^2, xy/r^2, $(3z^2-r^2)/r^2$ and $(x^2-y^2)/r^2$ respectively. Then the wave functions of the states under consideration are, apart from the closed shell configuration, expressed as follows.

$^6A_{1g}$: $d\epsilon^3(^4A_{2g})d\gamma^2(^3A_{2g})$ ground states

$$|^6A_{1g}(5/2)\rangle = [\xi\eta\zeta uv] \quad . \quad . \quad . \quad . \quad . \quad . \quad (2.1)$$

$^4A_{1g}$: $d\epsilon^3(^4A_{2g})d\gamma^2(^3A_{2g})$

$$|^4A_{1g}(3/2)\rangle = \{3([\xi\eta\zeta u\bar{v}]+[\xi\eta\zeta\bar{u}v]) - 2([\bar{\xi}\eta\zeta uv]+[\xi\bar{\eta}\zeta uv]+[\xi\eta\bar{\zeta}uv])\}/\sqrt{30} \quad . \quad . \quad . \quad . \quad (2.2)$$

^4E_g: $d\epsilon^3(^2E_g)d\gamma^2(^3A_{2g})$ and $d\epsilon^3(^4A_{2g})d\gamma^2(^1E_g)$

$$|^4E_g^{(1)}(3/2)\rangle = \frac{\alpha}{\sqrt{6}}\{2[\xi\eta\bar{\zeta}uv]-[\bar{\xi}\eta\zeta uv]-[\xi\bar{\eta}\zeta uv]\} + \frac{\beta}{\sqrt{2}}\{[\xi\eta\zeta u\bar{v}]-[\xi\eta\zeta\bar{u}v]\} \quad . \quad . \quad . \quad . \quad (2.3a)$$

$$|^4E_g^{(2)}(3/2)\rangle = \frac{\alpha}{\sqrt{2}}\{[\bar{\xi}\eta\zeta uv]-[\xi\bar{\eta}\zeta uv]\} + \frac{\beta}{\sqrt{2}}\{[\xi\eta\zeta u\bar{u}]-[\xi\eta\zeta v\bar{v}]\}. \quad . \quad . \quad . \quad . \quad (2.3b)$$

For simplicity, here we mention only the states with maximum M_s values which are shown in the parentheses, and each of the square bracket notations stands for a normalized Slater determinant obtained by accommodating electrons into the orbitals mentioned in such a way that the spin of electrons in the orbitals without upper bar is up and with bar is down. The coefficients α and β are

$$\alpha=(4/7)^{1/2} \quad \text{and} \quad \beta=(3/7)^{1/2}. \quad . \quad . \quad . \quad . \quad . \quad (2.4)$$

If we choose $\alpha=(3/7)^{1/2}$ and $\beta=-(4/7)^{1/2}$, we get the wave functions of the upper ^4E_g states from ^4D of the free ion which we will denote by $^4E_g{}^*$ in the following.

The states $^4A_{1g}$ and $^4E_g^{(1)}$ and $^4E_g^{(2)}$ have the same energy $10B+5C$ measured from the ground state $^6A_{1g}$, where $B=F_2-5F_4$ and $C=35F_4$

are Racah's parameters and are considered to be measures of the Coulomb repulsion between electrons. If we adjust these parameters so that the calculated energy values of $^4A_{1g}$, $^4T_{1g}$ and $^4T_{2g}$ agree with the experimental ones 25 000, 18 800 and 23 000 cm^{-1} respectively (Holmes and McClure 1957), it turns out to be necessary to put $C/B = 4$ and $\Delta/10 \simeq B \simeq 800\,cm^{-1}$.

For the sake of calculation in the following sections, we shall here determine the wave functions of the $^4T_{1g}$ states. By solving the three-dimensional secular equation of the energy matrix for $^4T_{1g}$ states given by Tanabe and Sugano, with the values $B = 800\,cm^{-1}$, $C = 3200\,cm^{-1}$, $\Delta = 8000\,cm^{-1}$, we can determine the coefficients λ_n, μ_n and ν_n of the wave functions

$$|^4T_{1g}{}^{(nz)}(3/2)\rangle = \lambda_n[\xi\eta\zeta\bar{\zeta}u] + \frac{\mu_n}{\sqrt{2}}\{[\xi\bar{\xi}\zeta uv] + [\eta\bar{\eta}\zeta uv]\} + \nu_n[\xi\eta uv\bar{v}] \qquad (2.5)$$

as follows.

Table 1.

n	Energy in cm^{-1} measured from $^6A_{1g}$	λ_n	μ_n	ν_n
1	18 950	0·977	0·144	−0·156
2	34 200	0·040	0·597	0·801
3	42 700	−0·208	0·788	−0·580

Two other components $|^4T_{1g}{}^{(nx)}\rangle$ and $|^4T_{1g}{}^{(ny)}\rangle$ of each triply degenerate orbital state are easily obtained by appropriate transformation of the coordinate axes.

In some calculations, it is more convenient to express the wave functions in terms of the *weak field language*. Since $^4A_{1g}$ and the lower ^4E_g states come from the ^4G states of the free ion and they do not couple with other multiplets through the cubic field, we can express the wave functions of these states by linear combinations of the M_L eigenfunctions $|M_L\rangle$ of the ^4G states. The explicit forms are as follows:—

$$|^4A_{1g}\rangle = (7/12)^{1/2}|\,0\,\rangle + (5/24)^{1/2}\{|\,4\,\rangle + |-4\rangle\} \quad . \quad (2.6)$$

$$|^4E_g{}^{(1)}\rangle = (5/12)^{1/2}|\,0\,\rangle - (7/24)^{1/2}\{|\,4\,\rangle + |-4\rangle\} \quad . \quad (2.7\,a)$$

$$|^4E_g{}^{(2)}\rangle = (1/2)^{1/2}\{|\,2\,\rangle + |-2\rangle\}. \quad . \quad . \quad . \quad . \quad . \quad . \quad (2.7\,b)$$

§ 3. Splitting of the Levels

The level structure shown in fig. 1 is obtained by neglecting the non-cubic components of the ligand field and the spin-dependent forces. If we take the effects of these forces into account, the degeneracy of the energy levels may be partly removed, and it gives rise to fine structure in the absorption spectra. In this section, we shall consider the effects of these perturbations on the energy levels under consideration.

Recently it has been shown that an appreciable amount of covalencies exist even in the so-called ionic complexes (Owen 1955). This effect is especially noticeable for $d\gamma$ electrons because the overlap of $d\gamma$ orbitals with the ligands is larger than that of the $d\epsilon$ orbitals. We shall, therefore, examine the influence of the difference of covalencies between $d\gamma$ and $d\epsilon$ orbitals on the splitting of the energy level $\{^4A_{1g}; {}^4E_g\}$.

3.1. *Spin–Orbit and Spin–Spin Interactions*

From eqns. (2.6) and (2.7) it is easily seen that the spin–orbit interaction, which is expressed by $\lambda \mathbf{L}.\mathbf{S}$ for the $(2L+1)(2S+1)$ states with given L and S, has no matrix element within each of the manifolds $^6A_{1g}(^6S)$ and $\{^4A_{1g}; {}^4E_g\}(^4G)$. Therefore, the changes of energy by this spin–orbit interaction are given by the second order perturbation terms:

$$\delta E_a \simeq \sum_b \frac{|\langle a|\zeta \sum_i \mathbf{l}_i.\mathbf{s}_i|b\rangle|^2}{\Delta E_{ab}}. \quad . \quad . \quad . \quad . \quad . \quad (3.1)$$

Since $\Delta E_{ab} \simeq 10^4\,\mathrm{cm}^{-1}$ and $\zeta \simeq 300\,\mathrm{cm}^{-1}$, splittings δE_a have the order of magnitude $10^1\,\mathrm{cm}^{-1}$, which can hardly be detected by the experiments.

Usually the first order effect of the spin–spin interaction has the same order of magnitude as the second order one of the spin–orbit interaction. In an (L, S) term, the spin–spin interaction is given by the expression (Pryce 1950 *a*, *b*)

$$-\rho\{(\mathbf{L}.\mathbf{S})^2+\tfrac{1}{2}(\mathbf{L}.\mathbf{S})-\tfrac{1}{2}L(L+1)S(S+1)\}. \quad . \quad . \quad . \quad (3.2)$$

From the spectra of free Mn^{2+} ion (Moore 1952), the coefficient is found to be $\rho = 0{\cdot}334\,\mathrm{cm}^{-1}$. Though the operator $\rho(\mathbf{L}.\mathbf{S})^2$ has matrix elements between the twelve states of $\{^4A_{1g}; {}^4E_g\}$, splittings caused by this perturbation are shown to be at most of order $25\rho \simeq 8\,\mathrm{cm}^{-1}$.

3.2. *Effects of Covalency*

We shall consider the effects of covalency only for the $d\gamma$ electrons. In the simple molecular orbital treatment, this effect is taken into account by describing each of the electron orbitals as a proper linear combination of the $d\gamma$ and the ligand orbitals:

$$\cos\theta|3d\gamma\rangle + \sin\theta|\sigma\rangle, \quad . \quad . \quad . \quad . \quad . \quad . \quad (3.3)$$

where $|\sigma\rangle$ stands for an appropriate linear combination of the σ-orbitals of the ligands.

Since the greater part of the contribution of the interelectronic Coulomb repulsion comes from the charge clouds in the proximity of the nucleus of the central atom, it may be a reasonable approximation in the evaluation of the Coulomb and exchange integrals to replace the radial part of the $d\gamma$ orbitals by $\cos\theta$ times of the original one and neglect the contribution from the second term of (3.3). In this approximation, Tanabe and

Sugano's energy matrices of the relevant levels (Tanabe and Sugano 1954, I, p. 764) are modified as follows:

$^4E_g(^4D, {}^4G)$

$d\epsilon^3(^2E_g)d\gamma^2(^3A_{2g})$	$9B_0+3C_0+4B'+2C'$	$-2\sqrt{3}B'$
$d\epsilon^3(^4A_{2g})d\gamma^2(^1E_g)$	$-2\sqrt{3}B'$	$6B'+3C'+8B''+2C''$

$^4A_{1g}(^4G): d\epsilon^3(^4A_{2g})d\gamma^2(^3A_{2g})$ $\quad 10B'+5C'$, . . . (3.4)

where energy of the ground state $^6A_{1g}$ is chosen as zero, and $B'=B_0\cos^2\theta$, $B''=B_0\cos^4\theta$, $C'=C_0\cos^2\theta$ and $C''=C_0\cos^4\theta$.

Fig. 2

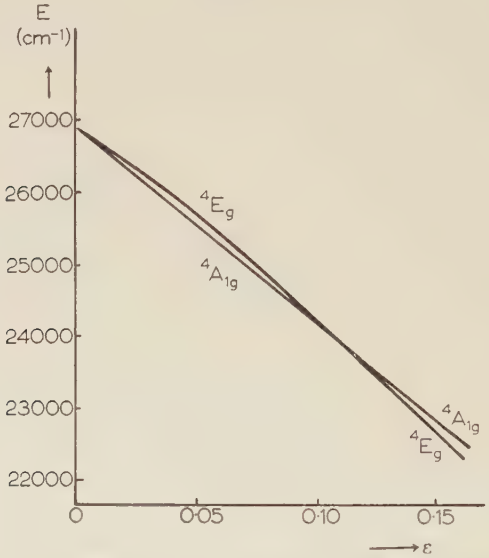

Variation of the energy levels as functions of the covalency parameter $\epsilon=1-\cos^2\theta$ is shown in fig. 2. Even in the case of the free ion, B_0 and C_0 cannot be determined so that all calculated spectral lines agree with experiment. Hence, we have assumed $C_0/B_0=4$ and used $B_0=900\,\mathrm{cm}^{-1}$ obtained from the $^4G\longleftrightarrow{}^6S$ separation $26\,900\,\mathrm{cm}^{-1}$ of the free ion in drawing fig. 2. From these curves, the covalency parameter ϵ is found to be about $0{\cdot}08\sim0{\cdot}10$, and, if our assumptions are not wrong, the $^4A_{1g}$ level is lower than the ^4E_g doubly degenerate one by about $100\,\mathrm{cm}^{-1}$.

Since $B\simeq800\,\mathrm{cm}^{-1}$ obtained in § 2 is regarded as some average of B_0, B' and B'', $B'\simeq800\,\mathrm{cm}^{-1}$ is a quite reasonable value. However, it is to be noted that this argument is valid only for the choice of the same ratio $C/B=C_0/B_0$.

3.3. *Distorted Field*

Since the crystal structure is known for only a few of the manganous salts, it is impossible to predict the level structure for each salt quantitatively from the theoretical point of view. However, it can be shown

group-theoretically that the trigonal field does not remove the two-fold degeneracy of the E levels. In this sense the trigonal distortion is rather special. We shall, therefore, treat here the effects of the rhombic distortion and see how it affects each of the three orbital states of our $\{^4A_{1g}; {}^4E_g\}$ level.

Let us assume the potential of the form

$$\text{where} \qquad \Delta V = \sum_{i=1}^{5} \Delta v(x_i, y_i, z_i) \qquad . \quad . \quad . \quad . \quad . \quad . \quad (3.5)$$

$$\Delta v(x,y,z) = A_2\left\{z^2 - \frac{1}{2}(x^2+y^2)\right\} + A_4\frac{\sqrt{3}}{4}(2z^4 - x^4 - y^4 + 12x^2y^2 - 6y^2z^2 - 6z^2x^2)$$
$$+ B_2\frac{\sqrt{3}}{2}(x^2-y^2) + B_4\frac{3}{4}(-6z^2x^2 + 6y^2z^2 + x^4 - y^4), \qquad . \quad (3.6\,a)$$

or

$$\sqrt{\frac{5}{4\pi}}\,\Delta v(r,\theta,\phi) = A_2 r^2 Y_2^{\,0} + A_4 r^4\left\{\sqrt{\frac{5}{12}}\,Y_4^{\,0} - \sqrt{\frac{7}{24}}\,(Y_4^{\,4} + Y_4^{-4})\right\}$$
$$+ B_2 r^2(Y_2^{\,2} + Y_2^{-2})/\sqrt{2} + B_4 r^4(Y_4^{\,2} + Y_4^{-2})/\sqrt{2}. \qquad . \quad . \quad (3.6\,b)$$

Then we get the following non-vanishing matrix elements related to the states $\{^4A_{1g}; {}^4E_g\}$:

$$\langle {}^4E_g^{(1)}|\Delta V|{}^4A_{2g}\rangle = -\frac{4\sqrt{3}}{7\sqrt{7}}\,B_2\langle r^2\rangle + \frac{6}{7\sqrt{7}}B_4\langle r^4\rangle \qquad . \quad . \quad (3.7)$$

and

$$\langle {}^4E_g^{(2)}|\Delta V|{}^4A_{2g}\rangle = \frac{4\sqrt{3}}{7\sqrt{7}}\,A_2\langle r^2\rangle + \frac{6}{7\sqrt{7}}\,A_4\langle r^4\rangle, \qquad . \quad . \quad (3.8)$$

where $^4A_{2g}$ is the state obtained by the configuration $d\epsilon^3({}^4A_{2g})d\gamma^2({}^1A_{1g})$ and comes from the ^4F states of the free ion. In the strong field representation, the wave function of this state is expressed as follows:

$$|{}^4A_{2g}(3/2)\rangle = \{[\xi\eta\zeta u\bar{u}] + [\xi\eta\zeta v\bar{v}]\}/\sqrt{2}, \qquad . \quad . \quad . \quad (3.9)$$

and its energy measured from the ground $^6A_{1g}$ is $22B+7C$ irrespective of the cubic field strength. So, if we apply the second order perturbation theory, the energy denominator common to both $^4E_g^{(1)}$ and $^4E_g^{(2)}$ is $12B+2C \simeq 20B \simeq 16\,000\ \mathrm{cm}^{-1}$.

This result shows that the $^4A_{1g}$ state is affected neither by tetragonal nor rhombic distortion and that if the distortion is tetragonal ($B_2 = B_4 = 0$) only the $^4E_g^{(2)}$ state is depressed. For the rhombic field, if we carry out a partial diagonalization using first order perturbed wave functions, we can eliminate the matrix elements between the $^4A_{2g}$ and the $\{^4E_g^{(1)}, {}^4E_g^{(2)}\}$ states and get the following Hamiltonian matrix for the perturbed ^4E_g states:

$$-(\Delta E_A)^{-1}\begin{pmatrix} |W_1|^2 & W_1W_2^* \\ W_1^*W_2 & |W_2|^2 \end{pmatrix}, \qquad . \quad . \quad . \quad . \quad (3.10)$$

where

$$W_1 = \langle {}^4A_{2g}|\Delta V|{}^4E_g^{(1)}\rangle$$
$$W_2 = \langle {}^4A_{2g}|\Delta V|{}^4E_g^{(2)}\rangle$$

and $$\Delta E_A = E({}^4A_{2g}) - E({}^4E_g^{(1)}) = E({}^4A_{2g}) - E({}^4E_g^{(2)}).$$

The eigenstates are, therefore, linear combinations of perturbed $^4E_g^{(1)}$ and $^4E_g^{(2)}$ states and their eigenvalues are 0 and $-(|W_1|^2+|W_2|^2)/\Delta E_A$. Hence only one of them is depressed by the rhombic field.

Although it is quite difficult to know the magnitudes of the parameters A and B even when the crystal structure is known, it may safely be concluded from work on the cobalt salts (Abragam and Pryce 1951) that the splittings due to the non-cubic components of the crystal field are much larger than those due to the effects mentioned in (1) and (2).

§ 4. Odd Vibrations

In those hydrated salts where the crystal structure is known, the manganous ion is at a centre of symmetry. Under these conditions electric dipole transitions between the levels we are considering can only take place with the excitation of one quantum (or an odd number) of an odd vibration.

Fig. 3

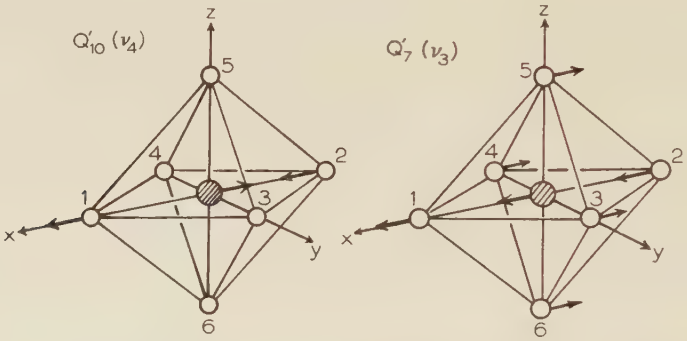

For the present purposes, it is a good approximation to regard each of the ligand molecules as a mass point because its internal molecular vibrations are in general of much higher frequencies. Then the problem is reduced to the vibrations of an octahedral XY_6 molecule. It is well known that the normal vibrations of this molecule can be classified into the modes of the symmetries $A_{1g}(1)$, $E_g(2)$, $T_{1u}(3)$, $T_{1u}(3)$, $T_{2g}(3)$ and $T_{2u}(3)$, where figures in the parentheses denote the degeneracies of the vibrations. The frequencies of these vibrations are usually denoted by ν_1, ν_2, ν_3, ν_4, ν_5 and $\nu_6(\nu_3<\nu_4)$ according to the above order.

Normal coordinates of the even vibrations A_{1g}, E_g and T_{2g} are given, for instance, in Van Vleck's paper (1939). For the present calculations, however, the normal coordinates of *odd* vibrations are necessary. Those of the T_{2u} vibrations can be readily obtained by symmetry consideration as

$$Q_{13}=(X_2+X_5-X_3-X_6)/2, \quad Q_{14}=(Y_3+Y_6-Y_1-Y_4)/2$$

and

$$Q_{15}=(Z_1+Z_4-Z_2-Z_5)/2. \quad . \quad . \quad . \quad . \quad . \quad . \quad (4.1)$$

It is easily seen that the x-components of the two T_{1u} vibrations are expressed by proper linear combinations of $(M_0/M)^{1/2}X_0$, $(X_1+X_4)/2$ and

$(X_2+X_3+X_5+X_6)/2$, where M and M_0 are the mass of a ligand and the central atom respectively. These must be orthogonal to each other and to the coordinate

$$Q_{16}=\{(M_0/M)X_0+(X_1+X_2+X_3+X_4+X_5+X_6)\}/(6+M_0/M)^{1/2} \quad (4.2)$$

of the translational motion in x-direction. The following set of the coordinates

$$Q_7'=\{4M_0^2/(M_0+2M)(M_0+6M)\}^{1/2}X_0+\{4M^2/(M_0+2M)(M_0+6M)\}^{1/2}$$
$$\times(X_1+X_4)-\{(M_0+2M)/4(M_0+6M)\}^{1/2}(X_2+X_3+X_5+X_6), \quad (4.3a)$$

and

$$Q_{10}'=\{2M_0/(M_0+2M)\}^{1/2}X_0-\{M_0/2(M_0+2M)\}^{1/2}(X_1+X_4) \quad (4.3b)$$

satisfies the conditions. In terms of these coordinates, the part of the vibrational potential energy which depends upon the x-components of the T_{1u} coordinates may be expressed as

$$U_{1u}=\tfrac{1}{2}(Q_7'\ Q_{10}')\begin{pmatrix}a & q\\ q & b\end{pmatrix}\begin{pmatrix}Q_7'\\ Q_{10}'\end{pmatrix}. \quad . \quad . \quad . \quad . \quad (4.4)$$

Actual normal modes Q_7 and Q_{10} are given by two such ortho-normal linear combinations of Q_7' and Q_{10}' that diagonalize this 2×2 matrix:

$$Q_7=Q_7'\cos\theta+Q_{10}'\sin\theta \quad \text{and} \quad Q_{10}=Q_7'\sin\theta-Q_{10}'\cos\theta. \quad (4.5)$$

To get the explicit expression of Q_7 and Q_{10}, therefore, we must make some assumptions as to the forces between constituents of the XY_6 molecules.

The simplest assumption which Liehr and Ballhausen (1957) adopted in their calculation is the so-called valence force model proposed by Wilson (Yost *et al.* 1934). In the following, for simplicity, we shall assume $M_0/M=3$, which is the ratio of the mass of Mn atom to that of a water molecule. Then in this model, our matrix is given by

$$\begin{pmatrix}\frac{18}{5}K_\alpha & \frac{12}{5}\sqrt{\frac{2}{3}}K_\alpha\\ \frac{12}{5}\sqrt{\frac{2}{3}}K_\alpha & \frac{5}{3}(K-2K_1)+\frac{16}{15}K_\alpha\end{pmatrix}, \quad . \quad . \quad (4.6a)$$

where K is the X–Y force constant, K_1 the interaction constant for the effect of extension of the X–Y bond, and K_α denotes the constant for the bending of the valence bonds.

Another typical assumption is the central field model. Let the mutual potential of the central X atom and a ligand Y be $f(r)$, and that between two ligands be $g(r)$. Then, for $M_0/M=3$ as before, we get

$$\begin{pmatrix}\frac{9}{5}g''+\frac{27}{20}\frac{f'}{R} & \frac{33}{20}\sqrt{\frac{2}{3}}\frac{f'}{R}-\frac{9}{5}\sqrt{\frac{2}{3}}g''\\ \frac{33}{20}\sqrt{\frac{2}{3}}\frac{f'}{R}-\frac{9}{5}\sqrt{\frac{2}{3}}g'' & \frac{5}{3}f''+\frac{6}{5}g''+\frac{7}{30}\frac{f'}{R}\end{pmatrix}, \quad . \quad (4.6b)$$

where R is the equilibrium X–Y distance, and

$$f'' = (d^2f/dr^2)_{r=R},\ f' = (df/dr)_{r=R} \text{ and } g'' = (d^2g/dr^2)_{r=\sqrt{2}R}.$$

The interaction between three pairs of opposite ligands, $3g(2R)$, has been neglected in deriving the matrix (4·6 *b*).

In the case of aquo-complexes, covalency of the forces is expected to be very small, so in the former model $K - 2K_1$ is much larger than K_γ. If we adopt the latter model and regard the six water molecules as dipoles of moment μ, we may put $g(r) = (3/2)\mu^2 r^{-3}$. Since the distance $\sqrt{2}\,R$ between two adjacent waters is larger than twice of the ionic radius of oxygen atom, exchange repulsion between water molecules is neglected in this expression. Then, using the equilibrium condition $f'(R) + \sqrt{2}^3 g'(\sqrt{2}R) = 0$, we get $f' = Rg''$ and the matrix (4·6 *b*) is reduced as

$$\begin{pmatrix} \frac{63}{20}g'' & -\frac{\sqrt{6}}{20}g'' \\ -\frac{\sqrt{6}}{20}g'' & \frac{5}{3}f'' + \frac{43}{30}g'' \end{pmatrix} . \quad . \quad . \quad . \quad (4.6\,b')$$

Thus, in both models, the off-diagonal elements are found to be quite small compared with the differences of diagonal elements. It is, therefore, reasonable to assume that Q_7' and Q_{10}' express the actual normal modes to a good approximation. In fact, the choice of normal modes by Liehr and Ballhausen corresponds to the very small θ of the expression (4.5).

In this approximation, the frequencies ν_3 and ν_4 are given by

$$M\lambda_3 = \begin{cases} \frac{18}{5}K_\alpha & \text{(valence force)} \quad (4.7\,a) \\ \frac{63}{20}g'' & \text{(central force)} \quad (4.7\,b) \end{cases}$$

$$M\lambda_4 = \begin{cases} \frac{5}{3}(K - 2K_1) + \frac{16}{15}K_\alpha & \text{(valence force)} \quad (4.8\,a) \\ \frac{5}{3}f'' + \frac{43}{30}g'', & \text{(central force)} \quad (4.8\,b) \end{cases}$$

where $\lambda_j = 4\pi^2\nu_j^2$. On the other hand, frequency of the T_{2u} vibration is given by

$$M\lambda_6 = \begin{cases} 2K_\alpha & \text{(valence force)} \quad (4.9\,a) \\ \frac{3}{4}g''. & \text{(central force)} \quad (4.9\,b) \end{cases}$$

So the ratio $\nu_6/\nu_3=(\lambda_6/\lambda_3)^{1/2}$ is

$$\frac{\nu_6}{\nu_3}=\begin{cases}0{\cdot}75 & \text{(valence force)} \quad (4.10a)\\ 0{\cdot}49. & \text{(central force)} \quad (4.10b)\end{cases}$$

For the sake of comparison, we shall give here the expressions for the frequencies ν_1, ν_2, ν_5 of the even vibrations as

$$\left.\begin{aligned} M\lambda_1&=\begin{cases}K+10K_1 & \text{(valence force)}\\ f''+4g'' & \text{(central force)}\end{cases}\\ M\lambda_2&=\begin{cases}K-2K_1 & \text{(valence force)}\\ f''-\dfrac{3}{4R}f'+g'' & \text{(central force)}\end{cases}\\ M\lambda_5&=\begin{cases}4K_\alpha & \text{(valence force)}\\ 2g''+\dfrac{1}{2R}f' & \text{(central force)}\end{cases}\end{aligned}\right\} \quad (4.11)$$

The perturbation responsible for the mixing of odd states is given by

$$H_v=\sum_{j=7}^{15}V_j\,.\,Q_j, \qquad V_j=(\partial V/\partial Q_j)_{Q=0}, \quad . \ . \ . \quad (4.12)$$

where V is the ligand field acting on the $3d$ electrons. This may be expressed in terms of the cartesian coordinates of the ligands as

$$H_v=V_{1x}(X_2+X_3+X_5+X_6-4X_0)+V_{2x}(X_1+X_4-2X_0)+V_{3x}Q_{13}+\ldots \quad (4.13)$$

where $$V_{jx}=\sum_i v_{jx}\,(x_i, y_i, z_i) \quad \text{etc.}, \quad . \ . \ . \ . \ . \ . \quad (4.14)$$

and x_i, y_i and z_i are the coordinates of i-th electron. V_j's in (4.12) are easily derived from V_{jx} etc. by using the relation between Q's and X's (4.3), or

$$X_2+X_3+X_5+X_6-4X_0=\frac{6}{\sqrt{5}}Q_7+\frac{4}{3}\sqrt{\frac{6}{5}}Q_{10} \quad (4.15a)$$

$$X_1+X_4-2X_0=\sqrt{\frac{10}{3}}\,Q_{10}. \quad . \ . \ . \ . \quad (4.15b)$$

as $$V_7=\frac{6}{\sqrt{5}}V_{1x} \quad \text{and} \quad V_{10}=\left(\frac{8}{5}V_{1x}+2V_{2x}\right)\sqrt{\frac{5}{6}}. \quad . \quad (4.16)$$

We shall assume here that the field V is due to the six point dipoles of moment μ vibrating about the equilibrium positions $(\pm R, 0, 0)$, $(0, \pm R, 0)$ and $(0, 0, \pm R)$ without changing their directions given by $(\pm 1, 0, 0)$,

$(0, \pm 1, 0)$ and $(0, 0, \pm 1)$ respectively. Then v_{1x}, v_{2x} and v_{3x} are written explicitly as follows:

$$\left.\begin{aligned} v_{1x} &= 3\mathscr{Y}_{11} + \frac{15}{8}(\sqrt{6}\,\mathscr{Y}_{31} - \sqrt{10}\,\mathscr{Y}_{33}) \\ &\quad + \frac{105}{16}\left(\frac{9}{\sqrt{15}}\,\mathscr{Y}_{51} + \frac{7}{\sqrt{70}}\,\mathscr{Y}_{53} + \frac{7}{\sqrt{14}}\,\mathscr{Y}_{55}\right), \\ v_{2x} &= -6\mathscr{Y}_{11} + 5(\sqrt{6}\,\mathscr{Y}_{31} - \sqrt{10}\,\mathscr{Y}_{33}) \\ &\quad - \frac{21}{4}\left(\sqrt{15}\,\mathscr{Y}_{51} - \sqrt{\frac{35}{2}}\,\mathscr{Y}_{53} + \sqrt{\frac{63}{2}}\,\mathscr{Y}_{55}\right), \\ v_{3x} &= -\frac{75}{4}\left(\sqrt{\frac{2}{3}}\,\mathscr{Y}_{31} + \sqrt{\frac{2}{5}}\,\mathscr{Y}_{33}\right) \\ &\quad + \frac{735}{8}\left(-\sqrt{\frac{1}{15}}\,\mathscr{Y}_{51} + \sqrt{\frac{1}{70}}\,\mathscr{Y}_{53} + \sqrt{\frac{1}{14}}\,\mathscr{Y}_{55}\right), \end{aligned}\right\} \tag{4.17}$$

where
$$\mathscr{Y}_{lm} = \sqrt{\frac{4\pi}{2l+1}}\,\frac{(-\mathrm{Y}_l^m + \mathrm{Y}_l^{-m})}{\sqrt{2}}\,\frac{e\mu r^l}{R^{l+3}} \quad (l, m = 1, 3, 5, \ldots). \tag{4.18}$$

§ 5. Calculation of the Intensities

For the sake of brevity, here we ignore the effects of the perturbations discussed in § 3, and use the wave functions given in § 2 as the unperturbed ones. Since electric dipole transitions between ground states and various $3d^5$ excited states are highly forbidden because of the same parity and different multiplicities of the initial and final state, to compute the transition probabilities, we must take the change of wave functions up to the second order taking account of H_v, the interaction with odd vibrations, and $H_{so} = \zeta \sum \mathbf{l}_i \cdot \mathbf{s}_i$, the spin–orbit interaction, as perturbations. Then transition probability between a pair of such perturbed states $|^6g : n\rangle$ and $|^4f : n'\rangle$ is proportional to the square modulus of the matrix element $\langle {}^4f\,; n'|P|^6g\,; n\rangle$ of the electric dipole moment vector $P = \sum e\,\mathbf{r}_i$, where each of n and n' stands for a set of the vibrational quantum numbers. Bearing in mind that the ground state $^6\mathrm{A}_{1g}$ is the only sextet obtained from $3d^5$ configuration and that H_{so} has no matrix element between $^6\mathrm{A}_{1g}(=\,^6\mathrm{S})$ and $\{^4\mathrm{A}_{1g}\,;\,^4\mathrm{E}_g\}$ originated from ^{4}G, we get

$$\begin{aligned} &\langle {}^4f\,;\, n'|P|^6g\,;\, n\rangle \\ &= \sum_{\mu,k} \frac{\langle {}^4f\,;\, n'|H_v|^4\mu\,;\, n\rangle\langle {}^4\mu\,;\, n|P|^4k\,;\, n\rangle\langle {}^4k\,;\, n|H_{so}|^6g\,;\, n\rangle}{(E_f - E_\mu)(E_g - E_k)} \\ &+ \sum_{\mu,k} \frac{\langle {}^4f\,;\, n'|P|^4\mu\,;\, n'\rangle\langle {}^4\mu\,;\, n'|H_v|^4k\,;\, n\rangle\langle {}^4k\,;\, n|H_{so}|^6g\,;\, n\rangle}{(E_g - E_k)(E_g - E_\mu)} \\ &+ \sum_{\mu,\nu} \frac{\langle {}^4f\,;\, n'|H_v|^4\mu\,;\, n\rangle\langle {}^4\mu\,;\, n|H_{so}|^6\nu\,;\, n\rangle\langle {}^6\nu\,;\, n|P|^6g\,;\, n\rangle}{(E_\mu - E_f)(E_\nu - E_f)} \\ &+ \sum_{\mu,\nu} \frac{\langle {}^4f\,;\, n'|P|^4\mu\,;\, n'\rangle\langle {}^4\mu\,;\, n'|H_{so}|^6\nu\,;\, n'\rangle\langle {}^6\nu\,;\, n'|H_v|^6g\,;\, n\rangle}{(E_\mu - E\ )(E_\nu - E\ )}. \end{aligned}$$

The intermediate states denoted by Greek letters are of odd parity, and lie far beyond the $3d^5$ states. The even intermediate states ^4k which couple with the ground sextet through the spin–orbit interaction are the $^4T_{1g}$ states mentioned in § 2. So the energy denominators of the third and fourth terms are much larger than those of the first and second terms. We may, therefore, neglect the third and fourth terms in the following calculations.

The remaining terms are still unmanageable because of the many unknown intermediate states with odd parity. Main contribution will, however, come from the states in which one of the five $3d$ electrons is promoted to the $4p$ orbits owing to the large overlap of the wave functions. It will, therefore, be a good approximation to replace the energy differences $E_\mu - E_g \simeq E_\mu - E_f$ by their appropriate mean value ΔE. Then the sum over the odd intermediate states can be carried out according to the closure properties of the eigenfunctions

$$\sum_m \langle f|A|m\rangle\langle m|B|i\rangle = \langle f|AB|i\rangle.$$

Thus we get

$$\langle {}^4f;\, n'|P|{}^6g;\, n\rangle = \frac{2}{\Delta E}\sum_k \frac{\langle {}^4f;\, n'|PH_v|{}^4k;\, n\rangle\langle {}^4k;n|H_{so}|{}^6g;\, n\rangle}{E_k - E_g}. \quad (5.1)$$

Let us first consider the matrix element $\langle {}^4k|H_{so}|{}^6g\rangle$. The ^6S states couple only with ^4P states through the spin–orbit interaction H_{so}, and the ^4P states are mixed in the $^4T_{1g}$ states mentioned in § 2 in such a way as

$$\langle {}^4P_\tau(M_s)|{}^4T_{1g}{}^{(n\tau)}(M_s)\rangle = \frac{i}{\sqrt{5}}\{\sqrt{2}(\lambda_n + \nu_n) - \mu_n\}, \quad . \quad . \quad (5.2)$$

where $\tau = x, y, z$. Using this relation and the Racah coefficients, we can determine the matrix elements of H_{so}, which are shown in table 2, where $\sigma_n = \zeta\{\sqrt{2}(\lambda_n + \nu_n) - \mu_n\}/\sqrt{5}$.

Table 2. Matrix elements of H_{so}

	$^4T_{1g}{}^{(nx)}(\frac{3}{2})$	$^4T_{1g}{}^{(nx)}(\frac{1}{2})$	$^4T_{1g}{}^{(ny)}(\frac{3}{2})$	$^4T_{1g}{}^{(ny)}(\frac{1}{2})$	$^4T_{1g}{}^{(nz)}(\frac{3}{2})$	$^4T_{1g}{}^{(nz)}(\frac{1}{2})$
$^6A_{1g}(\frac{5}{2})$	$-\sqrt{\frac{5}{2}}\sigma_n i$		$\sqrt{\frac{5}{2}}\sigma_n$			
$^6A_{1g}(\frac{3}{2})$		$-\sqrt{\frac{3}{2}}\sigma_n i$		$\sqrt{\frac{3}{2}}\sigma_n$	$\sqrt{2}\sigma_n i$	
$^6A_{1g}(\frac{1}{2})$	$-\sigma_n i/2$		$\sigma_n/2$			$\sqrt{3}\sigma_n i$
$^6A_{1g}(-\frac{1}{2})$		$-\sqrt{3}\sigma_n i/2$		$\sqrt{3}\sigma_n/2$		
$^6A_{1g}(-\frac{3}{2})$						
$^6A_{1g}(-\frac{5}{2})$						

Matrix elements of PH_v can be reduced to

$$\langle {}^4f;\, n'|PH_v|{}^4k;\, n\rangle = \sum_j \langle n'|Q_j|n\rangle\langle {}^4f|PV_j|{}^4k\rangle$$
$$= \sum_j \langle n'|Q_j|n\rangle\langle {}^4f|\sum_s p(\mathbf{r}_s)v_j(\mathbf{r}_s)|{}^4k\rangle, \quad . \quad (5.3)$$

where use has been made of the fact that p and v_j are both odd functions of the one-electron coordinates $\mathbf{r}_s$. Since our interest lies in the absorption

spectra at very low temperatures, we may assume that $|n\rangle$ expresses the state of no vibration. Then $|n'\rangle$ must be the state in which only j-th vibration is excited; $n_j=1$. For such vibrational states

$$\langle n'|Q_j|n\rangle=\sqrt{(\hbar/2M\omega_j)}, \qquad . \quad . \quad . \quad . \quad (5.4)$$

where ω_j is the angular frequency of the vibration associated with the normal coordinate Q_j. Thus one gets

$$\langle {}^4f;\, n'|PH_v|{}^4k;\, n\rangle=\sum_j\sqrt{\frac{\hbar}{2M\omega_j}}\,\langle {}^4f|\sum_s p(\mathbf{r}_s)v_j(\mathbf{r}_s)|{}^4k\rangle. \quad . \quad (5.5)$$

Since p and v_j are independent of the spin variables, non-vanishing matrix elements of (5.5) are obtained only between the states with same M_s, and are independent of the value M_s. Using the wave functions (2.2), (2.3) and (2.5) for $M_s=3/2$, one can reduce the matrix elements into the sum of one-electron integrals. Table 3 shows those associated with the z-component of the ${}^4\mathrm{T}_{1g}$ states. Matrix elements between $\{{}^4\mathrm{A}_{1g};\,{}^4\mathrm{E}_g\}$ and $\{{}^4\mathrm{T}_{1g}{}^{(nx)},\,{}^4\mathrm{T}_{1g}{}^{(ny)}\}$ can be easily derived by appropriate transformations of the coordinate axes.

Table 3. $\langle {}^4f|\sum_s p(\mathbf{r}_s)v_j(\mathbf{r}_s)|{}^4\mathrm{T}_{1g}{}^{(nz)}\rangle$

${}^4f$	${}^4\mathrm{T}_{1g}{}^{(nz)}$
${}^4\mathrm{A}_{1g}$	$-(5/6)^{1/2}(\lambda_n+\nu_n)\langle v|p\cdot v_j|\zeta\rangle$
${}^4\mathrm{E}_g{}^{(1)}$	$(\lambda_n+\nu_n)\langle v|p\cdot v_j|\zeta\rangle/\sqrt{42}$
${}^4\mathrm{E}_g{}^{(2)}$	$-(3/14)^{1/2}(\lambda_n+\nu_n)\langle u|p\cdot v_j|\zeta\rangle-4\mu_n\langle\xi|p\cdot v_j|\eta\rangle/\sqrt{7}$

Ultimately, it is found that all matrix elements can be expressed in terms of the following nine one-electron integrals:

$$\left.\begin{aligned}
\langle\zeta|v_7\,y|u\rangle&=3\sqrt{\frac{3}{5}}\left(\frac{4}{7}\left\langle\frac{r^2}{R^2}\right\rangle+\frac{5}{14}\left\langle\frac{r^4}{R^4}\right\rangle+\frac{10}{11}\left\langle\frac{r^6}{R^6}\right\rangle\right)\frac{e\mu}{R^2},\\
\langle\zeta|v_{10}y|u\rangle&=\sqrt{10}\left(-\frac{12}{35}\left\langle\frac{r^2}{R^2}\right\rangle+\frac{13}{21}\left\langle\frac{r^4}{R^4}\right\rangle+\frac{9}{11}\left\langle\frac{r^6}{R^6}\right\rangle\right)\frac{e\mu}{R^2},\\
\langle\zeta|v_{13}y|u\rangle&=\frac{25}{14}\sqrt{3}\left\langle\frac{r^4}{R^4}\right\rangle\frac{e\mu}{R^2},\\
\langle\zeta|v_7\,y|v\rangle&=\frac{3\sqrt{5}}{2}\left(\frac{5}{7}\left\langle\frac{r^4}{R^4}\right\rangle+\frac{14}{11}\left\langle\frac{r^6}{R^6}\right\rangle\right)\frac{e\mu}{R^2},\\
\langle\zeta|v_{10}y|v\rangle&=\sqrt{\frac{10}{3}}\left(\frac{65}{21}\left\langle\frac{r^4}{R^4}\right\rangle-\frac{21}{11}\left\langle\frac{r^6}{R^6}\right\rangle\right)\frac{e\mu}{R^2},\\
\langle\zeta|v_{13}y|v\rangle&=5\left(\frac{5}{14}\left\langle\frac{r^4}{R^4}\right\rangle+\frac{7}{11}\left\langle\frac{r^6}{R^6}\right\rangle\right)\frac{e\mu}{R^2},\\
\langle\zeta|v_7\,y|\eta\rangle&=\frac{2}{\sqrt{5}}\left(-\frac{9}{7}\left\langle\frac{r^2}{R^2}\right\rangle-\frac{15}{7}\left\langle\frac{r^4}{R^4}\right\rangle+\frac{30}{11}\left\langle\frac{r^6}{R^6}\right\rangle\right)\frac{e\mu}{R^2},\\
\langle\zeta|v_{10}y|\eta\rangle&=4\sqrt{\frac{5}{6}}\left(\frac{9}{35}\left\langle\frac{r^2}{R^2}\right\rangle-\frac{26}{21}\left\langle\frac{r^4}{R^4}\right\rangle+\frac{9}{11}\left\langle\frac{r^6}{R^6}\right\rangle\right)\frac{e\mu}{R^2},\\
\langle\zeta|v_{13}y|\eta\rangle&=0.
\end{aligned}\right\}\quad . \quad (5.6)$$

In deriving these, use has been made of the expressions (4.16) and (4.18).

§ 6. Results and Comparison with Experiments

To work out the intensities or oscillator strengths numerically, it is necessary to evaluate the values of $\langle r^2/R^2\rangle$, $\langle r^4/R^4\rangle$ and $\langle r^6/R^6\rangle$. Analytical functions of Slater type (Slater 1930) and numerical Hartree–Fock

Table 4.

	$\langle r^2/R^2\rangle$	$\langle r^4/R^4\rangle$	$\langle r^6/R^6\rangle$
Hartree–Fock	0·075	0·012	0·004
Slater	0·21	0·07	0·04

functions (Hartree 1955) give entirely different results. Though the latter are of course more reliable in the case of the free ion, if we use these values and $R = 2{\cdot}35 \times 10^{-8}$ cm and $\mu = 4 \times 10^{-18}$ e.s.u. cm, it is found impossible to obtain correct order of magnitude for the intensities. In fact, if one calculates Δ by using the same model, the relationship

$$\Delta = 10Dq = \frac{25}{3}\frac{e\mu}{R^2}\left\langle\frac{r^4}{R^4}\right\rangle, \qquad \ldots\ldots \quad (6.1)$$

gives

$$\left\langle\frac{r^4}{R^4}\right\rangle = 0{\cdot}054$$

for the same values of R, μ and $\Delta = 8000\,\mathrm{cm}^{-1}$. Since the wave functions may be considerably distorted in the crystal, it is quite difficult to estimate correct $\langle r^n\rangle$ values. In effect, this difficulty is related to the validity of the ligand field theory itself. Several attempts of non-empirical calculation of Δ reveal this situation (Kleiner 1952, Tanabe and Sugano 1956). We shall, therefore, treat these as empirical parameters, and tentatively assume the following two sets of values:

Case I:

$$\langle r^2/R^2\rangle = 0{\cdot}17, \quad \langle r^4/R^4\rangle = 0{\cdot}05 \text{ and } \langle r^6/R^6\rangle = 0{\cdot}025. \qquad (6.2a)$$

Case II:

$$\langle r^2/R^2\rangle = 0{\cdot}20, \quad \langle r^4/R^4\rangle = 0{\cdot}05 \text{ and } \langle r^6/R^6\rangle = 0{\cdot}01. \qquad (6.2b)$$

The spin–orbit interaction parameter is found from the free ion spectra as $\zeta = 300\,\mathrm{cm}^{-1}$. The mean energy difference between odd parity states ΔE is assumed $120\,000\,\mathrm{cm}^{-1}$ from the spectral data of the $3d^44p$ configuration states (Moore 1952). It is to be noted that if we consider only $3d^44p$ configuration in intermediate states the terms containing $\langle r^6/R^6\rangle$ never appear in (5.6). For this reason we have assumed rather small values for $\langle r^6/R^6\rangle$ instead of using different ΔE value for these terms.

For the vibration of the Mn^{2+} aquo-complexes, there are no experimental data of the frequencies. However, for several aquo-complexes of other iron group elements, frequency ν_1 of the A_{1g} vibration has been determined from the structure of the optical spectra (Schultz 1942).

From these values, one can presume $\nu_1 = 250 \sim 300\,\mathrm{cm}^{-1}$ for hydrated manganous complexes. As is seen in § 4, $\nu_4 = (5/3)^{1/2}\nu_1$, so that one gets $\nu_4 = 320 \sim 400\,\mathrm{cm}^{-1}$. Since the Jahn–Teller effect can give rise to the $E_g(\nu_2)$ vibrations which appear as sharper peaks than those of the A_{1g} (ν_1) vibration because of its weaker coupling with the environment, the frequency attributed to the A_{1g} vibration by Schultz might be ν_2 of the E_g vibration. However, we can see, from eqn. (4.11) that the two frequencies are very nearly equal in that $K \gg K_1$ and $f'' \gg g''$. Hence this estimate of ν_4 need not be altered.

As to the frequencies ν_3 and ν_6, no information has been obtained experimentally. Though Liehr and Ballhausen (1957) adopted the valence force model, the central force model would be more appropriate for the aquo-complexes. If we use the simple model discussed in § 4 and assume $g(r) = (3/2)\mu^2 r^{-3}$ with $\mu = 4 \times 10^{-18}$ e.s.u. cm (this value makes allowance for the induced dipole moment on the water molecules), eqns. (4.7*b*) and (4.9*b*) give

$$\nu_3 = 170\,\mathrm{cm}^{-1} \quad \text{and} \quad \nu_6 = 85\,\mathrm{cm}^{-1}. \qquad . \; . \; . \; . \qquad (6.3)$$

The calculated oscillator strengths thus obtained are shown in table 5. These are the values averaged over the polarization direction of the incident light. The intensities of the transition accompanying excitation of the high frequency T_{1u} vibrations are in general small because of the factor (5.4).

Table 5. Calculated oscillator strengths

Electronic transition	Associated vibration	Calculated oscillator strengths	
		Case I	Case II
$^6A_{1g} \rightarrow {}^4A_{1g}$	$T_{1u}(\nu_4)$	2×10^{-8}	3×10^{-8}
$^6A_{1g} \rightarrow {}^4A_{1g}$	$T_{1u}(\nu_3)$	6	4
$^6A_{1g} \rightarrow {}^4A_{1g}$	$T_{2u}(\nu_6)$	7	4
$^6A_{1g} \rightarrow {}^4E_g^{(1)}$	$T_{1u}(\nu_4)$	0·04	0·10
$^6A_{1g} \rightarrow {}^4E_g^{(1)}$	$T_{1u}(\nu_3)$	4	5
$^6A_{1g} \rightarrow {}^4E_g^{(1)}$	$T_{2u}(\nu_6)$	0·8	0·8
$^6A_{1g} \rightarrow {}^4E_g^{(2)}$	$T_{1u}(\nu_4)$	0·04	0·10
$^6A_{1g} \rightarrow {}^4E_g^{(2)}$	$T_{1u}(\nu_3)$	4	5
$^6A_{1g} \rightarrow {}^4E_g^{(2)}$	$T_{2u}(\nu_6)$	0·8	0·8

Magnetic dipole transition, if it exists, would give an intensity of the same order of magnitude. However, in our case, we need not consider it, because magnetic dipole transition takes place only between the states with the same L and S and we cannot expect any perturbation which mixes the ^6S and ^4G states appreciably with each other.

Experimental spectra have been obtained for various manganous salts (Gielessen 1935, Pappalardo 1957). For most of these salts, however, it cannot be allowed to treat $[Mn(H_2O)_6]^{2+}$ as an isolated molecule. We

can, therefore, compare our theoretical results only with the spectra of $MnSiF_6 . 6H_2O$ obtained at 20°K by Pappalardo.

He observed three comparatively intense absorption peaks in the region $24\,500 \sim 26\,000\,cm^{-1}$ of the wave number. The middle one at $25\,330\,cm^{-1}$ is considered to be a double peak of separation $14\,cm^{-1}$. So one can regard these as four lines centred at 25 420, 25 337, 25 323 and $25\,075\,cm^{-1}$ respectively. We may ascribe the first and second of these lines to the transitions ${}^6A_{1g} \rightarrow {}^4A_{1g}$ accompanying the excitation of lower $T_{1u}(\nu_3)$ and T_{2u} vibration respectively, because the separation of these two peaks, $83\,cm^{-1}$, is quite consistent with our estimate of ν_3 and ν_6. Then the remaining two may be attributed to the transition ${}^6A_{1g} \rightarrow {}^4E_g^{(2)}$ and ${}^6A_{1g} \rightarrow {}^4E_g^{(1)}$ with the excitation of the lower frequency T_{1u} vibrations. Then some of the other lines can also be assigned as shown in table 6. It is, however, impossible to discover transitions corresponding to the faint lines found at 24 946 and $24\,896\,cm^{-1}$. Furthermore, lines corresponding to the transitions ${}^6A_{1g} \rightarrow {}^4A_{1g} + h\nu_4$ and ${}^6A_{1g} \rightarrow {}^4E_g^{(2)} + h\nu_6$ are not observed in spite of their comparatively large intensities predicted by our theory. The wave number corresponding to the transition ${}^6A_{1g} + h\nu_6 \rightarrow {}^4A_{1g}$ is expected near $25\,170\,cm^{-1}$. The intensity of this transition is, however, quite small at 20°K because of the Boltzmann factor $\exp(-h\nu_6/kT) \simeq 0{\cdot}003$.

Table 6

Wave number in cm^{-1}	Observed oscillator strength	Assignment	Calculated oscillator strength	
			Case I	Case II
25 420	6×10^{-8}	${}^6A_{1g} \rightarrow {}^4A_{1g} + h\nu_3$	6×10^{-8}	4×10^{-8}
25 337	7	${}^6A_{1g} \rightarrow {}^4A_{1g} + h\nu_6$	7	4
25 323		${}^6A_{1g} \rightarrow {}^4E_g^{(2)} + h\nu_3$	4	5
25 170		${}^6A_{1g} + h\nu_6 \rightarrow {}^4A_{1g}(?)$	0·02	0·01
25 075	3	${}^6A_{1g} \rightarrow {}^4E_g^{(1)} + h\nu_3$	4	5
25 002		${}^6A_{1g} \rightarrow {}^4E_g^{(1)} + h\nu_6$	0·8	0·8
24 946		?		
24 896		?		

§ 7. Conclusion

Though some of the details are still unexplained, the general features of the observed spectra are explained and the calculated intensities give correct orders of magnitude. To make a decisive assignment, some more detailed experimental information, for instance crystal structure, direction of the polarization, etc., are awaited.

It may be stated that the forces responsible for the vibrations can be described by central force model rather than by valence forces.

Acknowledgments

The authors wish to thank Dr. R. Englman for stimulating discussions. One of them (S. K.) is grateful for a Scholarship from the Nishina Memorial Foundation.

References

Abragam, A., and Pryce, M. H. L., 1951, *Proc. roy. Soc.* A, **206,** 173.
Broer, L. J. F., Gorter, C. J., and Hoogschagen, J., 1945, *Physica*, **11,** 231.
Gielessen, J., 1935, *Ann. Phys., Lpz.* **22,** 537.
Hartree, D. R., 1955, *Proc. Camb. phil. Soc.*, **51,** 126.
Holmes, O. G., and McClure, D. S., 1957, *J. chem. Phys.*, **26,** 1686.
Jørgensen, C. K., 1954, *Acta Chem. Scand.*, **8,** 1502; 1957, *Energy Levels of Complex and Gaseous Ions* (København).
Kleiner, W. H., 1952, *J. chem. Phys.*, **20,** 1784.
Liehr, A. D., and Ballhausen, C. J., 1957, *Phys. Rev.*, **106,** 1161.
Moffitt, W., and Ballhausen, C. J., 1956, *Annual Rev. phys. Chem.*, **7,** 107.
Moore, C., 1952, *Atomic Energy Levels, National Bureau of Standards Circular* 467, Vol. II.
Orgel, L. E., 1955, *J. chem. Phys.*, **23,** 1004.
Owen, J., 1955, *Proc. roy. Soc.* A, **227,** 183.
Pappalardo, R., 1957, *Phil. Mag.*, **2,** 1397.
Pryce, M. H. L., 1950 a, *Phys. Rev.*, **80,** 1107; 1950 b, *Proc. phys. Soc. Lond.* A **63,** 25.
Satten, R. A., 1957, *J. chem. Phys.*, **27,** 286.
Schultz, M. L., 1942, *J. chem. Phys.*, **10,** 194.
Slater, J. C., 1930, *Phys. Rev.*, **36,** 57.
Tanabe, Y., and Sugano, S., 1954, *J. phys. Soc. Japan*, **9,** 753, 766; 1956, *Ibid.*, **11,** 864.
Van Vleck, J. H., 1937, *J. phys. Chem.* **41,** 67; 1939, *J. chem. Phys.*, **7,** 72.
Yost, D. M., Steffens, C. C., and Gross, S. T., 1934, *J. chem. Phys.*, **2,** 311.

Dislocations and Cracks in Anisotropic Elasticity†

By A. N. Stroh
Department of Physics, University of Sheffield

[Received March 13, 1958]

Abstract

The solution of the elastic equations is considered for the case in which the state of the solid is independent of one of the three Cartesian coordinates. The stresses due to a dislocation, a wall of parallel dislocations, and a crack in an arbitrary non-uniform stress field are obtained. The results hold for the most general anisotropy in which no symmetry elements of the crystal are assumed.

§ 1. Introduction

Eshelby *et al.* (1953) have developed the theory of anisotropic elasticity for a three dimensional state of stress in which the stress is independent of one of the Cartesian coordinates, and have applied this to find the stress field of a dislocation. In the present paper, which follows their treatment, the stresses due to a dislocation are treated more fully, and the interactions of dislocations considered; also, the stresses round a crack subjected to an arbitrary non-uniform applied stress are obtained. The object will be to present the results in a form which is, analytically, as simple as possible. It is hoped that, in applications of the theory, this will often allow of the properties of the system studied to be deduced without the need for numerical computation, and that when such computation is unavoidable, as when definite numerical values are required, the labour involved will be reduced to a minimum. For this purpose, the properties of a number of constants introduced in the theory and which are related to the elastic constants are investigated in some detail (§ 3). In § 2 some general relations are considered; most of these are given in Eshelby *et al.* but are included here, both for ease of reference, and so that the whole theory may be presented in a uniform notation.

§ 2. General Equations

The stresses σ_{ij} are related to the elastic displacements u_k by the equations

$$\sigma_{ij}=c_{ijkl}\partial u_k/\partial x_l, \qquad (1)$$

where $i, j, k, l=1, 2, 3$ and the convention of summing over a repeated Latin suffix is used. The elastic moduli c_{ijkl} have the symmetry properties

$$c_{ijkl}=c_{jikl}=c_{ijlk}=c_{klij}. \qquad (2)$$

† Communicated by the Author.

It is often convenient to replace the pairs of suffices (i, j) and (k, l) by single suffices M and N according to the scheme that 11 corresponds to 1, 22 to 2, 33 to 3, 23 to 4, 31 to 5, and 12 to 6. Besides securing some brevity in writing, this has the advantage that it enables the elastic constants to be considered as the elements of a matrix, but has the disadvantage that it does not make the tensor character of the constants apparent. In the sequal either four suffix notation c_{ijkl} or two suffix notation c_{MN} will be used according as to which is the more convenient in each case. In addition to the symmetry relations (2) the elastic moduli are subjected to further restrictions which arise because the elastic energy density must be everywhere positive. If the elastic strains are $e_1 = \partial u_1/\partial x_1, \ldots\ldots, e_6 = \partial u_1/\partial x_2 + \partial u_2/\partial x_1$, the energy density is

$$\tfrac{1}{2} c_{MN} e_M e_N > 0, \qquad \ldots\ldots\ldots \quad (3)$$

provided not all the e_M are zero. The condition for (3) is that the determinant $|c_{MN}|$ and its principal minors of all orders should be positive.

On substituting (1) in the equilibrium equations

$$\partial \sigma_{ij}/\partial x_j = 0. \qquad \ldots\ldots\ldots \quad (4)$$

we obtain

$$c_{ijkl} \partial^2 u_k/\partial x_j \partial x_l = 0. \qquad \ldots\ldots\ldots \quad (5)$$

Now we suppose that u_k is independent of x_3, and, following Eshelby *et al.* take

$$u_k = A_k f(x_1 + p x_2). \qquad \ldots\ldots\ldots \quad (6)$$

where $f(z)$ is an analytic function of the complex variable z; (6) is a solution of eqns. (5) provided the constant vector A_k satisfies the equations

$$(c_{i1k1} + p c_{i1k2} + p c_{i2k1} + p^2 c_{i2k2}) A_k = 0. \qquad \ldots \quad (7)$$

Values of A_k, not identically zero, can be found to satisfy these equations if p is a root of the sextic equation

$$|c_{i1k1} + p c_{i1k2} + p c_{i2k1} + p^2 c_{i2k2}| = 0. \qquad \ldots\ldots \quad (8)$$

Eshelby *et al.* have proved that eqn. (8) has no real root, so that the roots occur in complex conjugate pairs. The three roots with positive imaginary part will be denoted by $p_\alpha (\alpha = 1, 2, 3)$ with complex conjugates $\bar{p}_\alpha$; the corresponding values of A_k obtained from eqns. (7) are $A_{k\alpha}$ and $\bar{A}_{k\alpha}$. Summation over α, which of course is not a tensor suffix, and generally over Greek suffices will always be indicated explicitly. It will be assumed that the roots p_α are all distinct; equal roots may be regarded as the limiting case of distinct roots. A general expression for the displacement may then be written

$$u_k = \sum_\alpha A_{k\alpha} f_\alpha(z_\alpha) + \sum_\alpha \bar{A}_{k\alpha} \overline{f_\alpha(z_\alpha)}, \qquad \ldots\ldots \quad (9)$$

where $z_\alpha = x_1 + p_\alpha x_2$.

It is convenient to express the stresses in terms of a vector, the components of which will be denoted by ϕ_i; with the stresses independent of x_3, eqns. (4) are satisfied identically if the stresses are derived from the ϕ_i by the relations

$$\sigma_{i1} = -\partial \phi_i/\partial x_2, \quad \sigma_{i2} = \partial \phi_i/\partial x_1. \qquad \ldots\ldots \quad (10)$$

These equations determine in terms of the ϕ_i all the components of the stress except σ_{33}. But since in the present case σ_{33} is linearly dependent on the other stress components (the equation showing this is just the condition, expressed in terms of the stresses, that the strain $e_3 = \partial u_3/\partial x_3$ be zero), we may regard the problem as solved when the remaining five components of stress, or equivalently the functions ϕ_i, are determined. Since

$$\partial\phi_1/\partial x_1 = \sigma_{12} = -\partial\phi_2/\partial x_2, \quad \ldots\ldots (11)$$

ϕ_1 and ϕ_2 may be expressed in terms of a single function χ by

$$\phi_1 = -\partial\chi/\partial x_2, \quad \phi_2 = \partial\chi/\partial x_1; \quad \ldots\ldots (12)$$

however the theory takes on a more symmetrical form if this is not done, and we shall generally prefer not to introduce χ. Eshelby *et al.* have shown that the resultant force acting across a curve C is $\Delta\phi_i$, where $\Delta\phi_i$ is the change in ϕ_i on going along the curve. It may also be shown that the moment about the x_3 axis of the forces acting across C is

$$\Delta(x_2\phi_1 - x_1\phi_2 + \chi).$$

From eqns. (1), (9) and (10) we obtain

$$\phi_i = \sum_\alpha L_{i\alpha} f_\alpha(z_\alpha) + \sum_\alpha \bar{L}_{i\alpha}\overline{f_\alpha(z_\alpha)}, \quad \ldots\ldots (13)$$

where the three vectors $L_{i\alpha}$ are defined by

$$L_{i\alpha} = (c_{i2k1} + p_\alpha c_{i2k2}) A_{k\alpha}, \quad \ldots\ldots (14)$$

or alternatively,

$$L_{i\alpha} = -(p_\alpha^{-1} c_{i1k1} + c_{i1k2}) A_{k\alpha}, \quad \ldots\ldots (15)$$

these expressions being equivalent by eqns. (7). For (11) to hold, we must have

$$L_{1\alpha} + p_\alpha L_{2\alpha} = 0, \quad \ldots\ldots (16)$$

a relation which also follows directly from (14) and (15). Use of eqn. (16) will simplify the expressions for the $L_{i\alpha}$ and so we shall prefer to express our results in terms of the $L_{i\alpha}$ rather than the $A_{k\alpha}$; as will be seen in § 7 the $L_{i\alpha}$ can be obtained in terms of the p_α without first determining the $A_{k\alpha}$. Nevertheless, in the general case, these expressions still remain rather cumbersome, and we proceed first to develop the theory as far as possible without introducing the explicit values of the $A_{k\alpha}$ or $L_{i\alpha}$.

§ 3. Properties of $A_{k\alpha}$, $L_{i\alpha}$ and some Related Constants

From the vectors $\bar{A}_{i\alpha}$ and $L_{i\alpha}$ we may form the 3×3 matrix whose elements are $\bar{A}_{i\beta} L_{i\alpha}$; this matrix we now prove has skew-Hermitian symmetry. For from (14) we have

$$\bar{p}_\beta \bar{A}_{i\beta} L_{i\alpha} = \bar{p}_\beta \bar{A}_{i\beta} c_{i2k1} A_{k\alpha} + \bar{p}_\beta \bar{A}_{i\beta} c_{i2k2} p_\alpha A_{k\alpha},$$

and from (15)

$$\bar{A}_{i\beta} L_{i\alpha} p_\alpha = -\bar{A}_{i\beta} c_{i1k1} A_{k\alpha} - \bar{A}_{i\beta} c_{i1k2} p_\alpha A_{k\alpha};$$

subtracting these two equations,

$$\bar{A}_{i\beta} L_{i\alpha}(\bar{p}_\beta - p_\alpha) = \bar{A}_{i\beta} c_{i1k1} A_{k\alpha} + \bar{p}_\beta \bar{A}_{i\beta} c_{i2k2} p_\alpha A_{k\alpha} + (\bar{p}_\beta \bar{A}_{i\beta} c_{i2k1} A_{k\alpha} + \bar{A}_{i\beta} c_{i1k2} p_\alpha A_{k\alpha}). \quad \ldots\ldots (17)$$

Now each of the three terms on the right of (17) has Hermitian symmetry, and so the left side must also; that is

$$\bar{A}_{i\beta}L_{i\alpha}(\bar{p}_\beta - p_\alpha) = A_{i\alpha}\bar{L}_{i\beta}(p_\alpha - \bar{p}_\beta),$$

or since $(\bar{p}_\beta - p_\alpha)$ has negative imaginary part and so is not zero

$$\bar{A}_{i\beta}L_{i\alpha} = -A_{i\alpha}\bar{L}_{i\beta}, \qquad \ldots\ldots \quad (18)$$

which is the required relation.

Since $A_{k\alpha}$, $\bar{A}_{k\alpha}$ form a set of six vectors in three dimensional space, not more than three of them can be linearly independent; the three vectors $A_{k\alpha}$, corresponding to the three roots p_α with positive imaginary part, do however form such a linearly independent set. For suppose that this were not so and that a relation

$$\sum_\alpha \xi_\alpha A_{k\alpha} = 0 \qquad \ldots\ldots \quad (19)$$

existed with not all the ξ_α zero. Multiply eqn. (17) by $\xi_\alpha\bar{\xi}_\beta$ and sum over α and β. The left hand side becomes

$$\sum_\alpha\sum_\beta \bar{\xi}_\beta\bar{A}_{j\beta}L_{j\alpha}(\bar{p}_\beta - p_\alpha)\xi_\alpha = -\sum_\beta \bar{L}_{j\beta}\bar{p}_\beta\bar{\xi}_\beta\sum_\alpha A_{j\alpha}\xi_\alpha - \sum_\beta \bar{A}_{j\beta}\bar{\xi}_\beta\sum_\alpha L_{j\alpha}p_\alpha\xi_\alpha = 0$$

on using (18) and (19); also after using (19) and its complex conjugate the only term that remains on the right-hand side is

$$(\sum_\beta \bar{\xi}_\beta\bar{p}_\beta\bar{A}_{i\beta})c_{i2k2}(\sum_\alpha \xi_\alpha p_\alpha A_{k\alpha}) = 0.$$

But $[c_{i2k2}]$, being a principal minor of the 6×6 matrix $[c_{MN}]$, is by (3) positive definite; hence

$$\sum_\alpha \xi_\alpha p_\alpha A_{k\alpha} = 0. \qquad \ldots\ldots \quad (20)$$

From eqn. (7) we obtain

$$c_{i1k1}\sum_\alpha \xi_\alpha p_\alpha{}^{-1}A_{k\alpha} + (c_{i1k2} + c_{i2k1})\sum_\alpha \xi_\alpha A_{k\alpha} + c_{i2k2}\sum_\alpha \xi_\alpha p_\alpha A_{k\alpha} = 0,$$

or using (19) and (20)

$$c_{i1k1}\sum_\alpha \xi_\alpha p_\alpha{}^{-1}A_{k\alpha} = 0;$$

again by (3) $|c_{i1k1}| \neq 0$, so that

$$\sum_\alpha \xi_\alpha p_\alpha{}^{-1}A_{k\alpha} = 0. \qquad \ldots\ldots \quad (21)$$

Now for a fixed value of k, (19), (20) and (21) may be regarded as a set of three equations in the three unknowns $\xi_\alpha A_{k\alpha}$; the determinant of these equations is equal to $(p_1-p_2)(p_2-p_3)(p_3-p_1)/p_1p_2p_3$, which is not zero if all the p_α are distinct; hence the only solution is $\xi_\alpha A_{k\alpha} = 0$. But $A_{k\alpha}$ is not identically zero and so we must have $\xi_\alpha = 0$, or no relation of the form (19) with non-zero ξ_α is possible.

Next we prove that the linear independence of the $L_{i\alpha}$ follows from that of the $A_{k\alpha}$; in the course of establishing this result some constants which will also be needed later are introduced. Again we suppose that the $L_{i\alpha}$ are not linearly independent so that we can write

$$\sum_\alpha \xi_\alpha L_{i\alpha} = 0 \qquad \ldots\ldots \quad (22)$$

with not all the ξ_α zero. From (14) we have

$$\sum_\alpha \sum_\beta \bar{\xi}_\beta \bar{A}_{i\beta} L_{i\alpha} p_\alpha^{-1} \xi_\alpha = \sum_\beta \bar{\xi}_\beta \bar{A}_{i\beta} c_{i2k1} \sum_\alpha p_\alpha^{-1} \xi_\alpha A_{k\alpha} + \sum_\beta \bar{\xi}_\beta \bar{A}_{i\beta} c_{i2k2} \sum_\alpha \xi_\alpha A_{k\alpha}, \quad (23)$$

and the left-hand side is seen to be zero on using (18) and the conjugate of (22). Also, from (15) we have

$$c_{i1k1} \sum_\alpha p_\alpha^{-1} A_{k\alpha} \xi_\alpha + c_{i1k2} \sum_\alpha A_{k\alpha} \xi_\alpha = - \sum_\alpha L_{i\alpha} \xi_\alpha = 0. \quad . \quad . \quad . \quad (24)$$

Now the determinant $|c_{i1k1}|$ is by (3) positive and not zero, and hence the matrix $[s'_{ik}]$ reciprocal to $[c_{i1k1}]$ exists. Then from (24)

$$\sum_\alpha p_\alpha^{-1} A_{k\alpha} \xi_\alpha = - s'_{ki} c_{i1l2} \sum_\alpha \xi_\alpha A_{l\alpha},$$

and substituting this in (23), we obtain

$$(\sum_\beta \bar{\xi}_\beta \bar{A}_{i\beta}) \beta_{il} (\sum_\alpha \xi_\alpha A_{l\alpha}) = 0, \quad . \quad . \quad . \quad . \quad . \quad . \quad (25)$$

where

$$\beta_{il} = c_{i2l2} - c_{i2k1} s'_{kj} c_{j1l2}. \quad . \quad . \quad . \quad . \quad . \quad . \quad . \quad (26)$$

The expression

$$\beta_{il} \cdot |c_{j1k1}| = \begin{vmatrix} c_{1111} & c_{1121} & c_{1131} & c_{11l2} \\ c_{2111} & c_{2121} & c_{2131} & c_{21l2} \\ c_{3111} & c_{3121} & c_{3131} & c_{31l2} \\ c_{i211} & c_{i221} & c_{i231} & c_{i2l2} \end{vmatrix}$$

is easily verified by expanding the determinant on the right by its 4th row and 4th column. With

$$\Delta_1 = |c_{j1k1}| = \begin{vmatrix} c_{11} & c_{15} & c_{16} \\ c_{15} & c_{55} & c_{56} \\ c_{16} & c_{56} & c_{66} \end{vmatrix}, \quad . \quad . \quad . \quad . \quad (27)$$

we have

$$\left.\begin{aligned} \Delta_1 \beta_{22} &= \begin{vmatrix} c_{11} & c_{12} & c_{15} & c_{16} \\ c_{12} & c_{22} & c_{25} & c_{26} \\ c_{15} & c_{25} & c_{55} & c_{56} \\ c_{16} & c_{26} & c_{56} & c_{66} \end{vmatrix}, \\ \Delta_1 \beta_{33} &= \begin{vmatrix} c_{11} & c_{14} & c_{15} & c_{16} \\ c_{14} & c_{44} & c_{45} & c_{46} \\ c_{15} & c_{45} & c_{55} & c_{56} \\ c_{16} & c_{46} & c_{56} & c_{66} \end{vmatrix}, \\ \Delta_1 \beta_{23} = \Delta_1 \beta_{32} &= \begin{vmatrix} c_{11} & c_{14} & c_{15} & c_{16} \\ c_{12} & c_{24} & c_{25} & c_{26} \\ c_{15} & c_{45} & c_{55} & c_{56} \\ c_{16} & c_{46} & c_{56} & c_{66} \end{vmatrix}, \end{aligned}\right\} \quad . \quad . \quad . \quad (28)$$

and the remaining elements of β_{il} are zero. It follows from (3) that

$$\beta_{22} > 0, \text{ and } \beta_{33} > 0. \quad . \quad . \quad . \quad . \quad . \quad . \quad (29)$$

Further, consider the determinant

$$\Delta = \begin{vmatrix} c_{11} & c_{12} & c_{14} & c_{15} & c_{16} \\ c_{12} & c_{22} & c_{24} & c_{25} & c_{26} \\ c_{14} & c_{24} & c_{44} & c_{45} & c_{46} \\ c_{15} & c_{25} & c_{45} & c_{55} & c_{56} \\ c_{16} & c_{26} & c_{46} & c_{56} & c_{66} \end{vmatrix}; \quad . \quad . \quad . \quad (30)$$

$\beta_{22}\Delta_1$ is the cofactor of c_{44} in Δ, $\beta_{33}\Delta_1$ of c_{22}, and $-\beta_{23}\Delta_1$ of c_{24}. Hence it follows from Jacobi's theorem that

$$\beta_{22}\beta_{33} - \beta_{23}^2 = \Delta/\Delta_1 > 0. \quad . \quad . \quad . \quad . \quad (31)$$

On account of (29) and (31) eqn. (25) can be true only if

$$\sum_\alpha \xi_\alpha A_{2\alpha} = 0 \text{ and } \sum_\alpha \xi_\alpha A_{3\alpha} = 0. \quad . \quad . \quad . \quad . \quad (32)$$

The third equation,

$$\sum_\alpha \xi_\alpha A_{1\alpha} = 0, \quad . \quad . \quad . \quad . \quad . \quad . \quad . \quad (33)$$

does not follow from (25); it may however be deduced in a similar way but starting from the equation formed from (15) in a manner analogous to that by which (23) was formed from (14). Then (32) and (33) show that the linear dependance of the $L_{i\alpha}$ implies that of the $A_{k\alpha}$ which has already been proved untrue; hence the linear independence of the $L_{i\alpha}$ is established.

In deriving (33) we would have to introduce constants γ_{il} analogous to β_{il} and which will also be needed later. The non-zero components of γ_{il} are

$$\left.\begin{aligned} \Delta_2\gamma_{11} &= \begin{vmatrix} c_{11} & c_{12} & c_{14} & c_{16} \\ c_{12} & c_{22} & c_{24} & c_{26} \\ c_{14} & c_{24} & c_{44} & c_{46} \\ c_{16} & c_{26} & c_{46} & c_{66} \end{vmatrix}, \\ \Delta_2\gamma_{33} &= \begin{vmatrix} c_{22} & c_{24} & c_{25} & c_{26} \\ c_{24} & c_{44} & c_{45} & c_{46} \\ c_{25} & c_{45} & c_{55} & c_{56} \\ c_{26} & c_{46} & c_{56} & c_{66} \end{vmatrix}, \\ \Delta_2\gamma_{13} = \Delta_2\gamma_{31} &= \begin{vmatrix} c_{12} & c_{14} & c_{15} & c_{16} \\ c_{22} & c_{24} & c_{25} & c_{26} \\ c_{24} & c_{44} & c_{45} & c_{46} \\ c_{26} & c_{46} & c_{56} & c_{66} \end{vmatrix}, \end{aligned}\right\} \quad . \quad . \quad . \quad (34)$$

where

$$\Delta_2 = |c_{j2k2}| = \begin{vmatrix} c_{22} & c_{24} & c_{26} \\ c_{24} & c_{44} & c_{46} \\ c_{26} & c_{46} & c_{66} \end{vmatrix}. \quad . \quad . \quad . \quad (35)$$

Also $\gamma_{11} > 0$, $\gamma_{33} > 0$, and $\gamma_{11}\gamma_{33} - \gamma_{13}^2 = \Delta/\Delta_2 > 0$. . . (36)

Now having established that the $L_{i\alpha}$ are linearly independent, we are able to introduce three vectors $M_{\alpha i}$, reciprocal to the $L_{i\alpha}$, and which are defined by

$$M_{\alpha i}L_{i\beta}=\delta_{\alpha\beta}. \qquad (37)$$

From (37) the relation

$$\sum_{\alpha}L_{i\alpha}M_{\alpha j}=\delta_{ij} \qquad (38)$$

follows. Also eqn. (18) may now be written

$$\sum_{\alpha}\bar{A}_{j\alpha}\bar{M}_{\alpha i}=-\sum_{\alpha}A_{i\alpha}M_{\alpha j}. \qquad (39)$$

Since, for each α, eqn. (7) determine only the ratios of the components, $A_{i\alpha}$ (and hence $L_{i\alpha}$ and $M_{\alpha i}$) contains an arbitrary factor independent of i but which may depend on α. However this factor does not appear in the product $A_{i\alpha}M_{\alpha j}$ so that $\sum A_{i\alpha}M_{\alpha j}$ is unambiguously defined. A related tensor which will play an important role in the theory is

$$B_{ij}=\tfrac{1}{2}i\sum_{\alpha}(A_{i\alpha}M_{\alpha j}-\bar{A}_{i\alpha}\bar{M}_{\alpha j}); \qquad (40)$$

B_{ij} is clearly real, and being equal to the imaginary part of a skew-Hermitian matrix (cf. eqn. (39)) is itself symmetric.

Finally we seek a relation between B_{ij} and $L_{i\alpha}$, $M_{\alpha i}$ not involving the $A_{i\alpha}$ explicitly. From eqns. (15) and (38) we have

$$\delta_{ij}=\sum_{\alpha}L_{i\alpha}M_{\alpha j}=-c_{i1k1}\sum_{\alpha}A_{k\alpha}p_{\alpha}^{-1}M_{\alpha j}-c_{i1k2}\sum_{\alpha}A_{k\alpha}M_{\alpha j},$$

and from (14),

$$\sum_{\alpha}L_{i\alpha}p_{\alpha}^{-1}M_{\alpha j}=c_{i2k1}\sum_{\alpha}A_{k\alpha}p_{\alpha}^{-1}M_{\alpha j}+c_{i2k2}\sum_{\alpha}A_{k\alpha}M_{\alpha j}.$$

From these two equations we obtain, on using (26) and (40),

$$\frac{1}{2i}(Q_{ij}-\bar{Q}_{ij})=-\beta_{ik}B_{kj}, \qquad (41)$$

where

$$Q_{ij}=\sum_{\alpha}L_{i\alpha}p_{\alpha}^{-1}M_{\alpha j}. \qquad (42)$$

In the same way with

$$P_{ij}=\sum_{\alpha}L_{i\alpha}p_{\alpha}M_{\alpha j}, \qquad (43)$$

we obtain

$$\frac{1}{2i}(P_{ij}-\bar{P}_{ij})=\gamma_{ik}B_{kj}. \qquad (44)$$

The matrices $[P_{ij}]$ and $[Q_{ij}]$ are reciprocals of one another, as is easily seen on forming their product and using (37) and (38).

Since $[\beta_{ik}]$ and $[\gamma_{ik}]$ are singular matrices, neither (41) nor (44) alone can be solved for B_{kj}. However taken together (41) and (44) are sufficient to determine B_{kj} and when numerical values are required it will usually be easier to solve them than first to determine the $A_{i\alpha}$ and to use the definition (40).

§ 4. Dislocations

Consider the following displacements, which are of the form (9):

$$u_k = \frac{1}{2\pi i}\sum_\alpha A_{k\alpha} D_\alpha \log z_\alpha - \frac{1}{2\pi i}\sum_\alpha \bar{A}_{k\alpha}\bar{D}_\alpha \log \bar{z}_\alpha. \quad . \quad . \quad . \quad (45)$$

Along a closed path encircling the x_3 axis, u_k changes by an amount

$$b_k = \sum_\alpha (A_{k\alpha} D_\alpha + \bar{A}_{k\alpha}\bar{D}_\alpha). \quad . \quad . \quad . \quad . \quad . \quad (46)$$

Also from (13) the stress functions corresponding to the displacements (45) are

$$\phi_i = \frac{1}{2\pi i}\sum_\alpha L_{i\alpha} D_\alpha \log z_\alpha - \frac{1}{2\pi i}\sum_\alpha \bar{L}_{i\alpha}\bar{D}_\alpha \log \bar{z}_\alpha; \quad . \quad . \quad . \quad (47)$$

the change in ϕ_i along a closed path about the x_3 axis is

$$\Delta\phi_i = \sum_\alpha (L_{i\alpha} D_\alpha + \bar{L}_{i\alpha}\bar{D}_\alpha), \quad . \quad . \quad . \quad . \quad (48)$$

and it has been noted (§ 2) that this change in ϕ_i just represents the resultant force F_i acting.

Thus in general (45) represents the displacements due to a dislocation with Burgers vector b_i, together with a line of body force F_i, along the x_3 axis. Since the D_α and $\bar{D}_\alpha$ constitute a set of six independent constants we may expect that it will always be possible to choose them to correspond to any given values of b_i and F_i. We now determine these constants so that we have a pure dislocation without a line of force along its axis, that is we take $F_i = 0$.

It is always possible to express D_α in terms of new constants d_j by the relation

$$D_\alpha = \tfrac{1}{2} i M_{\alpha j} d_j;$$

then substituting this in (48) we see that $F_i = 0$ if d_j is real. Equations (46), (47) and (40) now show that the stress functions

$$\phi_i = \frac{1}{4\pi}\sum_\alpha (L_{i\alpha} M_{\alpha j} \log z_\alpha + \bar{L}_{i\alpha}\bar{M}_{\alpha j} \log \bar{z}_\alpha)\, d_j \quad . \quad . \quad . \quad (49)$$

represent a dislocation with Burgers vector

$$b_i = B_{ij} d_j \quad . \quad . \quad . \quad . \quad . \quad . \quad . \quad . \quad (50)$$

for all real values of the vector d_j. It will be seen later that the determinant $|B_{ij}|$ is not zero; hence given the value of b_i it is always possible to solve eqns. (50) for d_j, so that (49) can represent a dislocation with arbitrary Burgers vector. However the stresses are more closely related to the vector d_j than to b_i and so we shall usually prefer to express our results in terms of the former. (The nature of d_j may perhaps be made clearer by reference to the isotropic case where d_j are the components of $G\mathbf{b}$ for a screw dislocation and of $G\mathbf{b}/(1-\nu)$ for an edge, with G the rigidity and ν Poisson's ratio). The stresses derived from (49) by eqns. (10) are

$$\sigma_{i1} = -(1/4\pi)\sum_\alpha (L_{i\alpha} p_\alpha z_\alpha^{-1} M_{\alpha j} + \bar{L}_{i\alpha}\bar{p}_\alpha \bar{z}_\alpha^{-1}\bar{M}_{\alpha j})\, d_j, \quad . \quad (51)$$

and

$$\sigma_{i2} = (1/4\pi)\sum (L_{i\alpha} z_\alpha^{-1} M_{\alpha j} + \bar{L}_{i\alpha}\bar{z}_\alpha^{-1}\bar{M}_{\alpha j})\, d_j. \quad . \quad . \quad . \quad (52)$$

The elastic energy per unit length of the material lying inside a cylinder with generators parallel to the x_3 axis, and which meets the plane $x_3=0$ in a curve C, can quite generally be written

$$U=\tfrac{1}{2}\int_C u_i\sigma_{ij}n_j\,ds, \qquad (53)$$

where n_j are the direction cosines of the outward normal to C. On using (10) this becomes

$$U=-\tfrac{1}{2}\int_C u_i(d\phi_i/ds)\,ds. \qquad (54)$$

Fig. 1

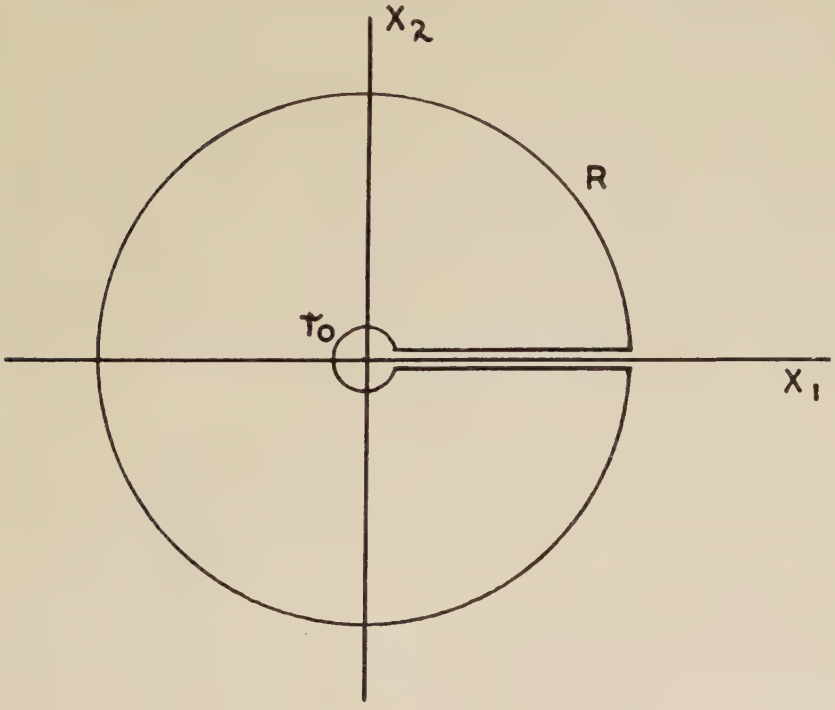

We apply (53) and (54) to calculate contribution to the energy of a dislocation from the material between radii R and r_0 $(R>r_0)$ from the x_3 axis (fig. 1). This region may be made simply connected by making a cut in the plane $x_2=0$ from $x_1=r_0$ to $x_1=R$; in the cut region we take the displacement u_i to be single valued but discontinuous across the cut. On the surface of the cylinder radius R, (54) gives a contribution to the energy of

$$U_R=-\tfrac{1}{2}\int_0^{2\pi} u_i(d\phi_i/d\theta)\,d\theta,$$

where we have taken $z_\alpha=x_1+p_\alpha x_2=R(\cos\theta+p_\alpha\sin\theta)$. From (49) we see that $d\phi_i/d\theta$ is independent of R, and from (45) that u_i is of the form

$$u_i=k\log R+g(\theta),$$

where k is a constant and $g(\theta)$ is independent of R. Thus the part of U_R involving R is

$$-\tfrac{1}{2}k\log R\int_0^{2\pi}(d\phi_i/d\theta)\,d\theta=0$$

since ϕ_i is single valued; U_R is thus independent of the radius R. From the surface of the inner cylinder of radius r_0 we obtain a similar contribution which will be of the same magnitude but, since the direction of the normal n_j is now reversed, opposite in sign. Thus the net contribution to the energy from the two curved surfaces is zero.

The displacements on the two sides of the cut differ by b_i, and the stress across the plane of the cut $x_2=0$ is, from (52),

$$\sigma_{12}=(1/4\pi x_1)\sum_\alpha(L_{i\alpha}M_{\alpha j}+\bar{L}_{i\alpha}\bar{M}_{\alpha j})d_j=d_i/2\pi x_1.$$

Hence (53) gives the energy as

$$U=(b_id_i/4\pi)\int_{r_0}^{R}dx_1/x_1=(b_id_i/4\pi)\log(R/r_0);\quad\ldots\quad(55)$$

using (50) we have the alternate expression for the energy of the dislocation

$$U=(B_{ij}d_id_j/4\pi)\log(R/r_0).\quad\ldots\quad(56)$$

Since U must be positive for all non-zero values of d_i, we see that $[B_{ij}]$ is positive definite. In particular the determinant $|B_{ij}|$ is positive and not zero; this establishes the statement made previously that eqn. (50) can always be solved to give d_j in terms of b_i.

§ 5. Interaction of Two Dislocations

The energy of interaction of two dislocations can most easily be found by the method due to Cottrell (1949) of forming one dislocation in the presence of the other. Consider a dislocation with Burgers vector $b_i^{(1)}$ lying along the x_3 axis and suppose a second dislocation with Burgers vector $b_i^{(2)}$ is formed parallel to the first and through the point $(X_1, X_2, 0)$. This dislocation may be formed by making a cut along the plane $x_2=X_2$ from $x_1=X_1$ to $x_1=\infty$, and giving the surfaces of the cut a relative displacement $b_i^{(2)}$. The work done in this process against the stresses of the first dislocation is

$$V=b_i^{(2)}\int_{X_1}^{\infty}\sigma_{i2}^{(1)}\,dx_1;$$

using (52) this becomes

$$V=-(b_i^{(2)}/4\pi)\sum_\alpha(L_{i\alpha}M_{\alpha j}\log Z_\alpha+\bar{L}_{i\alpha}\bar{M}_{\alpha j}\log\bar{Z}_\alpha)\,d_j^{(1)},\quad\ldots\quad(57)$$

where now $Z_\alpha=X_1+p_\alpha X_2$. Introducing polar coordinates $(r,\ \theta)$ (fig. 2) we have

$$\log Z_\alpha=\log r+\log(\cos\theta+p_\alpha\sin\theta).$$

Then from (57) and (38) we obtain the radial force

$$F_r=-\partial V/\partial r=b_i^{(2)}d_i^{(1)}/2\pi r;\quad\ldots\quad(58)$$

by using (50) this may also be written in the symmetrical form

$$F_r = B_{ij}\, d_i^{(1)} d_j^{(2)}/2\pi r. \qquad \ldots\ldots\ldots \quad (59)$$

The expression for the tangential component of the force is rather more complicated and is given by

$$F_\theta = -\frac{1}{r}\frac{\partial V}{\partial \theta} = -\frac{b_i^{(2)} d_j^{(1)}}{4\pi r} \sum_\alpha \left(L_{i\alpha} M_{\alpha j} \frac{p_\alpha \cos\theta - \sin\theta}{\cos\theta + p_\alpha \sin\theta} + \bar{L}_{i\alpha} \bar{M}_{\alpha j} \frac{\bar{p}_\alpha \cos\theta - \sin\theta}{\cos\theta + \bar{p}_\alpha \sin\theta} \right). \qquad \ldots \quad (60)$$

Fig. 2

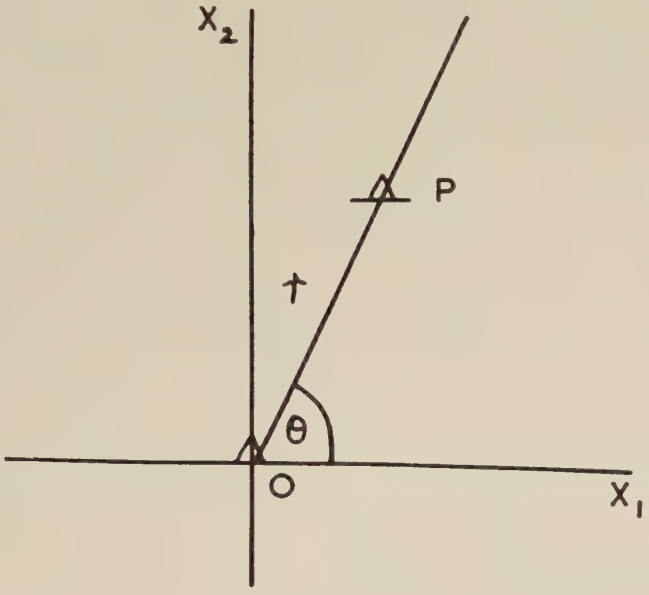

An important special case of the forces between dislocations is that of two like parallel edge dislocations in different slip planes; the well-known result of isotropic theory that the dislocations have an equilibrium position with the line joining them normal to the slip will not be true in general. For suppose the dislocations have Burgers vectors

$$b_i = (b,\ 0,\ 0) \qquad \ldots\ldots\ldots \quad (61)$$

so that the slip planes are parallel to the plane $x_2 = 0$, and let the dislocations pass through the origin and the point $(0,\ x_2,\ 0)$, the component of force in the slip plane may be found from (58) and (60), or more simply by noting that this force is

$$F_1 = b_i \sigma_{i2} = b\sigma_{12};$$

on using (51) and (38) this becomes

$$F_1 = -(b/4\pi x_2) \sum_\alpha (L_{2\alpha} M_{\alpha j} + \bar{L}_{2\alpha} \bar{M}_{\alpha j})\, d_j = -b\, d_2/2\pi x_2. \qquad . \quad (62)$$

The value of d_2 used here is to be obtained by solving eqns. (50) with b_i given by (61); it is shown in § 7, by consideration of a special case, that in general d_2 will not be zero, and so the dislocations will not be in equilibrium.

It is easily seen from (52) that σ_{12} changes sign as x_1 varies from $-\infty$ to $+\infty$, so that it will vanish at an odd number of points; that is two parallel edge dislocations have an odd number of equilibrium positions. It is convenient to characterize these by the angle θ between the line joining the dislocations and the slip plane, since, from the form of the forces (58) and (60), the equilibrium positions depend on θ but not on r. If, then, the dislocations at O and P in fig. 2 are in equilibrium, we can add any number of similar dislocations at different points along the line OP; every pair of dislocations, and hence the system as a whole, will be in equilibrium. Thus the values of θ corresponding to the equilibrium of a single pair of dislocations define possible orientations in which dislocation walls may be formed; moreover it is easily seen that these are the only orientations in which the dislocations forming a wall will be in equilibrium. In particular we are led to the conclusion that a wall of edge dislocations normal to the slip plane (a simple tilt boundary) will not be possible unless $\theta = \frac{1}{2}\pi$ is an equilibrium position for two dislocations, which, we have seen, is not always the case.

This last conclusion appears inconsistent with that obtained from the treatment of Frank (1950); in this the dislocations walls of least energy (and which are therefore the most stable) are obtained as those for which the material is unstrained at a distance from the walls. This gives the simple tilt boundary normal to the slip plane as the most stable arrangement which can be formed from edge dislocations all of the same kind; Frank's arguments are very general and should apply quite independently of the crystal symmetry. We therefore consider, in the next section, the stresses due to a wall of dislocations and verify that the remote stress field leads to results in agreement with Frank.

§ 6. Dislocation Walls

Consider a wall of like parallel dislocations, with arbitrary Burgers vector b_i; the dislocations are to be equally spaced in the wall, the distance between neighbouring dislocations being h. We take x_1 axis normal to the wall, and, as usual, x_3 axis parallel to the dislocation lines. The stresses due to the wall can be found by summing the stresses (51) and (52) over all the dislocations in the wall. Thus the stresses will be given by two expressions of the form (51) and (52) but with $z_\alpha^{-1} = (x_1 + p_\alpha x_2)^{-1}$ replaced by

$$\lim_{N\to\infty} \sum_{\nu=-N}^{N} \{x_1 + p_\alpha(x_2 - \nu h)\}^{-1} = \frac{\pi}{p_\alpha h} \cot \frac{\pi}{p_\alpha h}(x_1 + p_\alpha x_2). \quad . \quad (63)$$

When x_1 is large (63) reduces to $i\pi/p_\alpha h$; then from (51) and (38) we find

$$\sigma_{i1} = 0,$$

and from (52), (41), (42) and (50)

$$\sigma_{i2} = (i/4h) \sum_{\alpha} (L_{i\alpha} p_\alpha^{-1} M_{\alpha j} - \bar{L}_{i\alpha} \bar{p}_\alpha^{-1} \bar{M}_{\alpha j}) d_j$$
$$= \beta_{ik} B_{kj} d_j / 2h = \beta_{ik} b_k / 2h.$$

Since the only elements of β_{ik} which are not zero are those given in (28), the non-vanishing stresses are

$$\sigma_{22} = (\beta_{22} b_2 + \beta_{23} b_3)/2h,$$

and

$$\sigma_{23} = (\beta_{23} b_2 + \beta_{33} b_3)/2h.$$

These stresses clearly vanish if b_i is given by (61), and by (31) this is the only value of b_i for which they vanish. Thus the simple tilt boundary normal to the slip plane is the only type of boundary which can be formed from dislocations all of the same kind, and for which the remote stress field is zero. This agrees with Frank's results.

Fig. 3

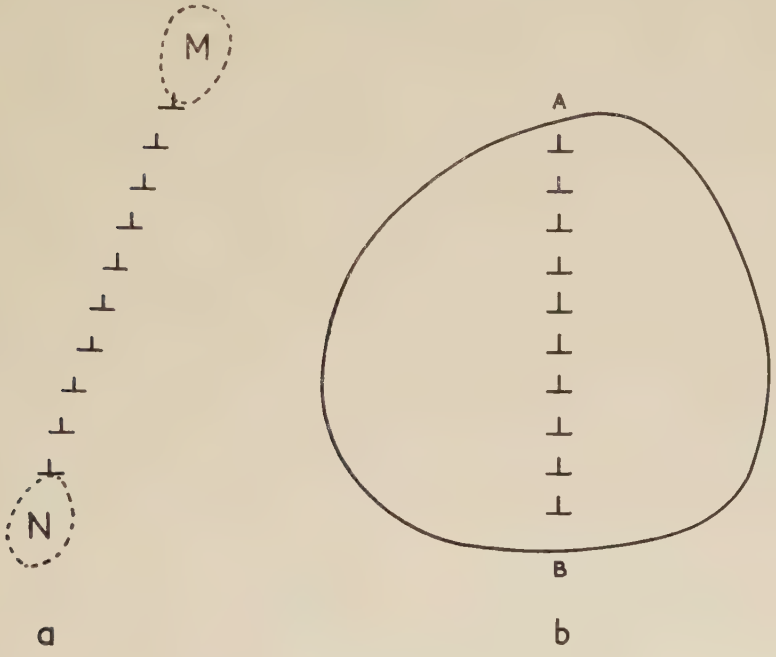

It remains to reconcile the treatment here with that of the previous section. Consider a wall built up of a finite number of dislocations. First suppose that the wall occurs in an infinite crystal (fig. 3 (*a*)); the treatment of § 5 will now be valid; but the present section fails to consider the regions of high stress concentration M and N at the ends of the wall, and so cannot give any information of the total energy and the equilibrium orientation of the wall in this case. Secondly, consider a finite crystal with the wall extending right across it (fig. 3 (*b*)); now the surface

of the crystal must be stress free and, to secure this, additional stresses (which possibly alter the equilibrium positions of the dislocations) must be added to the stresses of § 5. On the other hand suppose the stresses in the crystal are those obtained in this section, that is they are given by eqns. (51) and (52) with z_α^{-1} replaced by the expression (63); with the Burgers vector given by eqn. (61) the stress on the surface of the crystal is then negligibly small except within a distance of order h from the points A and B where the surface is met by the wall, and the stresses here are easily shown to give zero resultant force and moment; hence if the stresses on the surface are relaxed the change in the stress field will, by Saint-Venant's principle be confined to regions at the ends of the wall with dimensions of order h. Also the stress σ_{12} on each dislocation due to the others may be shown to be zero, and so the dislocations are in equilibrium. Thus the stress field has essentially been found.

We see then that there are two distinct physical situations: if the wall terminates inside the crystal, its orientation must be determined by the considerations of § 5; while if the wall extends right across the grain, the treatment of the present section will apply, and the wall will be normal to the slip plane.

However if the angle θ (fig. 2) defining the equilibrium between a pair of edge dislocations is a right angle, then incomplete walls will also be formed normal to the slip plane and the distinction between two cases largely disappears. Owing to the high symmetry of the lattices commonly occurring in metals, this will be so in a number of important instances. For if either the x_1 or the x_2 axis, i.e. either the slip direction or the normal to the slip plane, is a two fold axis, then the equilibrium positions of the dislocation at P must be arranged symmetrically on either side of the plane $x_1 = 0$; also the total number of equilibrium positions was seen in § 5 to be odd; hence an equilibrium position must occur on $x_1 = 0$. The only important case not covered by these symmetry requirements seems to be that of the body-centred cubic lattice with slip direction [111] and slip plane (11$\bar{2}$) or (12$\bar{3}$) (but not 1$\bar{1}$0)). Here dislocation walls may be expected in different orientations according as they are complete or incomplete.

On the other hand dislocation walls terminating inside the crystal may not occur with any great frequency as, owing to the high stress concentrations at their ends, they represent a state of high energy. They are unlikely to survive any prolonged heat treatment in which dislocation climb can occur; while even if only glide occurs, the nature of the stresses at the ends of the wall is such that dislocations will tend to be captured. and in this way the wall can extend across the crystal.

§ 7. Evaluation of the Constants

In this section we consider how the various constants we have introduced, and particularly the $L_{i\alpha}$, may be evaluated. It will be convenient to use instead of the elastic moduli c_{MN}, the elastic coefficients s_{MN}.

This also has the advantages for numerical work that compilations of experimental values, for example those of Schmid and Boas (1950), and of Hearmon (1946), usually give the values of s_{MN} rather than of c_{MN}.

The relation between stress and strain is then

$$e_M = s_{MN}\sigma_N. \quad . \quad . \quad . \quad . \quad . \quad . \quad . \quad . \quad . \quad (64)$$

In the present case the strain $e_3 = \partial u_3/\partial x_3$ is identically zero, and we may use this to eliminate the stress component $\sigma_3 = \sigma_{33}$ from eqns. (64); we obtain

$$e_M = S_{MN}\sigma_N, \quad . \quad . \quad . \quad . \quad . \quad . \quad . \quad . \quad . \quad (65)$$

where

$$S_{MN} = s_{MN} - s_{M3}s_{N3}/s_{33}. \quad . \quad . \quad . \quad . \quad . \quad . \quad . \quad (66)$$

Equation (66) gives $S_{M3} = S_{3N} = 0$, and omitting these elements from the matrix $[S_{MN}]$, we may show that the remaining 5×5 matrix is reciprocal to (30).

The constants β_{ij} and γ_{ij} are now easily expressed in terms of the S_{MN}; from Jacobi's theorem we obtain the non-zero elements in eqns. (28) and (34)

$$\left.\begin{aligned} \beta_{22} &= S_{44}/(S_{22}S_{44} - S_{24}^2), \\ \beta_{33} &= S_{22}/(S_{22}S_{44} - S_{24}^2), \\ \beta_{23} &= \beta_{32} = -S_{24}/(S_{22}S_{44} - S_{24}^2), \end{aligned}\right\} \quad . \quad . \quad . \quad . \quad (67)$$

and

$$\left.\begin{aligned} \gamma_{11} &= S_{55}/(S_{11}S_{55} - S_{15}^2), \\ \gamma_{33} &= S_{11}/(S_{11}S_{55} - S_{15}^2), \\ \gamma_{13} &= \gamma_{31} = -S_{15}/(S_{11}S_{55} - S_{15}^2). \end{aligned}\right\} \quad . \quad . \quad . \quad . \quad (68)$$

We now consider solutions of the elastic equations which involve only one of the roots p_α, that is we take the displacement to be of the simple form (6) rather than the more general form (9). The stress functions ϕ_i may then be written, on using (16), as

$$\left.\begin{aligned} \phi_1 &= -p_\alpha L_{2\alpha} f(x_1 + p_\alpha x_2), \\ \phi_2 &= L_{2\alpha} f(x_1 + p_\alpha x_2), \\ \phi_3 &= L_{3\alpha} f(x_1 + p_\alpha x_2). \end{aligned}\right\} \quad . \quad . \quad . \quad . \quad . \quad . \quad . \quad (69)$$

The stresses deduced from these functions must satisfy the compatibility conditions. Expressed in terms of the strains, the compatibility equations reduce, in the present case, to

$$\frac{\partial^2 e_1}{\partial x_2^2} + \frac{\partial^2 e_2}{\partial x_1^2} = \frac{\partial^2 e_6}{\partial x_1 \partial x_2}, \quad . \quad . \quad . \quad . \quad . \quad . \quad . \quad (70)$$

and

$$\frac{\partial e_4}{\partial x_1} - \frac{\partial e_5}{\partial x_2} = 0. \quad . \quad . \quad . \quad . \quad . \quad . \quad . \quad (71)$$

Inserting (65) in (70) and (71) and using (10) and (69) we obtain

$$L_{2\alpha}[p_\alpha{}^4S_{11}-2p_\alpha{}^3S_{16}+p_\alpha{}^2(2S_{12}+S_{66})-2p_\alpha S_{26}+S_{22}] - L_{3\alpha}[p_\alpha{}^3S_{15}-p_\alpha{}^2(S_{14}+S_{56})+p_\alpha(S_{25}+S_{46})-S_{24}]=0, \quad . \quad (72)$$

and

$$L_{2\alpha}[p_\alpha{}^3S_{15}-p_\alpha{}^2(S_{14}+S_{56})+p_\alpha(S_{25}+S_{46})-S_{24}] - L_{3\alpha}[p_\alpha{}^2S_{55}-2p_\alpha S_{45}+S_{44}]=0. \quad . \quad (73)$$

Eliminating $L_{2\alpha}$ and $L_{3\alpha}$ from (72) and (73) we find that p_α must be a root of the sextic equation

$$[p^4S_{11}-2p^3S_{16}+p^2(2S_{12}+S_{66})-2pS_{26}+S_{22}][p^2S_{55}-2pS_{45}+S_{44}] - [p^3S_{15}-p^2(S_{14}+S_{56})+p(S_{25}+S_{46})-S_{24}]^2=0. \quad . \quad (74)$$

Now eqns. (8) and (74) both just determine the values of p for which a solution with the displacements of the form (6) exists. Thus these two equations must be identical and we have simply expressed the coefficients in terms of the S_{MN} instead of the c_{MN}.

Now we recall that the vectors $L_{i\alpha}$ are undefined to the extent of an arbitrary constant factor (for each α); if $L_{2\alpha}\neq 0$ we choose this factor so that $L_{2\alpha}=1$. Then $L_{i\alpha}=(-p_\alpha, 1, l_\alpha)$, where l_α is a constant which has still to be determined. Substituting this value of $L_{i\alpha}$ in (73) we find

$$l_\alpha=[p_\alpha{}^3S_{15}-p_\alpha{}^2(S_{14}+S_{56})+p_\alpha(S_{26}+S_{46})-S_{24}]/[p_\alpha{}^2S_{55}-2p_\alpha S_{45}+S_{44}], \quad (75)$$

and l_α is determined provided p_α does not satisfy the equation

$$p^2S_{55}-2pS_{45}+S_{44}=0. \quad . \quad . \quad . \quad . \quad . \quad . \quad (76)$$

Then if none of the roots of (74) also satisfy (76), we may write

$$[L_{i\alpha}]=\begin{bmatrix} -p_1 & -p_2 & -p_3 \\ 1 & 1 & 1 \\ l_1 & l_2 & l_3 \end{bmatrix}; \quad . \quad . \quad . \quad . \quad . \quad . \quad (77)$$

and

$$[M_{\alpha i}]=L^{-1}\begin{bmatrix} l_3-l_2 & l_3p_2-l_2p_3 & p_3-p_2 \\ l_1-l_3 & l_1p_3-l_3p_1 & p_1-p_3 \\ l_2-l_1 & l_2p_1-l_1p_2 & p_2-p_1 \end{bmatrix}, \quad . \quad . \quad . \quad (78)$$

where L denotes the value of the determinant $|L_{i\alpha}|$. To determine B_{ij}, we must first evaluate P_{ij} and Q_{ij} defined in eqns. (42) and (43) and then solve (41) and (44). However, the expressions become increasingly complicated, and it is probably best to procede numerically at this point.

If eqns. (74) and (76) have a root in common we choose the labelling α so that this root is p_3. Comparing (74) and (76) we see that we must have

$$p_3{}^3S_{15}-p_3{}^2(S_{14}+S_{56})+p_3(S_{25}+S_{46})-S_{24}=0, \quad . \quad . \quad . \quad (79)$$

and (72) and (73) will be satisfied if L_{i3} is of the form (0, 0, 1). It is of course possible for eqn. (79) to be true without the coefficients vanishing identically, but this does not appear to be of much physical significance. A more important case is when (79) holds because the coefficients vanish identically; a sufficient condition for this is that the x_3 axis should be a

two-fold symmetry axis. Then (74) factorizes into a quartic and quadratic equation, and also (72) and (73) give $l_1 = l_2 = 0$. Thus

$$[L_{i\alpha}] = \begin{bmatrix} -p_1 & -p_2 & 0 \\ 1 & 1 & 0 \\ 0 & 0 & 1 \end{bmatrix}, \quad . \quad . \quad . \quad . \quad . \quad . \quad . \quad . \quad (80)$$

and

$$[M_{\alpha i}] = \begin{bmatrix} (p_2-p_1)^{-1} & p_2(p_2-p_1)^{-1} & 0 \\ -(p_2-p_1)^{-1} & -p_1(p_2-p_1)^{-1} & 0 \\ 0 & 0 & 1 \end{bmatrix}. \quad . \quad . \quad . \quad (81)$$

On account of the simple form of these matrices, the remaining constants are readily evaluated explicitly. From (43)

$$[P_{ij}] = \begin{bmatrix} p_1+p_2 & p_1p_2 & 0 \\ -1 & 0 & 0 \\ 0 & 0 & p_3 \end{bmatrix}, \quad . \quad . \quad . \quad . \quad . \quad . \quad . \quad (82)$$

and from (42)

$$[Q_{ij}] = \begin{bmatrix} 0 & -1 & 0 \\ 1/p_1p_2 & 1/p_1+1/p_2 & 0 \\ 0 & 0 & 1/p_3 \end{bmatrix}. \quad . \quad . \quad . \quad . \quad . \quad (83)$$

Also in the present case, the non-zero elements of β_{ij} and γ_{ij} reduce, by (67) and (68) to

$$\left.\begin{aligned} \beta_{22} &= S_{22}^{-1}, & \beta_{33} &= S_{44}^{-1}, \\ \text{and} \qquad \gamma_{11} &= S_{11}^{-1}, & \gamma_{33} &= S_{55}^{-1}, \end{aligned}\right\} \quad . \quad . \quad . \quad . \quad . \quad . \quad (84)$$

since $S_{24} = S_{15} = 0$. Then substituting (82), (83) and (84) in (41) and (44), we find

$$[B_{ij}] = \frac{1}{2i}\begin{bmatrix} S_{11}(p_1+p_2-\bar{p}_1-\bar{p}_2) & S_{11}(p_1p_2-\bar{p}_1\bar{p}_2) & 0 \\ S_{11}(p_1p_2-\bar{p}_1\bar{p}_2) & -S_{22}(1/p_1+1/p_2-1/\bar{p}_1-1/\bar{p}_2) & 0 \\ 0 & 0 & S_{55}(p_3-\bar{p}_3) \end{bmatrix}$$
$$. \quad . \quad . \quad (85)$$

By substituting this value of B_{ij} in eqns. (50), d_i may be expressed in terms of the Burgers vector, and hence the stresses of the dislocation may be obtained from (51) and (52) by a straight forward substitution.

In particular we note that if $b_i = (b, 0, 0)$, then $d_2 = 0$ only if $p_1p_2 = \bar{p}_1\bar{p}_2$; but this would imply a relation between the elastic coefficients which will not in general hold. The statement following eqn. (62) is thus verified.

§ 8. Cracks: The General Solution

Suppose we have an infinite crystal in which there is a crack along that portion of the plane $x_2 = 0$ which is given by $-1 \leqslant x_1 \leqslant 1$. An arbitrary stress is applied to the crystal such that in the absence of any stress relaxation due to the crack there would be a traction of $\tau_i(x_1)$ over the

surface of the crack. We must therefore add a stress field which produces a traction of $-\tau_i(x_1)$ over the surface of the crack and which vanishes at infinity.

We consider the semi-infinite regions $x_2>0$, and $x_2<0$ separately. In $x_2>0$ a displacement which has the form (9) and which remains finite at infinity is

$$u_k=\sum_\alpha A_{k\alpha}\int_0^\infty d\rho F_\alpha^+(\rho)\exp(i\rho z_\alpha)+\sum_\alpha \bar{A}_{k\alpha}\int_0^\infty d\rho\overline{F_\alpha^+(\rho)}\exp(-i\rho\bar{z}_\alpha). \quad (86)$$

The corresponding stress functions are

$$\phi_k=\sum_\alpha L_{k\alpha}\int_0^\infty d\rho F_\alpha^+(\rho)\exp(i\rho z_\alpha)+\sum_\alpha \bar{L}_{k\alpha}\int_0^\infty d\rho\overline{F_\alpha^+(\rho)}\exp(-i\rho\bar{z}_\alpha). \quad (87)$$

In the region $x_2<0$, we may take the stress functions to be

$$\phi_k=\sum_\alpha L_{k\alpha}\int_0^\infty d\rho F_\alpha^-(\rho)\exp(-i\rho z_\alpha)+\sum_\alpha \bar{L}_{k\alpha}\int_0^\infty d\rho\overline{F_\alpha^-(\rho)}\exp(i\rho\bar{z}_\alpha). \quad (88)$$

We have now to relate the solutions in the two regions. In the part of the plane $x_2=0$ outside the crack the material must be joined together, and the boundary condition on the stress is then that the components σ_{i2} should be continuous. In the crack the components take on prescribed values and so are a fortiore also continuous here. Hence $\sigma_{i2}=\partial\phi_i/\partial x_1$, is continuous over the whole plane $x_2=0$. Now an arbitrary constant can be added to ϕ_i without affecting the stresses, and if this constant is chosen suitably then ϕ_i will also be continuous across $x_2=0$. Putting $x_2=0$ in (87) and (88) and comparing the resulting equations we obtained the boundary conditions

$$\sum_\alpha L_{i\alpha}F_\alpha^+(\rho)=\sum_\alpha \bar{L}_{i\alpha}\overline{F_\alpha^-(\rho)}:$$

denoting these expressions by $\psi_i(\rho)$, we have

$$\left.\begin{aligned}F_\alpha^+(\rho)&=M_{\alpha i}\psi_i(\rho),\\ F_\alpha^-(\rho)&=M_{\alpha i}\overline{\psi_i(\rho)}.\end{aligned}\right\}\quad (89)$$

On substituting from (89) in (86) we obtain the displacement in the region $x_2>0$

$$u_k=\sum_\alpha A_{k\alpha}M_{\alpha i}\int_0^\infty \psi_i(\rho)\exp(i\rho z_\alpha)\,d\rho+\sum_\alpha \bar{A}_{k\alpha}\bar{M}_{\alpha i}\int_0^\infty\overline{\psi_i(\rho)}\exp(-i\rho\bar{z}_\alpha)\,d\rho. \quad (90)$$

In the region $x_2<0$, the displacement will be

$$u_k=\sum_\alpha A_{k\alpha}M_{\alpha i}\int_0^\infty\overline{\psi_i(\rho)}\exp(-i\rho z_\alpha)\,d\rho+\sum_\alpha \bar{A}_{k\alpha}\bar{M}_{\alpha i}\int_0^\infty\psi_i(\rho)\exp(i\rho\bar{z}_\alpha)\,d\rho. \quad (91)$$

Subtracting (90) and (91) we find that the difference in displacement on either side of the plane $x_2=0$ is

$$\Delta u_k=-2iB_{ki}\int_0^\infty\{\psi_i(\rho)\exp(i\rho x_1)-\overline{\psi_i(\rho)}\exp(-i\rho x_1)\}\,d\rho, \quad (92)$$

where B_{ki} is defined in eqn. (40). Outside the crack the displacement

must be continuous and so $\Delta u_k = 0$. Since $|B_{ki}| \neq 0$, this gives

$$\int_0^\infty \{\psi_i(\rho) \exp(i\rho x_1) - \overline{\psi_i(\rho)} \exp(-i\rho x_1)\} d\rho = 0, \quad |x_1| > 1. \quad . \quad (93)$$

Also substituting (89) in (87) we obtain the stress functions in the region $x_2 > 0$

$$\phi_k = \sum_\alpha L_{k\alpha} M_{xi} \int_0^\infty \psi_i(\rho) \exp(i\rho z_\alpha) d\rho + \sum_\alpha \bar{L}_{k\alpha} \bar{M}_{\alpha i} \int_0^\infty \overline{\psi_i(\rho)} \exp(-i\rho \bar{z}_\alpha) d\rho. \quad (94)$$

Now on the surface of the crack the stresses $\sigma_{k2} = \partial\phi_k/\partial x_1$, must be equal to $-\tau_k(x_1)$. Hence from (94) we obtain

$$i \int_0^\infty \{\psi_i(\rho) \exp(i\rho x_1) - \overline{\psi_i(\rho)} \exp(-i\rho x_1)\} \rho \, d\rho = -\tau_i(x_1), \quad -1 < x_1 < 1. \quad (95)$$

If we write $\psi_i = \psi_i' + i\psi_i''$ where ψ_i' and ψ_i'' are real. eqns. (93) and (95) become

$$\int_0^\infty \{\psi_i' \sin \rho x_1 + \psi_i'' \cos \rho x_1\} d\rho = 0 \qquad |x_1| > 1,$$

and

$$\int_0^\infty \{\psi_i' \sin \rho x_1 + \psi_i'' \cos \rho x_1\} \rho \, d\rho = \tfrac{1}{2}\tau_i(x_1) \qquad -1 < x_1 < 1.$$

These are equivalent to the two pairs of dual integral equations

$$\left.\begin{aligned} &\int_0^\infty \psi_i'(\rho) \sin \rho x_1 \, d\rho = 0 \qquad x_1 > 1, \\ &\int_0^\infty \psi_i'(\rho) \sin \rho x_1 \, . \, \rho \, d\rho = \tfrac{1}{4}\{\tau_i(x_1) - \tau_i(-x_1)\}, \quad 0 < x_1 < 1 \end{aligned}\right\} \quad . \quad (96)$$

and

$$\left.\begin{aligned} &\int_0^\infty \psi_i''(\rho) \cos \rho x_1 \, d\rho = 0 \qquad x_1 > 0, \\ &\int_0^\infty \psi_i''(\rho) \cos \rho x_1 \, . \, \rho \, d\rho = \tfrac{1}{4}\{\tau_i(x_1) + \tau_i(-x_1)\} \quad 0 < x_1 < 1. \end{aligned}\right\} \quad . \quad (97)$$

Equations (96) and (97) are special cases of a general set of dual integral equations studied by Titchmarsh (1937) and Busbridge (1938). Their general solution leads to

$$\psi_i'(\rho) = \frac{1}{2\pi} \int_0^1 \mu J_1(\mu\rho) \, d\mu \int_{-1}^1 \tau_i(\mu\xi)(1-\xi^2)^{-1/2} \xi \, d\xi, \quad . \quad . \quad (98)$$

and

$$\psi_i''(\rho) = \frac{1}{2\pi} \int_0^1 \mu J_0(\mu\rho) \, d\mu \int_{-1}^1 \tau_i(\mu\xi)(1-\xi^2)^{-1/2} \, d\xi. \quad . \quad . \quad (99)$$

On substituting (98) and (99) in eqn. (90) we obtain the displacements

$$\begin{aligned} u_k = &\frac{1}{2\pi} \sum_\alpha (A_{k\alpha} M_{\alpha j} + \bar{A}_{k\alpha} \bar{M}_{\alpha j}) \int_0^1 d\mu \int_{-1}^1 \tau_j(\mu\xi) \xi (1-\xi^2)^{-1/2} \, d\xi \\ &- \frac{1}{2\pi} \sum_\alpha A_{k\alpha} M_{\alpha j} \int_0^1 d\mu (z_\alpha^2 - \mu^2)^{-1/2} \int_{-1}^1 \tau_j(\mu\xi)(\mu + z_\alpha \xi)(1-\xi^2)^{-1/2} \, d\xi \\ &- \frac{1}{2\pi} \sum_\alpha \bar{A}_{k\alpha} \bar{M}_{\alpha j} \int_0^1 d\mu (\bar{z}_\alpha^2 - \mu^2)^{-1/2} \int_{-1}^1 \tau_j(\mu\xi)(\mu + \bar{z}_\alpha \xi)(1-\xi^2)^{-1/2} \, d\xi. \quad (100) \end{aligned}$$

This expression will be valid both in the region $x_2 > 0$, and in $x_2 < 0$ provided we choose the sign of $(z_\alpha^2 - \mu^2)^{1/2}$ so that

$$\arg (z_\alpha^2 - \mu^2)^{1/2} \to \arg z_\alpha \quad \text{as} \quad |z_\alpha| \to \infty.$$

The stress functions ϕ_k will be given by an expression of the form (100) but in which $A_{k\alpha}$ is replaced by $L_{k\alpha}$. Once the ϕ_k are determined the stresses are readily obtained by differentiation according to eqns. (10); it is to be remembered that the stresses obtained in this way are to be added to the stresses which would occur in the infinite material if the crack were absent.

A particular case of some importance is that in which the applied stress field is uniform. With τ_j constant, the equation corresponding to (100) for the stress functions reduces to

$$\phi_k = \tfrac{1}{2} \sum_\alpha \{L_{k\alpha} M_{\alpha j} [(z_\alpha^2 - 1)^{1/2} - z_\alpha] + \bar{L}_{k\alpha} \bar{M}_{\alpha j} [(\bar{z}_\alpha^2 - 1)^{1/2} - \bar{z}_\alpha]\} \tau_j.$$

From this we obtain the stresses

$$\sigma_{k1} = -\tfrac{1}{2} \sum_\alpha \{L_{k\alpha} M_{\alpha j} p_\alpha [z_\alpha (z_\alpha^2 - 1)^{-1/2} - 1] + \bar{L}_{k\alpha} \bar{M}_{\alpha j} \bar{p}_\alpha [\bar{z}_\alpha (\bar{z}_\alpha^2 - 1)^{-1/2} - 1]\} \tau_j,$$

$$\sigma_{k2} = \tfrac{1}{2} \sum_\alpha \{L_{k\alpha} M_{\alpha j} z_\alpha (z_\alpha^2 - 1)^{-1/2} + \bar{L}_{k\alpha} \bar{M}_{\alpha j} \bar{z}_\alpha (\bar{z}_\alpha^2 - 1)^{-1/2}\} \tau_j - \tau_k.$$

§ 9. The Stresses near the Tip of a Crack

The stresses near the tip of the crack are of special importance since there will be a large stress concentration here, and we shall consider now the nature of these stresses.

First we reduce the repeated integral in (100) to a single integral. This may be accomplished by replacing the variable ξ by $\eta = \xi\mu$ and changing the order of integration; we obtain

$$\phi_k = -\frac{1}{2\pi} \sum_\alpha \left\{ L_{k\alpha} M_{\alpha j} \int_{-1}^{1} \tau_j(\xi)\, d\xi \cos^{-1} \frac{z_\alpha \xi - 1}{z_\alpha - \xi} + \bar{L}_{k\alpha} \bar{M}_{\alpha j} \int_{-1}^{1} \tau_j(\xi)\, d\xi \cos^{-1} \frac{\bar{z}_\alpha \xi - 1}{\bar{z}_\alpha - \xi} \right\} \quad . \quad . \quad . \quad (101)$$

on dropping a constant term which can contribute nothing to the stresses. Then from (101) we obtain the stresses

$$\sigma_{k1} = -\frac{1}{2\pi} \sum_\alpha \left\{ L_{k\alpha} p_\alpha M_{\alpha j} (z_\alpha^2 - 1)^{-1/2} \int_{-1}^{1} \tau_j(\xi)\, d\xi (1 - \xi^2)^{1/2} (z_\alpha - \xi)^{-1} + \bar{L}_{k\alpha} \bar{p}_\alpha \bar{M}_{\alpha j} (\bar{z}_\alpha^2 - 1)^{-1/2} \int_{-1}^{1} \tau_j(\xi)\, d\xi (1 - \xi^2)^{1/2} (\bar{z}_\alpha - \xi)^{-1} \right\}, \quad . \quad (102)$$

and

$$\sigma_{k2} = \frac{1}{2\pi} \sum_\alpha \left\{ L_{k\alpha} M_{\alpha j} (z_\alpha^2 - 1)^{-1/2} \int_{-1}^{1} \tau_j(\xi)\, d\xi (1 - \xi^2)^{1/2} (z_\alpha - \xi)^{-1} + \bar{L}_{k\alpha} \bar{M}_{\alpha j} (\bar{z}_\alpha^2 - 1)^{-1/2} \int_{-1}^{1} \tau_j(\xi)\, d\xi (1 - \xi^2)^{1/2} (\bar{z}_\alpha - \xi)^{-1} \right\}. \quad . \quad (103)$$

Now we are interested in points near the tip of the crack where $z_\alpha = 1$; hence we write $z_\alpha = 1 + \zeta_\alpha$ and take $|\zeta_\alpha|$ small compared with unity. If r and θ are defined as in fig. 4 we have

$$\zeta_\alpha = r(\cos\theta + p_\alpha \sin\theta). \quad . \quad . \quad . \quad . \quad . \quad (104)$$

Then

$$\frac{1}{\pi}\int_{-1}^{1} \tau_j(\xi)(1-\xi^2)^{1/2}(z_\alpha - \xi)^{-1}\,d\xi \simeq \frac{1}{\pi}\int_{-1}^{1} \tau_j(\xi)(1+\xi)^{1/2}(1-\xi)^{-1/2}d\xi,$$

$$= T_j, \text{ say.} \quad . \quad . \quad . \quad . \quad . \quad . \quad (105)$$

T_j may be regarded as a suitably weighted average value of τ_j over the crack; it has been defined so that if τ_j is constant $T_j = \tau_j$. Substituting (105) in (102) and (103) and remembering that ζ_α is small, we obtain

$$\left.\begin{aligned} \sigma_{k1} &= -\tfrac{1}{2}\sum_\alpha \{L_{k\alpha}p_\alpha M_{\alpha j}(2\zeta_\alpha)^{-1/2} + \bar{L}_{k\alpha}\bar{p}_\alpha \bar{M}_{\alpha j}(2\bar{\zeta}_\alpha)^{-1/2}\}T_j, \\ \sigma_{k2} &= \tfrac{1}{2}\sum_\alpha \{L_{k\alpha}M_{\alpha j}(2\zeta_\alpha)^{-1/2} + \bar{L}_{k\alpha}\bar{M}_{\alpha j}(2\bar{\zeta}_\alpha)^{-1/2}\}T_j. \end{aligned}\right\} \quad . \quad (106)$$

Fig. 4

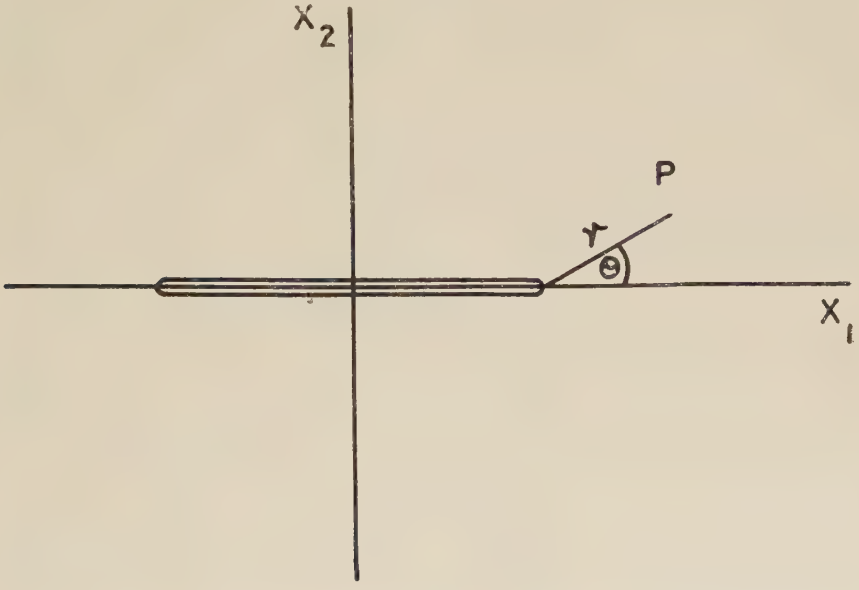

In particular we note that these stresses decrease with the distance from the tip of the crack as $r^{-1/2}$, just as in the isotropic case.

In the plane of the crack we have $\theta = 0$ and $\zeta_\alpha = r$, and so from (106) the stresses acting across this plane are

$$\sigma_{k2} = (2r)^{-1/2} T_k; \quad . \quad . \quad . \quad . \quad . \quad . \quad . \quad (107)$$

it is interesting to note that these stresses depend neither on the symmetry nor the elastic constants of the material.

If the length of the crack is $2c$ then we have only to replace r in eqns. (104) and (107) by r/c.

§ 10. The Energy of a Crack

If the two sides of the crack undergo a relative displacement Δu_k when the surface tractions τ_k are relaxed, the elastic energy of the material will change by an amount

$$U = \tfrac{1}{2}\int_{-1}^{1} \tau_k(x_1)\Delta u_k\, dx_1. \qquad (108)$$

Now Δu_k is given by eqn. (92) $(-1 < x_1 < 1)$, and substituting from (98) and (99) in this we obtain

$$\Delta u_k = \frac{2}{\pi} B_{kj} \int_{|x_1|}^{1} \frac{d\mu}{(\mu^2 - x_1^2)^{1/2}} \int_{-1}^{1} \tau_j(\mu\xi)(\mu + x_1\xi)\frac{d\xi}{(1-\xi^2)^{1/2}}. \qquad (109)$$

From (108) and (109) the energy of the crack may be written as

$$U = \tfrac{1}{2}\pi B_{jk} \int_{-1}^{1} |\mu|\, d\mu T_j(\mu) T_k(\mu), \qquad (110)$$

where

$$T_j(\mu) = \pi^{-1} \int_{-\pi/2}^{\pi/2} \tau_j(\mu \sin\theta)(1 + \sin\theta)\, d\theta. \qquad (111)$$

T_j as defined in eqn. (105) is related to the present $T_j(\mu)$ by

$$T_j = T_j(1).$$

In the particular case in which the applied stresses are uniform, $T_j(\mu) = \tau_j$ and the energy (110) becomes

$$U = \tfrac{1}{2}\pi B_{jk}\tau_j\tau_k;$$

or if the crack has length $2c$ then this energy is

$$U = \tfrac{1}{2}\pi B_{jk}\tau_j\tau_k c^2. \qquad (112)$$

Similarly, in the general case a factor c^2 must be inserted in eqn. (110).

References

Busbridge, I. W., 1938, *Proc. Lond. math. Soc.*, **44**, 115.

Cottrell, A. H., 1949, *Progress in Metal Physics*, I (London: Pergamon Press), p. 77.

Eshelby, J. D., Read, W. T., and Shockley, W., 1953, *Acta Met.*, **1**, 251.

Frank, F. C., 1950, *Report of Pittsburgh Conference on Plastic Deformation of Crystals* (Washington: Carnegie Institute of Technology and Office of Naval Research), p. 150.

Hearmon, R. F. S., 1946, *Rev. mod. Phys.*, **18**, 409.

Schmid, E., and Boas, W., 1950, *Plasticity of Crystals* (London: Hughes).

Titchmarsh, E. C., 1937, *Introduction to the theory of Fourier integrals* (Oxford: University Press).

The Capture of Slow Neutrons by Protons†

By A. R. Baker‡ and D. H. Wilkinson§
Cavendish Laboratory, Cambridge

[Received April 4, 1958]

Abstract

The result of a new experimental determination of the capture cross section of protons for slow neutrons is briefly reported. It is $\sigma_H = 0{\cdot}327 \pm 0{\cdot}004$ barns and is obtained by a comparison with the absorption of boron for slow neutrons.

A survey is presented of various direct and indirect methods for determining the neutron–proton capture cross section and the final value resulting from their inter-comparison is $\sigma_H = 0{\cdot}3315 \pm 0{\cdot}0017$ barns.

The cross section σ_H for the capture of slow neutrons by protons is the simplest process which may be expected to be markedly influenced by mesonic interaction effects (Austern and Sachs 1951, Austern 1953). Since these effects are expected to give a contribution of a few per cent to the cross section we must know σ_H with high accuracy. Other uncertainties in the evaluation of the interaction effect are due to lack of precise knowledge of other relevant two nucleon properties such as $r_t(-\epsilon, -\epsilon)$, the D-state percentage in the deuteron ground state and the effective n–p potentials. However these uncertainties are presently being reduced by both experimental and theoretical study and this is a suitable moment for an accurate evaluation of σ_H.

Several measurements of σ_H have appeared during the last decade. None however has used the traditional method of comparing the slow neutron density distributions due to a steady neutron source in water and a boron-rich solution. This method has the disadvantage that the bulky detectors usually used introduce a perturbation into the neutron distribution which cannot be evaluated with adequate reliability. We have however returned to this method and have overcome the difficulty by using as slow neutron detectors unmounted discs of boron loaded nuclear photographic emulsion of diameter 6 mm and thickness 100 μ. The perturbation in this case is small and can be accurately calculated owing to the simple form of the detectors. The neutron distribution was determined by counting under the microscope the individual events due to the reaction $^{10}B(n, \alpha)^7Li$ in 54 detecting discs in each of two cylindrical tanks of height 4 ft and diameter 5 ft, one filled with distilled water and the other with an aqueous solution of boric acid. The neutron source was a Po–Be mixture. A total of about 200 000 tracks was counted. As a

---

† Communicated by the Authors.
‡ Now at A.E.R.E., Harwell.
§ Now at the Clarendon Laboratory, Oxford.

result of this investigation we determined the ratio between σ_H and σ_B the cross section for slow neutron capture in our boron. The ratio between σ_B of our boron and of the standard Harwell boron was measured by a pile oscillator method. σ_B for the standard Harwell boron is taken as $769{\cdot}4 \pm 3{\cdot}8$ barns (at a neutron velocity of 2200 m/sec) from the work of Egelstaff (1957) which considers the work of many laboratories.

From this experiment we find the value $\sigma_H = 0{\cdot}3271 \pm 0{\cdot}0042$ barns. A full account of this work will be published by the first named author of this note.

We now attempt a comparison of the various data from which σ_H may be derived in order to arrive at the best current value for this constant. There are three chief approaches. In the first the mean life τ of thermal neutrons in water is measured directly. In the second a measurement is made of the ratio σ_B/σ_H which is then converted into a value for σ_H by using some independently determined value of σ_B. In the third we combine measurements of L (the diffusion length for slow neutrons in water) and D (the diffusion constant for slow neutrons in water) at the same temperature in order to arrive at a value for the mean life $\tau = L^2/D$.

Table 1. Direct Determinations of the Slow Neutron Mean Lifetime τ in Water Reduced to 22°C

Author	τ (μsec)
Antonov *et al.* (1955)	$206{\cdot}5 \pm 4{\cdot}2$
Bracci and Coceva (1956)	202 ± 6
von Dardel and Sjöstrand (1954)	$204{\cdot}4 \pm 2{\cdot}0$
Meads *et al.* (1956)	$203{\cdot}4 \pm 2{\cdot}6$
Mean value $\tau = 204{\cdot}3 \pm 1{\cdot}4$ μsec ($\chi^2 = 0{\cdot}54$; $P = 0{\cdot}9$)	

In table 1 we present the results of recent measurements of τ. We have rejected the measurements by von Dardel and Waltner (1953) and Scott *et al.* (1954) the former owing to the unknown and probably large effect of the perturbation by the detectors of the slow neutron density (see von Dardel and Sjöstrand 1954) and the second because of the uncertain allowance for the effect of higher harmonics. Where necessary slight corrections have been applied to the original results in order to reduce them to an effective water temperature of 22°C. This correction is particularly important for one of the measurements presented by Antonov *et al.* (1955) which was carried out at 80°C. The lifetime quoted for the results of these workers is obtained by averaging that determined at 23°C with the suitably corrected figure at 80°C. It is seen that these several results are in excellent accord with one another.

In table 2 we summarize the recent accurate determinations of σ_B/σ_H including that reported in this paper. The two U.S. results were originally determined relative to the standard U.S. boron. In quoting σ_B/σ_H in table 2 we have corrected this ratio to correspond to the standard Harwell boron using σ_B U.S./σ_B Harwell $= 0{\cdot}986 \pm 0{\cdot}003$ suggested by the work of Green *et al.* (1954)—see also Egelstaff (1957). The mean value of σ_B/σ_H given in table 2 therefore refers to standard Harwell boron. Again the accord between these various measurements is excellent.

Table 2. Measurements of σ_B/σ_H reduced to standard Harwell boron using the Ratio σ_B U.S./σ_B Harwell $= 0{\cdot}986 \pm 0{\cdot}003$

Author	σ_B/σ_H
Baker and Wilkinson (this paper)	2352 ± 28
Hamermesh *et al.* (1953)	2325 ± 28
Harris *et al.* (1953)	2306 ± 51
Mean value $\sigma_B/\sigma_H = 2338 \pm 18$ ($\chi^2 = 0{\cdot}86$; $P = 0{\cdot}7$)	

Table 3 summarizes recent measurements of the diffusion length L. In presenting these results we have corrected the quoted values for buckling where necessary and have reduced them to a value appropriate to 22°C on the assumption that L is proportional to the square root of the absolute temperature. We have admitted without further correction the

Table 3. Measurements of the Diffusion Length for Slow Neutrons in Water Reduced to 22°C

Author	L (cm)
Barkhov *et al.* (1957)	$2{\cdot}684 \pm 0{\cdot}020$
De Juren and Rosenwasser (1953)	$2{\cdot}735 \pm 0{\cdot}015$
Wright and Frost (1956)	$2{\cdot}700 \pm 0{\cdot}010$
Mean value $L = 2{\cdot}707 \pm 0{\cdot}008$ cm ($\chi^2 = 5{\cdot}3$; $P = 0{\cdot}1$) Adopted value $L = 2{\cdot}707 \pm 0{\cdot}012$ cm	

preliminary value due to Wright and Frost (1956) which may require subsequent revision. These values of L are seen to be in barely adequate accord with each other and for this and other reasons connected with the buckling correction and possible systematic errors we have preferred to increase the statistical error by 50%.

In table 4 we present recent results on the diffusion constant D. These we have reduced to an effective temperature of 22°C under the assumption

that a 1° rise in temperature increases D by 130 cm²/sec. This correction is a very small one and is in all cases well below the stated error of the measurements. These determinations are seen to be in good mutual accord.

Table 4. Measurements of the Diffusion Constant D for Slow Neutrons in Water Reduced to 22°C

Author	D (cm²/sec)
Antonov *et al.* (1955)	$34\,870 \pm 1000$
Bracci and Coceva (1956)	$34\,850 \pm 1100$
Campbell and Stelson (1956)	$34\,670 \pm 1000$
von Dardel and Sjöstrand (1954)	$36\,340 \pm 750$
Dio and Schopper (1958)	$35\,440 \pm 600$
Mean value $D = 35\,420 \pm 370$ cm²/sec ($\chi^2 = 2{\cdot}3$; $P = 0{\cdot}7$)	

When these values for L and D are combined we find the result $\tau = 206{\cdot}9 \pm 2{\cdot}8$ μsec.

In table 5 we compare the values of σ_H obtained by the three independent methods. In quoting the value derived from the ratio σ_B/σ_H we have used the above-mentioned value of σ_B for the Harwell boron.

Table 5. Summary of Determinations of σ_H. In quoting σ_H from σ_B/σ_H the value $\sigma_B = 769{\cdot}4 \pm 3{\cdot}8$ barns for standard Harwell boron has been used

Method	σ_H (barns)
Lifetime	$0{\cdot}3335 \pm 0{\cdot}0023$
σ_B/σ_H	$0{\cdot}3291 \pm 0{\cdot}0030$
L and D	$0{\cdot}3293 \pm 0{\cdot}0045$
Mean value $\sigma_H = 0{\cdot}3315 \pm 0{\cdot}0017$ barns ($\chi^2 = 1{\cdot}6$; $P = 0{\cdot}5$)	

We see that these results are in excellent mutual agreement and since they are independent of each other we quote the final mean value:

$$\sigma_H = 0{\cdot}3315 \pm 0{\cdot}0017 \text{ barns.}$$

References

Antonov, A. V., Isakoff, A. I., Murin, I. D., Neupocoyev, B. A., Frank, I. M., Shapiro, F. L., and Shtranick, I. V, 1955, *Int. Conf. on Peaceful Uses of Atomic Energy, Geneva*, **5**, 3.

Austern, N., 1953, *Phys. Rev.*, **92**, 670.

Austern, N., and Sachs, R. G., 1951, *Phys. Rev.*, **81**, 710.

Barkhov, L. M., Makarin, V. K., and Mukhin, K. N., 1957, *J. nuclear Energy*, **4**, 94.
Bracci, A., and Coceva, C., 1956, *Nuovo Cim.*, **4**, 59.
Campbell, E. C., and Stelson, P. H., 1956, *ORNL*-2076, p. 32.
von Dardel, G., and Sjöstrand, N. G., 1954, *Phys. Rev.*, **96**, 1245.
von Dardel, G., and Waltner, A. W., 1953, *Phys. Rev.*, **91**, 1284.
De Juren, J. A., and Rosenwasser, H., 1953, *J. Res. nat. Bur. Stand.*, **51**, 203.
Dio, W. H., and Schopper, E., 1958, *Nuclear Phys.*, **6**, 175.
Egelstaff, P. A., 1957, *J. nuclear Energy*, **5**, 41.
Green, A., Littler, D. J., Lockett, E. E., Small, V. G., Spurway, A. H., and Bowell, E., 1954, *J. nuclear Energy*, **1**, 144.
Hamermesh, B., Ringo, G. R., and Wexler, S., 1953, *Phys. Rev.*, **90**, 603.
Harris, S. P., Muehlhause, C. O., Rose, D., Shroeder, H. P., Thomas, G. E., and Wexler, S., 1953, *Phys. Rev.*, **91**, 125.
Meads, R. E., England, C. J., Collie, C. H., and Weeks, G. C., 1956, *Proc. phys. Soc. Lond.* A, **69**, 469.
Scott, F. R., Thomson, D. B., and Wright, W., 1954, *Phys. Rev.*, **95**, 582.
Wright, W. B., and Frost, R. T., 1956, *KAPL-M-WBW*-2.

CORRESPONDENCE

A Simple Formula for use with Carbon Thermometers at Low Temperatures

By O. V. Lounasmaa†
Clarendon Laboratory, Oxford

[Received March 10, 1958]

Several empirical or semi-empirical formulae have been proposed for use with carbon thermometers at low temperatures (Brown *et al.* 1951, Clement and Quinnell 1952, Lacaze and Peretti 1953, Hoare *et al.* 1955). Unfortunately, the mathematical forms of these are rather too complicated to be convenient when the amount of experimental data to be handled is large. A simpler formula was therefore sought, with the particular requirement that it be valid in the temperature range 4 to 12°K where frequent calibration is usually inconvenient.

The thermometer used was a 47 ohm, 0·25 watt radio resistor, taken from a 'Lab Minipack' card supplied by V.E.S. Wholesale Ltd., London. After removing the paint from the surface, an insulated copper wire was wound round it and bonded in place by Araldite 985E. The ends of the wire were soldered to a calorimeter whose temperature it was ultimately desired to measure; for present purposes it served simply as a gas thermometer bulb. This assembly formed part of an apparatus used for determining the entropy diagram of helium (Hill and Lounasmaa 1957). The details of the apparatus do not concern us here except that, as in most low temperature apparatus, thermometer calibrations against helium and hydrogen vapour pressures could conveniently be included in every experiment, whereas a gas thermometer calibration at intermediate temperatures involved a slight modification of the apparatus and so necessitated a separate experiment.

A first calibration in the range 4 to 12°K showed that when $1/R$ (R = thermometer resistance) is plotted against temperature an upward convex curve is obtained. On the other hand, $1/R'$, where $R' = R - R_0$, is nearly a linear function of temperature if the constant R_0 is suitably chosen. For a thermometer which had a resistance of 176·3 ohms at the hydrogen triple point (13·957°K) R_0 was found to be 94·0 ohms. When the calibration was repeated some months later, the thermometer having been cycled repeatedly between room temperature and helium temperatures in the meantime, little change was found. The resistance at the hydrogen triple point had increased by 1·6 ohms, but if R_0 was increased by the same amount the two curves of $1/R'$ against temperature coincided within the experimental accuracy. This is illustrated in the diagram,

† Now at the Wihuri Physical Laboratory, University of Turku, Finland.

where the temperature derivative of $1/R'$ is plotted as a function of temperature for the two runs.

As the quantity $d(1/R')/dT$ is sensibly constant, both with temperature and between experiments, the required relation may be written

$$T+\theta=A/R'$$

where θ and A are constants for a particular thermometer ; in the present case, $\theta \sim -1$ °K and $A \sim 1000$ ohm deg. It is to be emphasized that θ and A do not vary from run to run, provided that in each run R_0 is adjusted so as to bring R' to its standard value at one convenient temperature, preferably the hydrogen triple point. If the resistance measurements are to be made with a Wheatstone bridge, R' may be measured directly by inserting a resistance equal to R_0 in the balancing arm. The reduction of data then becomes particularly rapid, using either a desk calculator or tables of reciprocals and a large scale plot of $1/R'$ against T.

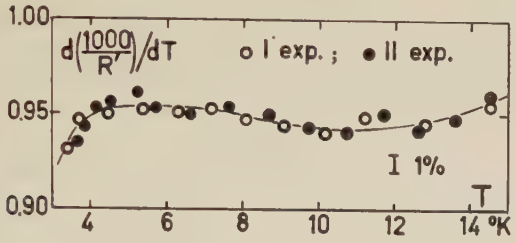

This calibration formula was tested and confirmed during a large number of experiments. With slight modifications its use can be extended to other temperatures.

References

Brown, A., Zemansky, M. W., and Boorse, H. A., 1951, *Phys. Rev.*, **84**, 1050.
Clement, J. R., and Quinnell, E. H., 1952, *Rev. sci. Instrum.*, **23**, 213.
Hill, R. W., and Lounasmaa, O. V., 1957, *Proceedings of the International Conference on Low Temperature Physics, Madison, U.S.A.* (in the press).
Hoare, F. E., Matthews, J. C., and Yates, B., 1955, *Proc. phys. Soc. Lond.* B, **68**, 388.
Lacaze, A., and Peretti, J., 1953, *J. Phys. Radium*, **14**, 350.

The Nucleation of Dislocation Loops during Cleavage

By S. Amelinckx
Laboratorium voor Kristalkunde, Rozier, 6, Gent, Belgium

[Received March 21, 1958]

It has been shown recently by Gilman (1956) that dislocation loops are nucleated by a propagating crack if the speed of the crack front falls below a certain critical value. Gilman deduced the presence of the loops from

etch patterns. The same phenomenon has been studied also by Forty (1957) who used interferometry and microscopic examination, and inferred the existence of loops from the geometry of the cleavage face.

We have developed recently a method for the decoration of dislocations in KCl which leaves the dislocation pattern after deformation practically undisturbed. This makes it possible to observe the dislocation loops in an even more direct way. Photograph 1 represents an example. The crystal was intentionally cleaved in such a way that the crack front stopped a number of times. The instantaneous position of the crack front can clearly be recognized on the photograph 1.

It is evident that a number of small dislocation loops have been formed. They are lying in two families of (110) planes. A large number of them are single loops. A few systems of concentric loops are however also visible, suggesting that surface sources have been active during a short time.

The decoration procedure is as follows. One uses KCl doped with 0·75% of $AgNO_3$ (by weight). The dislocations are already slightly decorated in the crystal as grown. A much better decoration, even of freshly introduced dislocations, can however be obtained if such crystals are x-irradiated for ± 6 h in contact with the window of a copper target x-ray tube operated at 40 kv, 20 ma, and subsequently annealed in air during 2 h at 600°c. At high magnification and in crystals irradiated and annealed for a longer period than those of which the patterns are shown, it is observed that the decoration consists mainly of small cubic cavities, similar but smaller in size than those found in hydrogene treated specimens (Amelinckx *et al.* 1958). The cavities are filled with gas under a pressure of a few atmospheres, and the walls are covered by silver. This can be deduced by dissolving the crystal in water and observing it under the microscope. Every time the dissolution front reaches a cavity a small gas bubble, a few times larger than the cavity giving rise to it. is produced. The nature of the gas was studied by means of mass-spectroscopy and by chemical means; details are given elsewhere (loc. cit.). It mainly consists of oxygen and nitrogen, resulting from the decomposition of the NO_3^- and NO_2^- radials under the influence of the ionizing radiation. The presence of oxydes of nitrogen could not be established.

The method has serious advantages, in that it leaves the pattern of freshly introduced dislocations largely undisturbed, probably as a consequence of their pinning under the influence of x-irradiation. Even the anneal at 600°c hardly disturbs the pattern. In particular the small half loops do not pop out as is invariably the case if they are not pinned. It is clear that this method is a promising tool for investigating the dislocation configuration after slip. Photograph 2, for example, shows the first stage of polygonization in KCl, i.e. the rearrangement of edge dislocations in their glideplane, so as to form vertical rows. Edge dislocations in their glideplane have also been observed in potassium bromide crystals decorated by means of gold (Barber *et al.* 1957).

A more detailed account will be published elsewhere.

Acknowledgments

I wish to thank Professor Dr. W. Dekeyser for the stimulating interest taken in this work which is part of a research programme (C.E.S.) supported by the " Institut pour l'encouragement de la Recherche Scientifique dans l'Industrie et l'Agriculture ".

References

Amelinckx, S., Maenhout-van der Vorst, W., and Dekeyser, W., 1958 (to be published).
Barber, D. J., Harvey, K. B., and Mitchell, J. W., 1957, *Phil. Mag.*, **2**, 704.
Forty, A. J., 1957, *Proc. roy. Soc.* A, **242**, 392.
Gilman, J. J., 1956, *J. appl. Phys.*, **27**, 1262.

Precipitate Instability During Unidirectional Extension of an Age Hardened Aluminium–Zinc–Magnesium Alloy

By I. J. Polmear and I. F. Bainbridge
Aeronautical Research Laboratories, Australian Defence Scientific Service, Melbourne, Australia

[Received March 17, 1958]

There has been much recent interest in the problem of the low fatigue properties exhibited by age hardened aluminium alloys. Current theories suggest that the poor properties are associated with the relative instability of the dispersed precipitate under conditions of cyclic stressing. Migration of solute atoms and over-ageing are thought to occur in heavily deformed localized regions. This produces zones which are relatively soft and in which subsequent plastic deformation tends to be concentrated leading, ultimately, to accelerated fatigue cracking.

There is some support for the suggestion that moving dislocations generate vacancies which increase solute diffusion rates in localized regions (Broom *et al.* 1956). Broom *et al.* (1957) have indicated that this proposal requires any structural changes to be associated with slip planes. Furthermore, since vacancies are generated during unidirectional extension as well as during fatigue, then some changes might be apparent in fractured tensile specimens. It was with the object of detecting such changes that these workers studied high purity alloys of aluminium–5·5% zinc–2·65% magnesium and aluminium–6% zinc–3% magnesium–1% copper. There was some evidence of slip band effects in polished and etched sections of the simpler ternary alloy but, because of a tendency to intercrystalline cracking in this material, work was concentrated on the quaternary alloy which had the basic composition of the commercial material DTD 683. Intense slip bands were observed in polished and etched sections from the interior of both tensile and fatigue specimens. However, modifications

to the distribution of the precipitate, as shown by Hanstock (1954) in fatigue-tested DTD 683 specimens, were not observed in either case.

We have also been studying metallographic changes associated with fatigue and tensile stressing of a series of high purity aluminium–zinc–magnesium alloys. Standard 0·25 in. diameter tensile specimens were machined to a diamond-turned surface finish from forged bar which had previously been heat treated. The heat treatment cycle, which consisted of $1\frac{1}{2}$ hours at 460°C, water quenching, and age hardening for 16 hours at 125°C, was chosen so that all alloys had a common U.T.S. of approximately 25 tons in^2. The specimens were tensile tested to failure, carefully centre sectioned in a longitudinal direction, and mounted in a cold setting resin. The centre section was mechanically polished and etched in Modified Kellers reagent (87·5% H_2O, 10% HNO_3, 1·5% HCl, 1·0% HF) which clearly showed the distribution of the precipitate and any deformation markings. The structural changes observed in a tensile specimen of an alloy of aluminium–5·1% zinc–3·0% magnesium are of interest in view of the earlier remarks.

The room temperature tensile test of the alloy gave the following results: 0·1% P.S., 20·6 tons in^2; U.T.S., 26·3 tons in^2; and elongation on a gauge length of $1\frac{1}{4}$ in. of 17·7%. Significant metallographic changes were confined to the necked section. In some grains widely spaced bands were observed which, because of their crystallographic nature, were presumed to indicate regions of intense slip. An example of this is shown in fig. 1, Pl. 27 where it is the distribution of the precipitate which is of particular interest. Intense precipitation has occurred in the region of the slip bands with consequent depletion of the surrounding matrix; a process which must have occurred during the comparatively short test period of approximately three minutes. Closer examination showed that the lines of precipitate and the coarse slip bands did not coincide. This is clearly evident in fig. 2, Pl. 27 where an actual plane on which slip displacement has occurred is revealed by a step in the grain boundary. It thus seems that coarse slip has occurred through the softer, depleted matrix which is the same result as that obtained for certain age hardened aluminium alloys tested in fatigue (Forsyth and Stubbington 1957).

A further example of precipitation caused by deformation in a tensile test is shown in fig. 3, Pl. 27. In this case the slip lines have been generated at the tip of an advancing internal crack and the distribution of the precipitate is similar to the bands of precipitate which Hanstock (1954) has observed in fatigue tested DTD 683 specimens.

The metallographic changes described above were less evident in alloys with a higher zinc : magnesium ratio where failure became progressively more intercrystalline or in alloys with a lower ratio of zinc : magnesium where deformation was more homogeneous. It thus appears that this alloy is particularly susceptible to structural changes when subjected to plastic deformation. This conclusion is significant as most of the commercial alloys based on the aluminium–zinc–magnesium system have closely similar zinc and magnesium contents.

ACKNOWLEDGMENT

This note is published with the permission of the Chief Scientist, Australian Defence Scientific Service, Department of Supply, Melbourne, Australia.

REFERENCES

BROOM, T., MOLINEUX, J. H., and WHITTAKER, V. N., 1956, *J. Inst. Metals*, **84**, 357.
BROOM, T., MAZZA, J. A., and WHITTAKER, V. N., 1957, *J. Inst. Metals*, **86**, 17.
FORSYTH, P. J. E., and STUBBINGTON, C. A., 1957, *J. Inst. Metals*, **85**, 339.
HANSTOCK, R. F., 1954, *J. Inst. Metals*, **83**, 11.

Measurements of Thermoelectricity Below 1°K

By D. K. C. MACDONALD, W. B. PEARSON and I. M. TEMPLETON
Division of Pure Physics, National Research Council, Ottawa, Canada

[Received March 20, 1958]

RECENT measurements of the absolute thermoelectric power S of the alkali metals down to $\sim 2°K$ (MacDonald *et al.* 1958) have shown that, even down to so low a temperature, there is very considerable variety in

Fig. 1

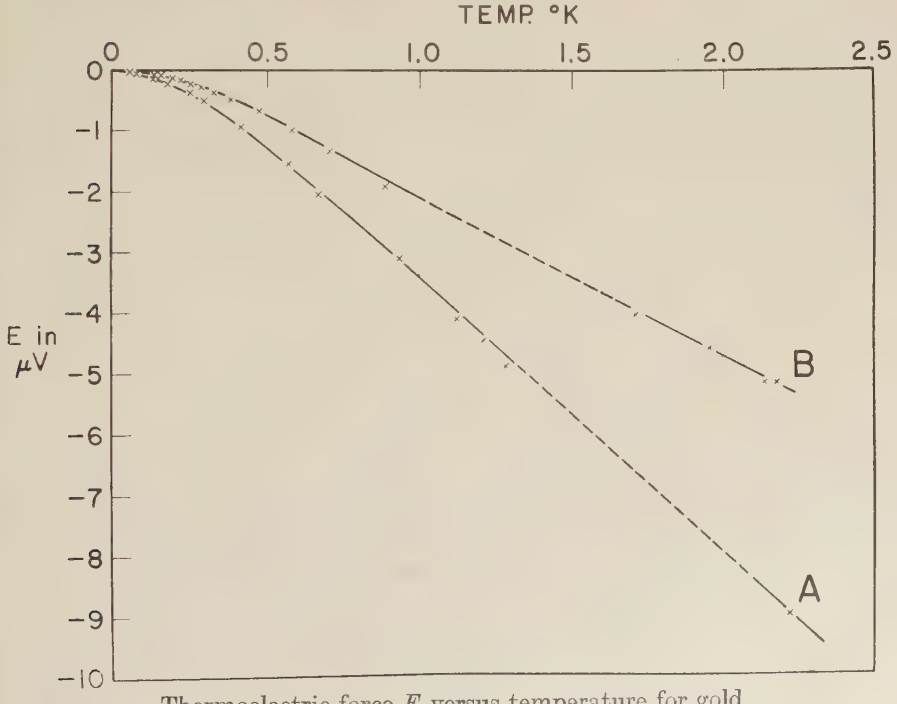

Thermoelectric force E versus temperature for gold.
Sample (A) (' specpure ') $R_{4\cdot2°K}/R_{294°K} \approx 3\cdot19 \times 10^{-3}$.
Sample (B) (lower purity, unannealed) $R_{4\cdot2°K}/R_{291°K} \approx 6\cdot39 \times 10^{-2}$.

the behaviour. In particular, the Thomson heats μ derived from our results ($\mu = T\, dS/dT$) show, in the case of rubidium and caesium, a rather remarkable oscillation with temperature: in caesium the Thomson heat shows a *positive* maximum at $\sim 3°K$ with a value as high as $\sim +2{\cdot}5\,\mu V/°C$.

We therefore decided to extend these measurements of thermoelectric power to the temperature region below 1°K; as far as we know, no measurements of thermoelectric power below 1°K have previously been reported. Before attempting to work with the alkali metals themselves,

Fig. 2

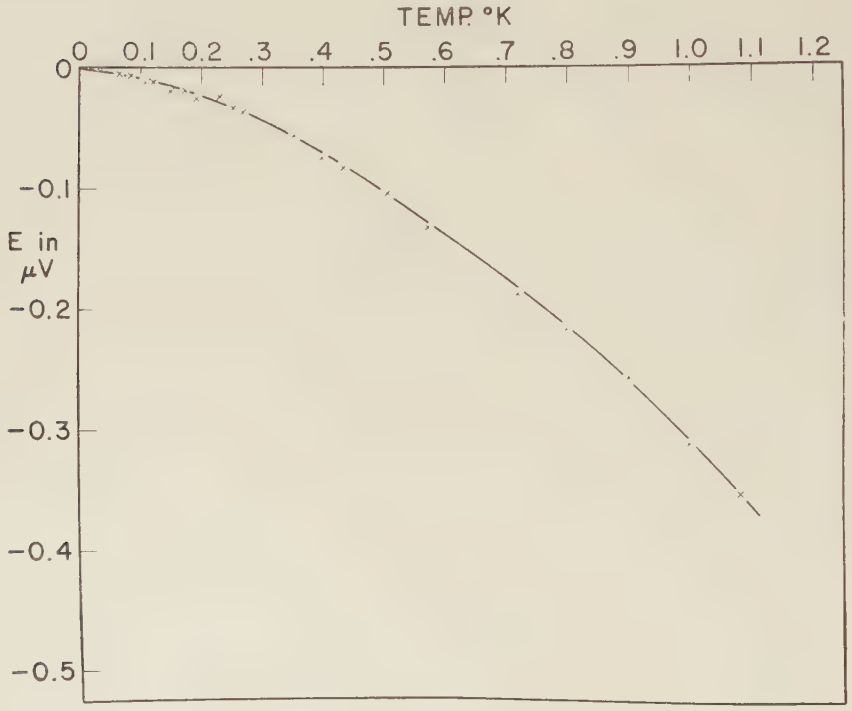

Thermoelectric force E versus temperature for silver.
$R_{4{\cdot}2°K}/R_{294°K} \approx 3{\cdot}85 \times 10^{-3}$.

we thought it best to try some preliminary experiments in this temperature region on the 'noble' metals, gold and silver, which are much easier to handle than the alkali metals. A few experiments on gold and silver specimens are now complete and the results appear of considerable interest in themselves.

Figures 1 and 2 show the observed thermoelectric force on two samples of gold and one of silver. The electromotive force itself can be measured with rather good precision (around 1%). No great accuracy, however, is claimed for the temperature measurement in these experiments.

Ferric Ammonium Alum was used as the refrigerant, and the correction from T^* to T was made using the recent scale resulting from the experiments of Cooke *et al.*† (1956); only a very rough form factor was used, however, for the salt pill which was an irregular cylinder.

It will be seen that the gold specimen referred to as A shows an absolute thermoelectric power of about $-4\mu V/°C$ around 0·5°K. Now the usual theory of electron transport predicts for a free electron model:

$$S \sim C_{el}/Ne \qquad . \quad . \quad . \quad . \quad . \quad . \quad . \quad . \quad (1)$$

where C_{el} is the electron specific heat per unit volume, and N the density of free electrons. For gold this would give $S \sim -3{\cdot}5 \times 10^{-9}$ volts/°C at $\sim 0{\cdot}5$°K, i.e. less than one thousandth of the observed value.

Of recent years there has been considerable interest in the ' phonon-drag ' effect to which attention was first drawn by Gurevich (1945, 1946). This recognizes that the heat flow in the *lattice* (i.e. a ' phonon-current ') can, through scattering of phonons by conduction electrons, ' drag ' these electrons with it so causing a thermoelectric current. The magnitude of this effect depends primarily on the *lattice* specific heat, C_{latt}, and a crude analysis indicates a maximum thermoelectric power of the order C_{latt}/Ne due to the ' phonon-drag '. In semiconductors it appears established that the ' phonon-drag ' can play quite a major role, and it also now appears quite probable that in metals at fairly low temperatures the effect may be important.

However, at 0·5°K. C_{latt}/C_{el} in gold is only the order of 10%, assuming reasonable theoretical values; consequently it appears impossible to look in this direction for an explanation of the relatively enormous thermoelectric power which we have observed at these very low temperatures.

A more detailed formula (e.g. Wilson 1953) for the ' normal ' thermoelectric power in a metal is:

$$S = \frac{\pi^2 k^2 T}{3e\zeta_0} \left\{ \frac{d \log n(E)}{d \log E} + \frac{d \log (\tau v^2(E))}{d \log E} \right\}_{E=\zeta_0} . \qquad . \quad . \quad . \quad (2)$$

(We note that $C_{el}/Ne = \pi^2 k^2 T/2e\zeta_0$, cf. eqn. (1).) For ideal free electrons the first factor in the brackets equals $\frac{1}{2}$, and the second is presumed (Wilson *loc. cit.*) to vary from $\frac{1}{2}$ at low temperatures to $\frac{5}{2}$ at high temperatures. One would clearly have to postulate enormous values (i.e. of the order of 10^3) for one or other of the logarithmic derivatives to account for the observed thermoelectric power in gold below 1°K.

These experimental results seem to us, therefore, to lie beyond the limits of current theoretical explanation. The interest of measurements in this temperature region is evident.

---

† We are grateful to Dr. A. H. Cooke for letting us have a copy of his data.

The magnitude of thermoelectric power observed in these metals also clearly points to their possible use as differential thermometers, for example, in calorimetry below 1°K.

References

Cooke, A. H., Meyer, H., and Wolf. W. P., 1956, *Proc. roy. Soc,* A, **237,** 395.
Gurevich, L., 1945, *J. Phys. U.S.S.R.*, **9,** 477; 1946, *Ibid.*, **10,** 67.
MacDonald, D. K. C., Pearson, W. B., and Templeton, I. M., 1958, *Proc. roy. Soc.* A (submitted for publication).
Wilson, A. H., 1953, *The Theory of Metals*, 2nd ed. (Cambridge: University Press).

REVIEWS OF BOOKS

Theoretical Physics (*3rd edition*). By Georg Joos and Ira M. Freeman. (London and Glasgow: Blackie & Son Ltd.) [Pp. 885.] 70*s*.

This new edition of the well-known textbook by Professor Joos is as useful and well written as earlier editions have been. It covers the whole of theoretical physics from vector analysis to quantum theory, including classical mechanics, relativity, electromagnetism, optics thermodynamics, statistical aspects of heat and the atomistic nature of electrical phenomena. This edition has been brought up to date by some short additions including a section on matrices and by a revision of the chapter on nuclear physics. The treatment throughout is a connected development of selected useful topics rather than exhaustive. The mathematics never becomes frighteningly formidable, while the application of the theory to well-known physical phenomena is continually pointed out. In particular " modern " physics, such as the vector model of the atom and detailed wave mechanical calculations, receives its due weight.

Only the nuclear physics chapter is really disappointing, in that it is general and discursive, instead of a theoretical discussion of selected aspects in accordance with the spirit of the rest of the book. Incidentally it contains one odd assertion—" probably every elementary particle has spin 1/2 ".

The book can be recommended strongly as a textbook for honours students and as a reference book for the shelf of any work-a-day physicist.

V. H.

An Introduction to Fourier Analysis and Generalised Functions. By M. J. Lighthill. (Cambridge University Press.) [Pp. 79.] 17*s*. 6*d*.

When talking to physicists about Dirac's delta function, it is customary to say " Of course, to the pure mathematicians, this is a very improper function, but it would take a lot of explanation to get it right, and in practice there is usually no difficulty ". To the bright boys of the class, we can now add " Professor Lighthill's little book shows the simplest and most elegant way of setting up a consistent formulation ". The theory of generalised functions, developed by Schwartz and Temple, seems to solve most of the epsilontic problems that arise in applied mathematics, without recourse to Lebesque integration and other sophistications. It is strongly recommended to undergraduates and research students who care for rigour (if not for the *rigor mortis* of absolutely pathological functions !).

J. M. Z.

Magneto-Hydrodynamics. Edited by R. K. M. Landshoff. (Stanford University Press. London : Oxford University Press.) [Pp. x+115.] 32*s*.

This book is essentially an edited collection of the papers by different authors presented at a symposium on Magnetohydrodynamics held in California at the end of 1956.

Five theoretical papers are followed by seven describing experimental work, though in the latter is included one on a hydromagnetic waveguide which gives the theory of an experiment only being planned at the time of writing.

The first paper is an interesting attempt to classify the problems of magnetohydrodynamics according to the relative importance of the many parameters involved. The next two are of the descriptive type common in this field

(in one, the reader is asked to visualize the use of a rolling pin on a lump of cosmic dough). There follow analytical treatments of a shock wave problem and the pinch effect. The experimental section is largely concerned with shock waves.

The papers are bound to be of interest to workers in the field, but surely this rather heterogeneous collection would have appeared more appropriately in the research journals than in a book. P. C. C.

Magnetohydrodynamics (*Interscience Tracts on Physics and Astronomy, No.* 4). By T. G. Cowling. (New York: Interscience Publishers, Inc. [Pp. viii + 115.]

This is a book to be commended, short but comprehensive. Its length seems inversely proportional to its authority, and careful reading, supplemented by the references, should give a good appreciation of magnetohydrodynamics.

Following a concise presentation of the fundamental mathematics, various problems are considered, grouped in respective chapters on magnetohydrostatics, wave motion, magnetic fields and instability, dynamo theories, and ionized gases. Many of the discussions are conducted in words, with quantitative injections from order of magnitude arguments: this reflects the impossibility of anything like a comprehensive mathematical treatment of the interlocked electromagnetic and hydrodynamic equations. On the other hand, some of the more analytical investigations do receive attention, results being quoted and derivations hinted at. Most of the theories are criticized, and reasons given for their rejection often outweigh those for acceptance: but some are commended with phrases like "the suggestion deserves attention", and Bullard's work on the dynamo theory draws the response "Thus the possibility of dynamo maintenance of cosmic magnetic fields can be regarded as finally established".

One evident omission is any discussion of magnetic field effects on shock waves, and it is perhaps disappointing that so little is said about the important case of anisotropic conductivity. P. C. C.

The Elements of Classical Thermodynamics. By A. B. Pippard. (Cambridge: University Press). [Pp. 159, Exercises and Index.] Clothbound 25*s.*; Students Edition, paper covers; 15*s.*

It has often been pointed out that thermodynamics is a subject of which it is easy to acquire knowledge but difficult to acquire understanding. One can readily become familiar with the manipulation of partial derivatives without a real appreciation of the concepts on which the structure of thermodynamics is based. Dr. Pippard's book, whilst paying adequate attention to technique, is particularly to be recommended for providing the reader with an *understanding* of thermodynamics. Many awkward points, which are glossed over in other treatises, are discussed clearly and comprehensively.

The book contains nine chapters and is restricted to the study of homogeneous systems. In the introductory chapter the author points out that classical thermodynamics approaches more closely to an ideal logical development than any other branch of natural science. The next three chapters which are devoted to the zeroth, first, and second laws keep this aspect well to the foreground; consideration is given to the approach of Caratheodory in developing the second law, as well as to the more usual Carnot cycle method. Chapters four, five and six consider various consequences and applications of the laws of thermodynamics; these include the Maxwell relations, various properties of the equation

of state, adiabatic changes, specific heats, the Joule Kelvin effect, radiation, and surface phenomena. Chapter five also contains a brief discussion of the third law of thermodynamics and Chapter six ends with a detailed account of the establishment of the absolute scale of temperature. Chapter seven deals with the thermodynamics inequalities and conditions of equilibrium, and contains as an illustrative example a discussion of the equilibrium between a liquid drop and its vapour.

The last two chapters which discuss respectively phase equilibrium and higher order transitions, constitute, in the opinion of the reviewer, the most valuable and original section of the book. Applications are drawn widely from modern research in solid state physics, and in themselves show how much help can be obtained from thermodynamics in elucidating these phenomena. The analysis of second order transitions, and the correlation of the difference between first and higher order phase transitions with the existence or non-existence of metastable states, should dispel the confusion with which this topic has long been surrounded.

The book is not intended for the complete beginner, but anyone with a rudimentary knowledge of thermodynamics cannot fail to derive benefit and stimulus from perusing its pages. The Cambridge University Press is to be warmly congratulated on the innovation of a paper-backed edition which brings the price to a very reasonable level. It is to be hoped that this experiment will be continued.

C. D.

Soviet Sputniks. (London : Soviet News, 1958.) [Pp. 52.] 1*s.* 3*d.*

This booklet gives a popular account of the Russian satellites, based on material published by Soviet scientists. As popular accounts go it is a good one and well illustrated, but it reads, unfortunately, as if the material has been extracted piecemeal with a pair of scissors and assembled with a pot of glue.

The method of launching is described after a brief historical introduction, but most of the book is taken up with the various phenomena that can be investigated by means of artificial satellites.

There is little propaganda and only once are we told how it is " far from accidental that it was the Soviet Union which first succeeded in building and launching satellites ". This is an opinion with which all may concur.

J. R. S.

BOOK NOTICES

Pressure Measurement in Vacuum Systems. By J. H. Leck. (Published on behalf of the Institute of Physics by Chapman & Hall Ltd.) [Pp. 144.] 30*s*.

Communication, Organization, and Science. By J. Rothstein. (Indian Hills, Colorado : Falcon's Wing Press.) [Pp. lxxxv+110.] $3.50.

Contributions to the Theory of Games. Volume III. Edited by M. Dresher, A. W. Tucker, and P. Wolfe. (Princeton University Press. London : Oxford University Press.) [Pp. vi+435.] 40*s*.

Edmund Burke and the Natural Law. By Peter J. Stanlis. (Ann Arbor : University of Michigan Press.) [Pp. xiii+311.] $5.75.

[The Editors do not hold themselves responsible for the views expressed by their correspondents.]

Fig. 2

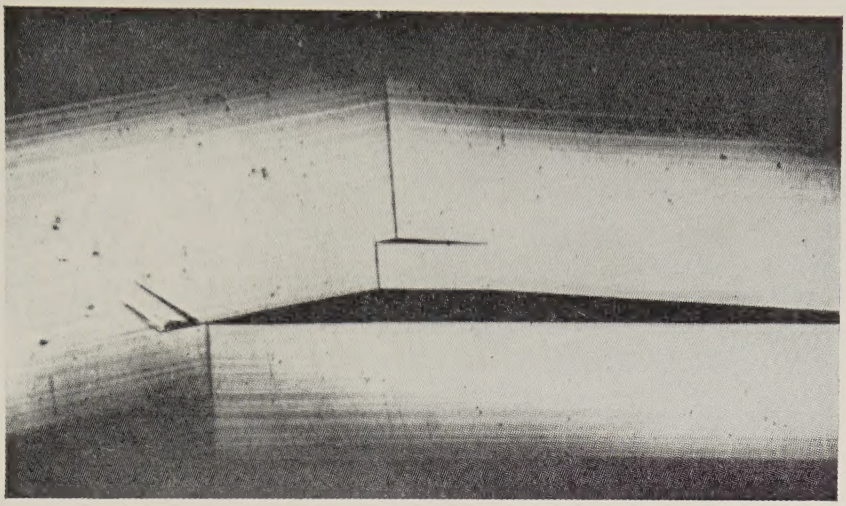

Single crystal of zinc under compression Gilman (1954).

Fig. 3

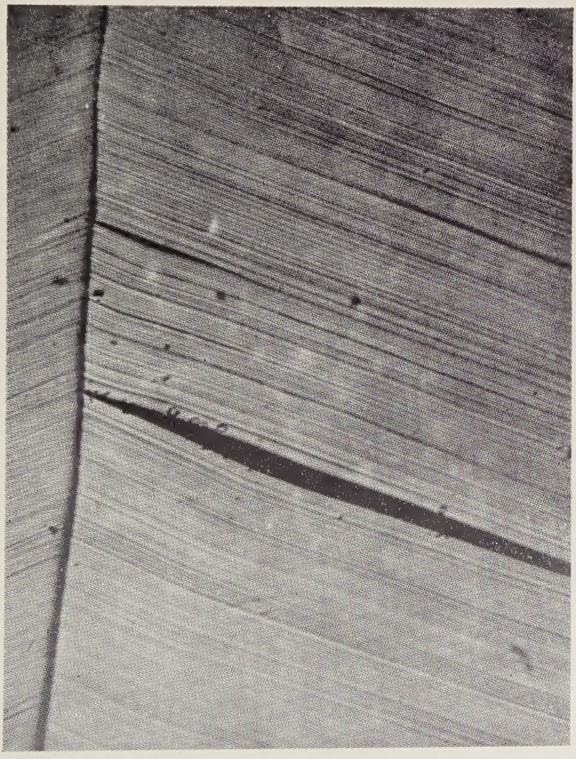

A

B

Symmetrical zinc bicrystal under tension Gilman (1957).

Photograph 1

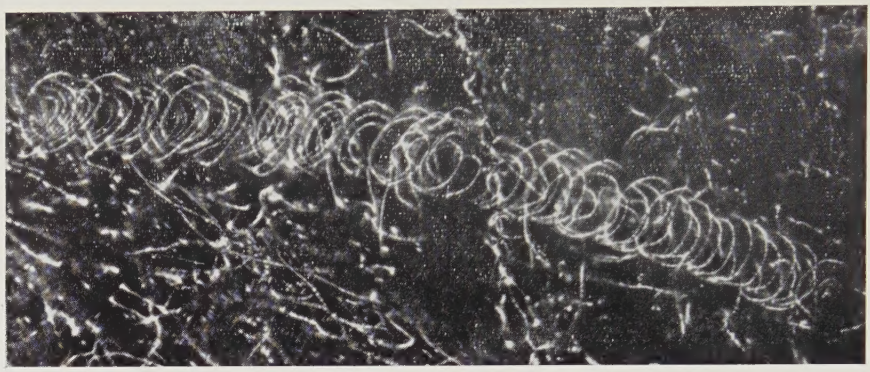

Dislocation loops along crack front in KCl crystal. Loops are lying in (110) and ($1\bar{1}0$) planes. Note systems of concentric loops ($\times 350$).

Photograph 2

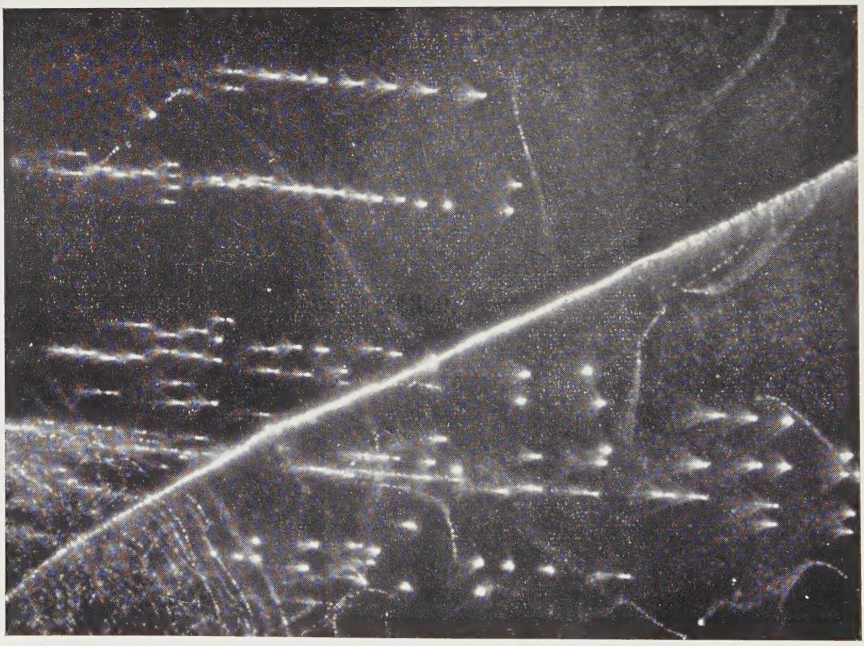

Dislocations in glide planes. Note the tendency to form vertical rows. The deformation was caused by indentation somewhere in the bottom left corner ($\times 500$).

Fig. 1

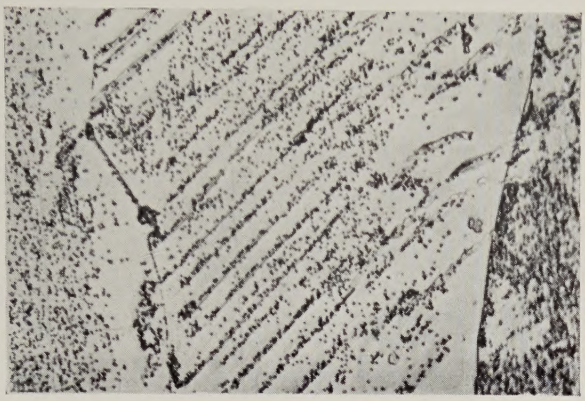

Precipitation in slip band regions. ×500.

Fig. 2

Lack of coincidence between lines of precipitate and slip bands. ×1300.

Fig. 3

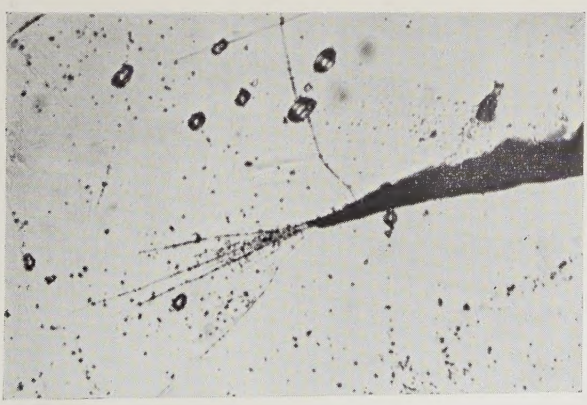

Precipitation associated with slip bands generated at the tip of an internal crack. ×500.